TECHNISCHE UNIVERSITÄT MÜNCHEN

Fakultät für Medizin

Neural correlates of anesthesia-induced unconsciousness in humans. Focus on subcortical influences measured by BOLD fMRI

Juliana Zimmermann

Vollständiger Abdruck der von der Fakultät für Medizin der Technischen Universität München zur Erlangung des akademischen Grades eines Doctor of Philosophy (Ph.D.) genehmigten Dissertation.

Vorsitz: Prof. Dr. Thomas Korn

Betreuer: Priv.-Doz. Dr. Christian Sorg

Prüfer*innen der Dissertation:

1.Priv.-Doz. Dr. Afra Wohlschläger
2. Prof. Dr. Gerhard Schneider

Die Dissertation wurde am 24.11.2022 bei der Technischen Universität München eingereicht und durch die Fakultät für Medizin am 23.01.2023 angenommen.

Abstract

Although general anesthesia has been widely used for over a century now, mechanisms of how anesthetic agents modulate consciousness are only partly understood. One topic of debate in anesthesia systems neuroscience is whether these effects are mainly explained by 'bottom-up' or 'top-down' processes. Using data of two independent previously-recorded simultaneous EEG-fMRI experiments in healthy volunteers, anesthetized with sevoflurane and propofol, respectively, the subcortical influences on neural correlates of anesthesia-induced unconsciousness measured by blood oxygenation fluctuations (BOLD) of functional MRI (fMRI) were explored. Three projects were conducted.

The first two projects focused on one of the most consistent neural correlate of anesthesia-induced unconsciousness: the reduction of the intrinsic functional connectivity in the so-called default mode network (DMN), i.e., reduced correlations of ongoing infra-slow activity BOLD fluctuations (intrinsic functional connectivity) among medial cingulate and lateral parietal-temporal cortices. While this finding has been replicated several times, its underlying mechanisms are incompletely understood. Experiments in animals and humans suggest that the subcortical neuromodulatory nuclei, such as the midbrain dopaminergic ventral tegmental area (VTA) and the cholinergic basal forebrain anterior part (a-cBF), which are projecting into the DMN, are also associated with the modulation of wakefulness, making these nuclei possible candidates of influencing DMN anesthesia-related effects. In the first project, using seed-based functional connectivity and mediation analyses, results showed that the connectivity reduction within the DMN during anesthesia-induced unconsciousness is mediated by the reduction of VTA-DMN connectivity. Reduction of a-cBF-DMN connectivity did not mediate within-DMN connectivity reduction, instead it was found a strong correlation between them, especially with sevoflurane anesthesia. This finding provides indirect evidence of the dopaminergic and cholinergic neuromodulatory influence on cortical DMN modulation during anesthesia-induced unconsciousness.

In the second project, we studied transient large-scale synchronizations of BOLD discrete events across DMN regions in a time window of ~50 seconds. Results from humans and animals suggest that transient large-scale synchronizations across the cortex are a hallmark of the awake state. This was measured by the Fano Factor (FF) and its distribution. The FF captures higher order correlation and global synchrony between discrete events and allows to quantify if the observed neural variability compares with the expected variability for a Poisson process. Results showed that during anesthetized states, BOLD synchronizations were reduced across the DMN. Interestingly, these reductions were

mediated by VTA-DMN connectivity, but not by a-cBF-DMN one, upon wakefulness post-anesthesia. We demonstrated that -beyond static functional connectivity- large-scale BOLD DMN synchronizations were affected during anesthesia-induced unconsciousness, and additionally, findings suggest that the recovery of the within-DMN organization might be influenced by the recovery of a coherent DMN and midbrain arousal system interaction. Taken together, these findings from the first two projects support the idea that anesthesia-induced cortical DMN changes with sevoflurane or propofol, respectively, might be modulated by neuromodulatory subcortical influences, especially by the midbrain VTA.

Finally, our third project focused on burst suppression state (BS) induced with 4vol% sevoflurane anesthesia. BS is a global electroencephalogram (EEG) pattern characterized by an alternating high-voltage activity (bursts) and isoelectric quiescence (flat line or suppression). This pattern has been identified as a global state of profound brain inactivation, physiologically seen during comatose states but also pharmacologically induced by deep anesthesia. Evidence from animal and human data suggest that cortical areas, thalamus, and the ascending arousal system (ARAS) participate in the generation of burst and suppression; however, the dynamics of this process is still unclear, especially when discerning global vs. local activity. We have studied functional connectivity of fMRI BOLD fluctuations from cortical, thalamus and ARAS regions up to 18 seconds before a bursting event. Events where labelled using EEG signal. To detect local differences when the global activity seems to govern, we have applied an event-like partial jackknife correlation approach, consisting in a repeatedly re-estimating the pair-wise correlation value between two regions after the removal of a single observation. The results indicate that just before the bursting global event, connectivity between ARAS and cortical regions, and thalamus and cortical areas increase significantly, compared to cortico-cortical connectivity. Thalamus-related results were supported by event-related BOLD response analyses. This suggests that subcortical activity, specially from the medial thalamus, could participate in the generation of single global bursting events during sevoflurane-induced burst suppression.

In total, we provide various evidence for prominent subcortical neuromodulatory influences on cortical particularly DMN blood oxygenation correlations during distinct states of anesthesia, supporting a general bottom-up arousal model of anesthesia-induced unconsciousness.

Zusammenfassung

Obwohl die Allgemeinanästhesie seit über einem Jahrhundert weit verbreitet ist, sind die konkreten Wirkmechanismen von Anästhetika auf das Bewusstsein nur teilweise bekannt. Dabei ist die Frage, ob die Effekte hauptsächlich durch "bottom-up"- oder "top-down"-Prozesse erklärt werden, ein zentraler Bestandteil der neurowissenschaftlichen Debatte. Ziel der vorliegenden Studien war es daher, subkortikale (bottom-up) Einflüsse auf neuronale Korrelate der narkosebedingten Bewusstlosigkeit zu untersuchen, anhand von Daten zweier unabhängiger EEG-fMRI Experimente an gesunden Probanden, die mit Sevofluran bzw. Propofol narkotisiert wurden. Die Schwankungen in der Blutsauerstoffsättigung (BOLD) der fMRI Messung waren das zentrale Hirnmaß in den drei nachfolgenden Projekten.

Die ersten beiden Projekte konzentrierten sich auf eines der beständigsten neuronalen Korrelate der anästhesiebedingten Bewusstlosigkeit: Die Verringerung der intrinsischen funktionellen Konnektivität im so genannten „Default Mode Network“ (DMN), d.h. eine verringerte Korrelation der infra-langsamen BOLD Schwankungen (intrinsische funktionelle Konnektivität) zwischen dem medialen cingulären Kortex sowie dem lateralen parieto-temporalen Kortex. Obwohl diese Beobachtung wiederholt, gefunden werden konnte, sind die zugrunde liegenden Mechanismen noch nicht vollständig geklärt. Tier- und Humanexperimente zeigten, dass subkortikale neuromodulatorische Kerne wie das dopaminerge ventrale tegmentale Areal (VTA) des Mittelhirns und der cholinerge vordere Teil des basalen Vorderhirns (a-cBF) zum einen mit der Modulation des Wachseins in Verbindung stehen, zum anderen in das DMN projizieren.
Das erste Projekt, basierend auf funktionellen Konnektivitäts- und Mediationsanalysen, zeigte, dass die Verminderung der funktionellen Konnektivität innerhalb des DMN während narkosebedingter Bewusstlosigkeit durch eine Reduktion der VTA-DMN-Konnektivität vermittelt wird. Weiter fanden wir, dass eine Verringerung der a-cBF-DMN-Konnektivität mit einer Verringerung der Konnektivität innerhalb des DMN korrelierte. Diese Ergebnisse liefern somit einen indirekten Beweis für den dopaminergen und cholinergen neuromodulatorischen Einfluss auf die kortikale DMN-Modulation während der anästhesieinduzierten Bewusstlosigkeit.

Im zweiten Projekt untersuchten wir vorübergehende Synchronisationen von diskreten BOLD-Ereignissen in DMN-Regionen in einem Zeitfenster von etwa 50 Sekunden. Studien an sowohl Menschen als auch Tieren deuten darauf hin, dass solche Synchronisationen im gesamten Kortex ein Kennzeichen des Wachzustands sein können. Dies wurde anhand des Fano-Faktors (FF) und seiner

Wahrscheinlichkeitsverteilung gemessen. Der FF erfasst Korrelationen höherer Ordnung und globale Synchronizität zwischen diskreten Ereignissen. Die Ergebnisse zeigten, dass während einer Narkose durch Sevofluran und Propofol die BOLD-Synchronisationen im gesamten DMN reduziert waren. Interessanterweise wurde diese Verringerung durch die VTA-DMN-Konnektivität nach der Narkose im Wachzustand vermittelt, jedoch nicht durch die a-cBF-DMN-Konnektivität. Die Ergebnisse deuten darauf hin, dass die Erholung der DMN-internen Synchronisation durch die Wiederherstellung einer kohärenten Interaktion zwischen DMN und dem Erregungssystem des Mittelhirns beeinflusst werden. Zusammengenommen unterstützen die Ergebnisse der ersten beiden Projekte die Idee, dass die durch Sevofluran oder Propofol induzierten kortikalen DMN-Veränderungen durch neuromodulatorische subkortikale bottom-up Einflüsse, insbesondere durch das VTA des Mittelhirns, moduliert werden könnten.

Das dritte Projekt schließlich befasste sich mit dem so-genannten Burst-Suppressions-Zustand (BS), der durch eine 4-Vol%-Sevofluran-Anästhesie ausgelöst wird. BS ist ein globales Elektroenzephalogramm (EEG)-Muster, das durch eine abwechselnde Hochspannungsaktivität (Bursts) und isoelektrische Ruhe (flache Linie oder „Suppression“) gekennzeichnet ist. Dieses Muster wird als ein globaler Zustand tiefgreifend veränderter Hirnaktivierung identifiziert, der ursprünglich bei komatösen Zuständen beobachtet wurde, jedoch auch pharmakologisch durch tiefe Anästhesie ausgelöst werden kann. Ergebnisse deuten darauf hin, dass kortikale Areale, der Thalamus sowie das aufsteigende Erregungssystem (ARAS) an der Erzeugung von Burst- oder Suppression-Ereignissen beteiligt sind. Wir haben deshalb die funktionelle Konnektivität von fMRI-BOLD-Fluktuationen aus kortikalen, Thalamus- und ARAS-Regionen bis zu 18 Sekunden vor einem Burst-Ereignis, indiziert durch EEG-Veränderungen, untersucht. Um lokale Unterschiede zu erkennen, wenn globale Aktivität sich verändert, haben wir einen Ereignis-ähnlichen partiellen Jackknife-Korrelationsansatz angewandt. Die Ergebnisse zeigen, dass kurz vor einem globalen Burst-Ereignis die Konnektivität zwischen ARAS und den kortikalen Regionen sowie zwischen Thalamus und den kortikalen Bereichen im Vergleich zur kortikalen Konnektivität signifikant zunimmt. Insgesamt deuten diese Ergebnisse darauf hin, dass subkortikale Aktivität, insbesondere aus dem medialen Thalamus, an der Erzeugung einzelner globaler Burst-Ereignisse, während eines sevofluraninduzierten Burst-Supression-Zustands beteiligt sind.

Diese Befunde zeigen, dass subkortikale neuromodulatorische Systeme während verschiedener Anästhesiezustände und unter Verwendung verschiedener Anästhetika die kortikale BOLD funktionelle Konnektivität beeinflussen, insbesondere die des DMN. Sie unterstützen das allgemeine Bottom-up-Arousal-Modell der anästhesieinduzierten Bewusstlosigkeit.

Table of Content

Abbreviations

a-cBF	anterior cholinergic basal forebrain
ACh	acetylcholine
AMPA	alpha-amino-3-hydroxy-5-methyl-4-isoxazolepropionic acid
ARAS	ascending reticular activating system
BIS	bispectral index
BOLD	blood oxygen level-dependent
BS	burst suppression
cBF	cholinergic basal forebrain
CI	confidence interval
CSF	cerebrospinal fluid
DARTEL	diffeomorphic anatomical registration based on exponentiated lie algebra
DMN	default mode network
DR	dorsal raphe
ECoG	electrocorticogram
EEG	electroencephalogram
EPI	echo-planar imaging
FC	functional connectivity
FF	Fano factor
fMRI	functional magnetic resonance imaging
FWE	family-wise error
GABA	gamma-aminobutyric acid
GLM	general lineal model
GM	grey matter
HRF	hemodynamic response function
iFC	intrinsic functional connectivity
IV	intravenous
JC	jackknife correlation
LC	locus coeruleus
LFP	local field potentials
mPFC	medial prefrontal cortex
MR	medial raphe
MRF	medial reticular formation
MRI	magnetic resonance imaging

NMDA	N-methyl-D-aspartate
NVC	neurovascular coupling
PAG	periaqueductal grey
PBC	parabrachial complex
PCA	principal component analysis
PCC	posterior cingulate cortex
PESTICA	physiologic estimation by temporal independent component analysis
PET	positron emission tomography
PFC	prefrontal cortex
PFC	prefrontal cortex
PJC	partial jackknife correlation
PO	pontis oralis
PPN	pedunculopontine nucleus
PSTH	peri-stimulus time histogram
rCBF	regional cerebral blood flow
rCBV	regional cerebral blood volume
rCMRO2	regional cerebral metabolic rate of oxygen
RF	radio-frequency
ROI	region of interest
RSN	resting state networks
SLOMOCO	slice oriented motion correction
SPECT	photon emission computed tomography
SRCC	small region confound correction
TE	echo time
TR	repetition time
VTA	ventral tegmental area

List of figures and tables

Figures.

Tables.

1. Introduction

1.1. General anesthesia and state of unconsciousness

Consciousness can be described as the presence of a subjective experience (Tononi & Koch, 2015). More specifically, it is defined based on two critical components: *(i)* arousal, which refers to the overall state of alertness (i.e., wakefulness), and *(ii)* awareness, which refers to the proper subjective experience (i.e., content of consciousness: awareness of environment and of the self) (Boly et al., 2013; Laureys, 2005). Both components are integral and interdependent parts of the human consciousness, i.e., arousal pathways originating in the brainstem activate awareness networks in the cerebral cortex, while cortical activity provides continuous feedback to subcortical and brainstem areas to sustain cognitive processes (Parvizi & Damasio, 2001). During clinical examination, arousal is assessed by the opening of the eyes, and awareness is inferred by the ability of the subject to follow commands (Boly et al., 2013; Lee et al., 2022).

Consciousness can be altered or modified in different ways, e.g., physiologically during sleep, pathologically after a brain insult such a traumatic brain injury, or pharmacologically with the use of anesthesia, which is a common practice in the clinical setting. This drug-induced reversible condition is called *general anesthesia* or *pharmacological sedation*. The aim of its use is to provide patients a state where they can tolerate painful or invasive procedures (Bonhomme et al., 2019) by inducing and maintaining specific behavioral and physiological traits, such as amnesia, analgesia, akinesia, and loss of consciousness (i.e., anesthesia-induced unconsciousness), while guaranteeing stability of the autonomic, cardiovascular, respiratory, and thermoregulatory systems (Brown et al., 2010). Besides the clinical setting, general anesthesia serves as a useful model to modulate consciousness levels in a controlled reversible way to understand neural-related processes involved in the induction of and emergence from unconsciousness; therefore, of great interest in biological and computational neuroscience research.

In this process, concentration of the administered anesthetic plays a decisive role, for instance, low-sedative levels produce analgesia, amnesia, distorted time perception, depersonalization, and increased sleepiness; higher doses usually induce a complete absence of response to commands, commonly recognized as ‘unconsciousness’ (Alkire et al., 2008). In humans, the process of sedation (and indirectly consciousness modulation), can be assessed through various physiological measures: *(i)* electroencephalogram (EEG) monitoring, specifically via visual inspection of the raw signal, or by

tracking changes in its spectral edge frequency or monitoring the depth of anesthesia with the bispectral index (BIS); *(ii)* behavioral quantification of reusability via the Ramsay Sedation Scale, which consists of four levels of sedation defined by responses to stimuli (corresponding to the levels 3 to 6 in the scale), a level of 'cooperative oriented and tranquil' (level 2), and a level for 'anxious, agitated, or restless' (level 1) (Sessler et al., 2008) ; and *(iii)* using a protocol based on end-tidal anesthetic agent concentration monitoring, currently used in clinical settings (Eger et al., 1965; Hendrickx & De Wolf, 2022). In rodents, besides EEG readouts, the assessment of the *loss or return of the righting reflex*, (i.e., a binary measure assessed by placing the animal in a supine position and measuring the time it takes to return to all fours) represent the two more prominent correlates of consciousness (Vincent et al., 2021).

General anesthesia is a complex process and can elicit different experiences in each subject. It has been proposed that these reflect different states of consciousness: *(i)* unconsciousness, i.e., a complete absence of a subjective experience, *(ii)* disconnected consciousness, i.e., a conscious experience without perception of the environment, and *(iii)* connected consciousness, i.e., episodes of oriented consciousness state potentially followed by explicit or implicit memories (Bonhomme et al., 2019; Sanders et al., 2012). Additionally to these, it has been described that higher-order brain functions and a disembodied self-awareness can be retained until high concentrations of the anesthetic drug (Sleigh et al., 2018). Furthermore, depending on the anesthetic agent of choice, experiences might drastically vary, specially by using dissociative anesthetics like ketamine, where subjects report hallucinations and vivid dreams (Mueller et al., 2018; Tucker et al., 1984). These complex alterations emerge as a function of the equilibrium between the pharmacodynamic properties of anesthetic agents and their concentration in the body (Bonhomme et al., 2019).
These premises immediately suggest that unresponsiveness does not strictly implicate being unconscious (Sanders et al., 2012), however, due to the complexity and the high inter-subject variability of experiences, the term anesthesia induced-unconsciousness has been classically used interchangeably with anesthesia-induced unresponsiveness throughout the published literature, as well as in this thesis.

The underlying mechanisms by which different anesthetic agents modulate consciousness remain unclear. The leading question to this problem relates to the primacy of bottom-up vs. top-down mechanisms of anesthesia-induced unconsciousness (Mashour, 2014). As posed in classic literature, the term 'bottom-up' relates to the effect of anesthesia on midbrain arousal pathways and diencephalic structures, such as thalamus and subcortical nuclei. These structures project to the

cortex and modulate wake-like behavior through the actions of distinct neurotransmitters such as dopamine or acetylcholine, i.e., *modulation of* the *arousal hierarchy* (Mashour, 2014). A further meaning of 'bottom-up' relates to the disruption of processes that occur from smaller to larger structural scales, e.g., from molecular, to the cellular, to the neuroanatomical, to the network level in the brain, i.e., *modulation of structural hierarchy* (Mashour, 2014) . On the other hand, 'top-down' or 'network level' mechanisms refer to primarily cortical changes induced by anesthesia incompatible with conscious processes (Dehaene & Changeux, 2011; Koch et al., 2016; Tononi, 2012), which can on the one hand reflect the effect on subcortical areas, or on the other hand either *precede* subcortical changes or be totally independent from them (Mashour, 2014). However, currently it is been discussed whether the disruption at the network level, might not be simply a signature of lower-order anesthetic actions but rather reflect a subcortical modulation of cortical dynamics (Mashour, 2014).

The aim of this thesis is to investigate characteristic cortical neural correlates of anesthesia-induced unconsciousness in humans, with a focus on subcortical influences measured by BOLD fMRI.

1.2. Neural correlates of anesthesia-induced unconsciousness

1.2.1. Micro-level: Anesthetic agent's molecular mechanisms

There are 5 main classes of anesthetic agents: intravenous (IV) anesthetics (e.g., etomidate, ketamine, propofol, thiopental), inhalational anesthetics (e.g., halothane, desflurane, enflurane, isoflurane, sevoflurane, etc.), IV sedatives (e.g., benzodiazepines), synthetic opioids (e.g., fentanyl and derivatives), and neuromuscular blocking drugs used to facilitate endotracheal intubation (e.g., succinylcholine, rocuronium, vecuronium, etc.). In the clinical setting, general anesthesia is most commonly achieved via induction with IV agents and analgesics followed by maintenance with volatic anesthetics (Smith et al., 2022). All general anesthetics -by definition- are administered to reach the end point of loss of consciousness, yet it is remarkable that such a structurally diverse group of drugs, ranging from simple inert gases, like halogenated ethers, to complex barbiturates and steroids, produce the same effect (Franks, 2008); from these, propofol and sevoflurane are the most used anesthetic agents (Brown et al., 2018).

At the molecular level, most of the anesthetic agents modulate neural activity through two main actions: depression of fast excitatory and enhancement of fast inhibitory synaptic transmission (Hao

et al., 2020; Hemmings, 2009; Hemmings et al., 2005). This can lead to the silencing of normal synaptic transmission and result in decreased excitation of the postsynaptic neurons. Alternatively, their effect might result from direct action on the process of exocytosis, either by inhibiting calcium entry into the presynaptic bouton or by direct action on the exocytotic machinery (Hao et al., 2020).

Propofol and sevoflurane target gamma-amino butyric acid type A ($GABA_A$) presynaptic receptors, the main inhibitory receptors in the brain expressed in around one-third of all synapses (Bloom & Iversen, 1971; Uhrig et al., 2014). This binding causes a receptor's conformational change, which induces the opening of postsynaptic chloride channels, enhances the inward chloride current and augments $GABA_A$-receptor-mediated inhibition of postsynaptic neuronal excitability (Brown et al., 2011; Campagna et al., 2003; Jones & Harrison, 1993; Peduto et al., 1991; Uhrig et al., 2014). Because a small numbers of inhibitory interneurons (20-30% of neocortical neurons) control large numbers of excitatory pyramidal neurons (70-80% of cortical neurons) (DeFelipe & Farinas, 1992; Markram et al., 2004), the hypnotic-induced enhancement of $GABA_A$ inhibition can efficiently inactivate large brain regions. This translates into a breakdown of the tight balance between neuronal inhibition and excitation characteristic of the awake state (Brown et al., 2011). Subcortical regions such as thalamus, striatum, as well as respiratory and arousal centers in the brainstem are similarly affected by these agents (Brown et al., 2018; Feldman et al., 2003; Franks, 2008).

Besides $GABA_A$ receptors, further ion channels are sensitive to clinically effective concentrations of sevoflurane, including 2-pore potassium channels, nicotinic acetylcholine, serotonin type 3, glycine and glutamate receptors (both, N-methyl-D-aspartate (NMDA) and alpha-amino-3-hydroxy-5-methyl-4-isoxazolepropionic acid (AMPA) receptors) (Brown et al., 2018; Campagna et al., 2003; Hemmings, 2009). The effect of these anesthetics on direct neurotransmitter release in the central nervous system has also been reported; dopamine and acetylcholine (ACh) are of main interest due to their association with the waking condition.

Regarding dopamine-reported changes with volatile anesthetics, halothane and isoflurane modulate presynaptic dopamine striatal release in a biphasic way: enhancing the spontaneous release of dopamine while inhibiting the NMDA-evoked release via $GABA_A$-receptor enhancement and depression of presynaptic NMDA receptor responses relative to the concentration of the anesthetic (Keita et al., 1999). In other studies, the presence of sevoflurane resulted in an increased dopamine release in rat brain cortical slices (Silva et al., 2007), while halothane (in clinical concentration) and isoflurane (in concentrations above clinical) reversibly inhibit dopamine transporters linked to a

reduced dopamine uptake by synaptosomes (el-Maghrabi & Eckenhoff, 1993). On the contrary, a study using an animal *in vitro* model of cerebral ischemia showed that sevoflurane slowed ischemia-induced dopamine release from striatal terminals (Toner et al., 2001). Finally, a recent study using c-FOs staining, calcium fiber photometry recording, optogenetics, chemo genetics, and fluorescent sensors, combined with behavioral tests and EEG analysis, showed that fluoresce signals of dopamine decreased in the induction of and increased in the emergence from sevoflurane anesthesia (Gui et al., 2021). Regarding effects of propofol, it has been reported that its presence increases dopamine metabolites in the somatosensory cortex (Shyr et al., 1997) but inhibited dopamine release in the rat nucleus accumbens (Schulte et al., 2000) and in medial prefrontal cortex (mPFC) (Wang et al., 2016). Such findings suggest that these anesthetics alter the normal physiology of dopaminergic neurotransmission in the brain, however, overall results are not conclusive.

ACh-related changes reports seem more consistent, for instance, animal experiments have reported a decrease of ACh basal release from the cortex and subcortex with administration of propofol (Gamou et al., 2010; Kikuchi et al., 1998; Nemoto et al., 2013) as well as with sevoflurane (Shichino et al., 1998; Shichino et al., 1997)

1.2.2. Macro-level: Large-scale network disruption

1.2.2.1 Ways to characterize large-scale network interactions in humans. Focus: functional connectivity of BOLD fMRI signal fluctuations

Beyond the activity of single neurons and mesoscopic systems, in which single brain circuits and brain areas are postulated to act as independent processors for specific functions (Mashour & Hudetz, 2018), this work will mainly focus on the collective function of brain areas working together as large-scale brain networks (Bressler & Menon, 2010).

The term *network* suggests the relation or interconnection that bring elements of a system together (Bassett & Sporns, 2017), and *large-scale* refers to neural systems that are distributed across the whole brain (Bassett & Sporns, 2017). To map the architecture of large-scale brain networks, signals recorded from different non-invasive neuroimaging methods can be used, such as: functional magnetic resonance imagining (fMRI), PET or neurophysiologic measures like EEG (Mashour & Hudetz, 2018). Connectivity between elements can be characterized as follows: *(i)* structural connectivity, i.e., definition of physical connections between brain regions and study mainly with tractography, a

measure providing a skeleton of connected brain areas which facilitates signaling along preferred pathways in the service of specific cognitive functions (Bassett & Sporns, 2017) ; *(ii)* (non-directed) functional connectivity, i.e., estimation of brain communication derived from statistical relations between recorded signals, using for example paired-wise Pearson's correlations coefficients; *(iii)* directed functional connectivity, i.e., estimation of intensity and direction of connections between brain regions, with for example, granger causality analyses, transfer entropy; and *(iv)* effective connectivity, i.e., analysis of directed causal links among network elements using a model-based approach, with for example, dynamic causal modeling (Bassett & Sporns, 2017). From these, functional connectivity is one of the most used methods to map large-scale intrinsic networks, which refers to the quantification of coherent activity between continuous fluctuations of the so-called blood oxygenation level dependent (BOLD) fMRI signal across areas in the brain. Interestingly, recent fMRI studies have demonstrated that large-scale synchronicity of BOLD fluctuations across brain areas can also be studied by analyzing the continuous BOLD signal as *discrete events*, by for example using the so-called *point process analysis* where positive peaks trespassing a certain threshold are defined as events within a time window (Hahn et al., 2021; Tagliazucchi et al., 2012; Zhang et al., 2020); this is followed by the calculation of synchronicity measures (*see section 1.2.2.3*).

The fMRI BOLD neuroimaging technique is a noninvasive method that depicts local changes of blood oxygenation along time in the brain. The signal readout is based on *(i)* the physical principles of nuclear magnetic resonance of hydrogen protons of water molecules present in the tissue and *(ii)* the regional fluctuation of deoxygenated/oxygenated blood in a specific brain region. This is usually recorded under the following MRI conditions: T2*-weighted imaging, gradient-echo echo-planar imaging, EPI, sequences (Buxton, 2013; Heeger & Ress, 2002; Ogawa et al., 1990). In more detail, in the presence of a strong magnetic field (e.g., produced in a 3.0 Tesla MRI scanner), the spins (or the magnetic properties of hydrogen protons) align to the external magnetic field (i.e., known as longitudinal magnetization), then, energy is applied as a radio-frequency excitation pulse (RF) changing the plane of magnetization from longitudinal to a transverse plane. When the RF pulse is switched off, the MRI scanner detect the energy emitted by the protons while returning to their initial state, a process called transverse relaxation. The presence of inhomogeneities in the magnetic field contributes to a faster transverse relaxation or signal decay rate, known as T2* (Buxton, 2013; Heeger & Ress, 2002; Ogawa et al., 1990). Signal decay is a dephasing process which results from random field fluctuations originated from the interaction of molecules with different magnetic properties; this leads to a random walk of their phases and results in the partial cancellation of the net signal (Buxton, 2013). In venous blood, the increase in deoxyhemoglobin concentration, a paramagnetic molecule, creates

local distortions in the magnetic field and consequently decreases the intensity in the image. On the contrary, the increase in oxyhemoglobin concentration, a weak diamagnetic particle, results in a local increase in the MR signal (Buxton, 2013; Heeger & Ress, 2002; Ogawa et al., 1990). Sampling rates of approx. 1-3 seconds are necessary to record T2* signal fluctuations in voxels (i.e., a 3-dimensional pixel, ~mm^3) of the whole-brain. This is interpreted as BOLD changes along time (Schulz et al., 2022).

The physiological underpinnings of BOLD signal fluctuations are still under investigation. The current understanding relies on the association between local neural activity and changes in blood oxygenation concentration via neurovascular coupling (NVC). NVC explains that an increase in local neural activity results in an increase of deoxyhemoglobin concentration elicited by local hyperemia (i.e., increase local blood inflow thus volume) to meet local oxygen tissue requirements (Buxton, 2013; Heeger & Ress, 2002; Ogawa et al., 1990). The temporal dynamics of this process follow the mathematical model of the NVC called the hemodynamic response function (HRF) (Boynton et al., 1996; Taylor et al., 2022): after a 2-s stimulus, the BOLD response begins ~2 s later, rises to a plateau 6-9 s after stimulus onset, and returns to baseline (Logothetis & Wandell, 2004).

Although this imaging modality suffers from methodological limitations, including biological and temporal ones, experiments in primates have showed that BOLD responses strongly correlate with neuronal-derived signals, such as local field potentials (LFP), which is an electrophysiological signal reflecting mostly the input and local processing of neuronal information (Logothetis et al., 2001; Logothetis & Wandell, 2004). Diverse experiments studying neuronal activity and concurrent hemo- and vasodynamic measurements have supported this association and have further validated its use for neuroimaging studies (Du et al., 2014; Goense et al., 2012; Goense & Logothetis, 2008; Schwalm et al., 2017; Shmuel & Leopold, 2008).

1.2.2.2. Large-scale mainly cortical intrinsic networks. Focus: default-mode network disruption

Imaging the brain during resting state, i.e., awake state in the absence of an explicit task performance or stimulation, revealed that the fMRI BOLD signal fluctuates spontaneously at slow frequencies between ∼0.01 to 0.15Hz, and that these are temporally correlated across specific brain areas or regions. This coherent ongoing activity is called 'intrinsic functional connectivity' (iFC) and is organized in specialized groups of regions that relate to specific aspects of cognition and behavior, these are known as 'resting-state networks' (RSNs) (Biswal et al., 1995; Biswal et al., 2010; Fox & Raichle, 2007).

Besides measurements during wakeful resting states, functional networks also show synchronous fluctuations during task paradigms (Fox et al., 2005) and persist – at least partially- independently of level of consciousness, e.g., during sleep (Fukunaga et al., 2006; Horovitz et al., 2008), with anesthesia (Boveroux et al., 2010; Greicius et al., 2008; Kafashan et al., 2016; Martuzzi et al., 2010; Vincent et al., 2007) and in disorders of consciousness such as vegetative state (but not in severe coma states or brain dead patients) (Boly et al., 2009; Threlkeld et al., 2018). This suggests that these specific correlated patterns reflect intrinsic processes and not merely structural connections (Mitra et al., 2018; Van Dijk et al., 2010). Furthermore, stage of sleep (Horovitz et al., 2009) and level of sedation (Peltier et al., 2005; Ranft et al., 2016; Wang et al., 2021) modulate intrinsic activity correlations, suggesting that the state of consciousness affects functional connectivity (Van Dijk et al., 2010).

Among all RSNs, the so-called default mode network (DMN) is the network associated with internally-focused tasks and engaged during self-referential processes, therefore the most studied in association with consciousness. This network encompasses two midline regions, *(i)* the precuneus and posterior cingulate cortex (PCC), and *(ii)* the ventral anterior cingulate cortex and parietal cortices (Buckner et al., 2008; Greicius et al., 2003; Raichle, 2015; Raichle et al., 2001). Disruption of the within-DMN iFC, more specifically reduced iFC, has been evidenced during slow wave sleep (Horovitz et al., 2009; Samann et al., 2011; Tagliazucchi et al., 2013), disorders of consciousness (Boly et al., 2009; Cauda et al., 2009; Norton et al., 2012; Vanhaudenhuyse et al., 2010), and anesthesia-induced unconsciousness with sevoflurane, propofol and ketamine (Boveroux et al., 2010; Golkowski et al., 2019; Greicius et al., 2008; Huang et al., 2014; Jordan et al., 2013; Martuzzi et al., 2010; Palanca et al., 2015; Ranft et al., 2016; Schrouff et al., 2011). However, further reports have also shown the presence of increased iFC, specifically of the PCC with areas outside of the DMN during light sedation with propofol (Stamatakis et al., 2010), with 0.5% concentration of sevoflurane (Martuzzi et al., 2010) and with midazolam (Greicius et al., 2008).

The specific processes explaining the disruption of intrinsic functional correlations within the DMN during anesthesia-induced unconsciousness are not known, two possible candidate 'bottom-up' mechanisms have been suggested: the breakdown of thalamocortical circuits and the disruption of neuromodulatory input from ascending neurotransmitter systems.

1.2.2.3. Large-scale BOLD synchronizations. Focus: alteration of cortical dynamics

Static functional connectivity studies mentioned above provide important information about the anatomical location of the effect of anesthesia, i.e., DMN regions, however the dynamics of these effects are missing. For instance, it is not clear how the administration of anesthesia interrupts the coherent functional interactions between DMN cortical regions typically seen during the awake state (Alkire et al., 2008). One could attribute this to the direct effect of anesthesia '*shutting-off*' the brain, however It has been hypothesized that the complex effects of anesthesia on the brain, thereby consciousness itself, involves a constant '*shaping and reshaping of an irreducible dynamic core*' (Cavanna et al., 2018; Tononi & Edelman, 1998). This means that loss of consciousness does not strictly imply an inactivation of neuronal activity, but consequent dynamic changes incompatible with the ability of the brain to sustain synchronous long-range interactions present during a wakeful/conscious state (Alkire et al., 2008; Barttfeld et al., 2015; Demertzi et al., 2019). For example, classic electrophysiological experiments in rodents studying cortical integration of sensory information during anesthesia showed that visual evoked responses in the occipital cortex after a light stimulus is preserved during anesthesia, however the later response in the association parietal cortex seen in the same experiment during wakefulness as well as its information exchange measure was attenuated (Imas et al., 2005). In humans, fMRI studies have shown a reconfiguration of cortical dynamics with propofol and sevoflurane-induced anesthesia, respectively, for instance findings with propofol revealed an increased cortico-cortical modularity pattern (Monti et al., 2013) as well as a decreased temporal dynamic repertoire within RSNs, including DMN (Golkowski et al., 2019; Hudetz et al., 2015). Similar results were found in monkeys (Barttfeld et al., 2015) and with sevoflurane (Golkowski et al., 2019). This evidence suggests that during anesthetized-induced states the flexibility of the brain to switch between configurations is impaired, carrying with it a reduction in large-scale synchronized activity necessary for information integration and processing characteristic of a conscious wakeful state (Cavanna et al., 2018).

This idea was supported by a recent fMRI study studying brain-wide large-scale synchronizations of infra-slow activity fluctuations during states with altered consciousness, such as non-rapid eye movement (non-REM) sleep in humans and propofol-induced sedation in monkeys (Hahn et al., 2021). They showed that these states were characterized by reduced transient large-scale BOLD synchronizations and introduced the study of synchronicity of the BOLD signal as discrete events across brain regions using the Fano Factor (FF) (i.e., variance of counts over the mean of counts) in specific time windows, a proxy of dynamic connectivity (Hahn et al., 2021). The probability of finding large-scale BOLD synchronicities (FF >>1) was reduced during unconscious states, instead local

synchronizations between few areas was the dominating pattern. Using a whole-brain computational model, the authors further showed that the fluctuations between synchronized and desynchronized states is a property of the awake state and the transition to states of unconsciousness are linked to a decrease in global excitability and large-scale functional connectivity (Hahn et al., 2021). Studies assessing BOLD transient large-scale synchronicity with the FF across specifically DMN regions, are still missing.

The specific neurophysiologic mechanism underlying the orchestration of the loss or recovery of excitability fluctuations are still unclear, neuromodulatory influences might participate in the process.

1.2.2.4. Thalamus-cortex interactions

It has been suggested that thalamocortical interactions are a fundamental part of the neural substrate of consciousness and its disruption/interruption a candidate mechanism underlying unconsciousness including anesthesia-induced unconsciousness (Alkire et al., 2000; Nakajima & Halassa, 2017; Poulet et al., 2012; Tononi & Koch, 2008).

Physiologically, the thalamus interacts with the cortex by relaying ascending and descending information to and from the cortex through layer-specific thalamo-cortical and cortico-thalamic pathways (Aru et al., 2019; Redinbaugh et al., 2020; Van Horn & Sherman, 2004). Current evidence suggests that this is not a passive process but an actively regulated one which modulates neural processing in the cortex according to behavioral context (O'Connor et al., 2002; Saalmann & Kastner, 2015; Saalmann et al., 2012) and conscious state (Redinbaugh et al., 2020; Schiff, 2008). Furthermore, specific regions in the thalamus have been associated with contributing to arousal regulation in rodents, e.g., injections of $GABA_A$ agonists in the midline thalamic region led to depression of arousal and decreased spontaneous movement (Miller & Ferrendelli, 1990; Miller et al., 1989), intra-thalamic micro infusion of nicotine (Alkire et al., 2007) or voltage-gated Kv1 potassium channel blockers in the central medial thalamus caused arousal behavior despite continuous administration of inhaled anesthetics (Alkire et al., 2009; Lioudyno et al., 2013), and optogenetic tonic activation of thalamic reticular nucleus decreased arousal (Lewis et al., 2015). In non-human primates, electric stimulation of the central thalamus, including mediodorsal nucleus intralaminar nuclei, evoked arousal behavior and neurophysiological signs of cortical arousal during propofol-induced unconsciousness (Bastos et al., 2021). In humans, focal injuries within the central thalamus generated disturbances of consciousness, including hypersomnia, coma and akinetic mutism (Castaigne et al., 1981; Schiff, 2008;

Schiff & Plum, 2000). Finally, it has been proposed that the mediodorsal thalamus coordinate communication across higher order cortical regions (including regions part of the DMN) (Pergola et al., 2018).

Regarding anesthesia-related effects, electrophysiological experiments have demonstrated that anesthetic agents compromise natural firing patterns of thalamic network neurons via hyperpolarization, therefore, reducing its membrane excitability (Angel, 1991; Ries & Puil, 1999; Steriade, 2001). It is hypothesized that this prevents normal synaptic transmission of sensory information relayed to the cortex and/or the engagement of thalamic neurons in intra-thalamic oscillations characteristic of wakefulness, in other words: thalamus is 'functionally disconnected' from the cortex (Alkire et al., 2000).

In the neuroimaging field, regional reduction of functional cerebral metabolism and blood flow during anesthesia-induced unconsciousness in subcortical areas, including the thalamus, have been described with halothane, isoflurane (Alkire et al., 2000; Alkire et al., 1999; White & Alkire, 2003), sevoflurane and propofol (Fiset et al., 1999; Kaisti et al., 2003; Kaisti et al., 2002). Results from resting-state fMRI studies have shown that during sevoflurane- and propofol-induced unconsciousness thalamic functional connectivity with cortical regions, including those within the DMN are reduced (Boveroux et al., 2010; Gili et al., 2013; Guldenmund et al., 2013; Nir et al., 2022; Palanca et al., 2015; Ranft et al., 2016; Schroter et al., 2012; Stamatakis et al., 2010), however an increased connectivity to primary motor, somatosensory areas, and insula have also been reported (Guldenmund et al., 2013; Martuzzi et al., 2010). Finally, a recent simultaneous EEG-fMRI study in anesthetized primates demonstrated that central thalamic deep brain stimulation restored wake-like behavior and restores thalamocortical and corticocortical static connectivity patterns as well as cortical dynamic connectivity despite a continuous administration of propofol (Tasserie et al., 2022),

Interestingly, central thalamic nuclei, specially the mediodorsal nuclei, receive strong input from neuromodulatory systems also associated with modulation of arousal and common targets of anesthetic agents, such as the dopaminergic system in the brainstem (Garcia-Cabezas et al., 2009; Garcia-Cabezas et al., 2007; Sanchez-Gonzalez et al., 2005), and the cholinergic system originating from both the brainstem and basal forebrain (Heckers et al., 1992; Kolmac & Mitrofanis, 1999; Parent et al., 1988; Steriade et al., 1988). This evidence suggests that first, the thalamus allows cortical arousal acting as a relay for corticocortical information processing, and second, that this might be indirectly orchestrated by neuromodulatory systems.

1.2.2.5. Brainstem-cortex interactions

The ascending reticular activating system (ARAS) is a complex network of highly specialized neurons organized in the brainstem and rostral pons as interdependent nuclei. Each nucleus has distinct anatomic and physiological features and project to the cortex directly (Edlow et al., 2012; Parvizi & Damasio, 2001; Starzl et al., 1951) or indirectly through the thalamus, via the intralaminar thalamic and further nuclei (Parvizi & Damasio, 2001; Steriade & Glenn, 1982; Van der Werf et al., 2002), and/or basal forebrain (Jones, 2004; Jones & Yang, 1985; Parvizi & Damasio, 2001). These pathways are neurotransmitter specific including serotoninergic fibers from the dorsal raphe (DR) and medial raphe (MR) nuclei, noradrenergic fibers from the locus coeruleus (LC), dopaminergic fibers from the ventral tegmental area (VTA), cholinergic fibers from the pedunculopontine nucleus (PPN) and laterodorsal tegmental nucleus, and glutamatergic fibers from the parabrachial complex (PBC) (Edlow et al., 2012; McCormick, 1992).

The conception that the ARAS plays a role in modulation of cortical activity, hence consciousness, can be traced back to the early 20th century with two main experiments (Parvizi & Damasio, 2003). In the first one, Bremer demonstrated that the transection of the brainstem of anesthetized cats at different levels produced different electrophysiological and behavioral outcomes. For instance, a section of the midbrain at the ponto-mesencephalic level (near the exit of the oculomotor nerve) produced a condition like coma, i.e., electroencephalographic characteristics of sleep plus unresponsiveness despite intense stimulation, whereas a section at a lower level, specifically at the spinomedullary junction, did not (Bremer, 1935). In the second experiment, Moruzzi and Magoun showed that an electrical stimulation of the reticular system in the brainstem resulted in high frequency/low amplitude EEG (electrophysiological correlate of wakefulness), whereas a high-level transection of the midbrain resulted in low frequency/high amplitude EEG and, similar as in the first experiment, continuous unresponsiveness despite stimulation (Moruzzi & Magoun, 1949). A subsequent experiment in cats causing lesions in cell bodies located in the mesencephalic reticular formation (including dopaminergic cells) did not result in alterations of cortical activation nor arousal (Denoyer et al., 1991). Nevertheless, more recent studies confirmed that lesions in the brainstem, including rostral pons, and/or its axonal projections, could generate a comatose state and related consciousness alterations in both animals (Fuller et al., 2011; Smith et al., 2000) and humans (Edlow et al., 2013; Parvizi & Damasio, 2003; Posner, 1978; Rosenblum, 2015; Snider et al., 2019). Currently, damage of

this circuitry represents an anatomical correlate for the diagnosis of disorders of consciousness, such as coma, persistent vegetative state, among others.

Resting-state fMRI studies have further demonstrated a close interaction between brainstem and cortex. For instance, seed-based functional connectivity analyses have evidenced correlated spontaneous BOLD fluctuations between ARAS nuclei and cortical regions (Bar et al., 2016; Zhang et al., 2016), including DMN regions particularly with the VTA (Bar et al., 2016; Murty et al., 2014; Nakamura et al., 2018; Peterson et al., 2017; Zhang et al., 2016). Critically, these intrinsic correlations are affected in psychiatric disorders, where the brainstem systems are disturbed, such as schizophrenia (Giordano et al., 2018; Gradin et al., 2013; Hadley et al., 2014; Xu et al., 2019), major depression or bipolar disorder (Nakamura et al., 2020; Wagner et al., 2017). As well as during anesthesia-induced unconsciousness (Nir et al., 2019; Nir et al., 2022; Spindler et al., 2021).

This evidence demonstrate that brainstem-cortical interaction might participate in the maintenance of consciousness (Parvizi & Damasio, 2001; Posner, 1978); however which specific nuclei in the brainstem are involved in the maintenance/emergence of consciousness in humans, and whether each of them contributes equally to this process is still unclear.

1.3. Anesthesia-induced unconsciousness in extreme brain states: burst suppression state

Burst suppression (BS) is an electroencephalographic pattern characterized by the alternation of periods of isoelectricity or flat line EEG (i.e., suppression) with high voltage activity (i.e., bursts) (Swank & Watson, 1949). This state occurs under pathologic conditions characterized by deeply depressed brain metabolic activity associated with profound unresponsiveness and unarousability. For instance, BS might arise spontaneously in anoxic brain injury, where it is a predictor of poor neurologic prognosis (Cloostermans et al., 2012; Rossetti et al., 2012), or can be reversibly induced for medical purposes with high doses of most general anesthetics (i.e., particularly those acting primarily by enhancing $GABA_A$ receptors, such as halogenated ethers or propofol) (Brown et al., 2010; Hartikainen et al., 1995; Niu et al., 2014; Purdon et al., 2015) and hypothermia (Stecker et al., 2001; Westover et al., 2015). Overdoses of further medication drugs and substances can induce BS, such as alcohol (Whishaw, 1976), baclofen (Ostermann et al., 2000) and carbamazepine (De Rubeis & Young, 2001). Pediatric patients with early infantile epileptic encephalopathy, i.e., Ohtahara syndrome, early

myoclonic encephalopathy, and Aicardi syndrome, also show BS pattern (Fariello et al., 1977; Ohtahara et al., 1987; Saneto & Sotero de Menezes, 2007). Is important to mention that BS is not present during sleep (Brown et al., 2010), suggesting that this state is an extreme brain state.

Regarding the morphology of the BS pattern: *(i)* it has been conventionally characterized as a global brain state where bursts can be detected simultaneously in all electrodes during EEG recordings, however asymmetry and asynchrony of the BS pattern has been reported in patients with structural lesions in the corpus callosum (Lambrakis et al., 1999) as well as in epilepsy patients (Lewis et al., 2013; Shanker et al., 2021) and animal models for epilepsy (Liou et al., 2019), as well as in rats (Ming et al., 2020), it is not clear whether asynchrony happens in healthy conditions; *(ii)* its spectral structure varies with the underlying condition and the anesthetic agent used, for instance it has been observed that bursts periods resembles the frequency spectrum that of the EEG period before the onset of BS (Lewis et al., 2013; Purdon et al., 2015; Shanker et al., 2021), also drug-specific features has been described in rodents (Akrawi et al., 1996; Kenny et al., 2014) and humans (Fleischmann et al., 2018); *(iii)* alternation of burst and suppression has a quasi-periodic nature, for instance inter- and intra-burst duration has a high variation (Ching et al., 2012; Shanker et al., 2021); *(iv)* this alternation happens in a slower timescale than other neural activity associated with an inactivated brain, such as sleep or simply lesser deep levels of anesthesia (Brown et al., 2010; Ching et al., 2012); and *(v)* there is a parametric sensitivity of suppression to the level of brain depression, e.g., with anesthesia, the deeper the anesthesia level, the longer the time spent in suppression with respect to the time in bursting activity, i.e., longer suppressions and shorter bursts (Brown et al., 2010; Hartikainen et al., 1995).

There are still no specific unifying mechanism explaining the generation and maintenance of BS, however there are two proposed hypotheses. The first one, the cortical hypersensitivity hypothesis, focus on the effect of cellular mechanisms of anesthetic agents on cortical neurons and a consequent disruption of the excitatory-inhibitory balance being shifted towards excitation (Ferron et al., 2009; Kroeger & Amzica, 2007). According to this theory, massive bursting activity causes an increased calcium influx into cells, thus a depletion of available extracellular calcium, which results in cortical silence reflected as a flat EEG and a general disconnection of neuronal networks (Ferron et al., 2009). During suppression phases, levels of interstitial calcium are restored, which enables any external or intrinsic signal to trigger a new burst in a hyper-excitable cortex (Ferron et al., 2009). A second mechanistic explanation based on a bio-physical computation model, the metabolic hypothesis, suggests that BS emerges to ensure basic cell function during states of lowered metabolism, such as general anesthesia, hypothermia, or brain injury. It suggests that a strong depressor causes an

imbalance between ATP consumption and production. This results in the opening of ATP-gated potassium channels hyperpolarizing neurons (suppression emergence) until enough ATP becomes available again to sustain a basic neuronal circuit (burst emergence). Bursting activity will deplete ATP reserves generated during suppression, hence perpetuating the cycle (Ching et al., 2012).

Regarding neuronal correlates for BS state, in vivo intracellular recordings in animals have demonstrated that during BS, bilateral cortical areas as well as brainstem showed periods of alternating bursts and suppression while the thalamus displayed slow wave activity (1-4Hz) or only increased firing rates during the periods of suppression in the cortex and brainstem. During burst periods, thalamic neurons showed an increased background noise accompanied by a decreased rhythmicity in their burst firing activity plus random single spikes, thalamic activity ceased with suppression periods longer than 30 seconds. Interestingly, post-synaptic stimulation in thalamocortical or corticothalamic pathways recovered normal cellular activity and a wake-like EEG (Steriade et al., 1994). This suggests that during BS there is a virtual disconnection in cortico-thalamic circuits and anesthetic-induced bursts are generated intrinsically by the cortex independently from thalamic input (Detsch et al., 2002; Steriade et al., 1994). This idea has been supported by experiments demonstrating that BS-like state can emerge spontaneously in isolated neocortical brain slices with continuous barbituric (Lukatch & MacIver, 1996) or general anesthetics (Lukatch et al., 2005) administration. However, other experiments support the notion that the thalamus is a key player in the generation and synchronization of the bursts during BS, e.g., *(i)* using somatosensory (Yli-Hankala et al., 1993), visual (Hartikainen et al., 1995; Hudetz & Imas, 2007; Kroeger & Amzica, 2007), or auditory (Hartikainen et al., 1995; Kroeger & Amzica, 2007) stimulation it is possible to evoke single bursts during BS via (presumably) thalamocortical afferents, which morphologically are analogous to spontaneously-generated bursts (Hudetz & Imas, 2007); *(ii)* selective thalamus inactivation experiments in focal-epilepsy rodent models during anesthesia-induced BS have demonstrated that bursts are triggered from the thalamus rather than from the cortex itself, however in controls, bursts originated from either the cortex or thalamus (Liou et al., 2019); and *(iii)* that thalamic activity modulates cortical burst onsets (Ming et al., 2020).

On the macroscopic scale, neuroimaging findings confirmed the cortico-subcortical deafferentation during suppression periods, however during bursting segments, subcortical areas (beyond the thalamus) might play an important role. For instance, a PET study of a pediatric patient with early myoclonic encephalopathy demonstrated hypoperfusion and hypometabolism of basal ganglia and thalamus and parietooccipital cortices, whereas an interictal single photon emission computed

tomography (SPECT) showed a hyper perfusion of the basal ganglia, thalamus, brainstem and frontoparietal cortices (Hirose et al., 2010). A further study applying source localization algorithms and connectivity measures in EEG of 13 neonates and infants with BS patterns showed that during bursting periods there is coherent activity between thalamus and brainstem as well as frontal and parietal cortices and that there is an upwards informational flow from the brainstem to the thalamus, and from the thalamus to the cortex. These was absent during suppression periods (Japaridze et al., 2015).

There is still no consensus whether BS is generated intrinsically in the cortex or is it modulated by subcortical sources. However, besides the thalamus, subcortical structures such as brainstem might play an important role in generation of bursts during BS. The ARAS complex has been proposed as an extra thalamic route gating spontaneous as well as stimulus-induced bursting activity in an inactivated cortex (Hudetz & Imas, 2007). This was demonstrated in rats, where micro stimulation of the reticular formation during isoflurane-induced BS caused decreased the length of the periods of suppression (Orth et al., 2006).

1.4. Anesthesia-induced unconsciousness and arousal: neuromodulatory brainstem influences – candidates

1.4.1. Dopaminergic system, ventral tegmental area, and modulation of arousal and wakefulness

The dopaminergic system consists of broadcasting network of dopaminergic neurons originating almost exclusively in the brainstem and organized as nuclei, particularly in the midline and rostral portion of the mesencephalon (Bjorklund & Dunnett, 2007; Dahlstroem & Fuxe, 1964). Dopamine is the predominant catecholamine neurotransmitter in the mammalian brain, it acts through two main receptor populations: D1-like receptors including subtypes D1 and D5, and D2-like receptor including subtypes D2, D3 and D4, which activate or inhibit cAMP/protein kinase A signaling respectively (Kebabian et al., 1984; Kebabian & Calne, 1979; Missale et al., 1998). Substantia nigra pars compacta and VTA are the two main dopaminergic nuclei. From these, the VTA send projections to key arousal-promoting brain regions, including thalamus (Garcia-Cabezas et al., 2009; Garcia-Cabezas et al., 2007; Sanchez-Gonzalez et al., 2005), DR, LC, pedunculopontine and laterodorsal tegmental areas, basal

forebrain, and lateral hypothalamus (Monti & Monti, 2007), but also to cortical regions related to cognition such as prefrontal cortex, anterior and posterior cingulate cortices (Edlow, 2021; Haber & Fudge, 1997; Morales & Margolis, 2017; Yetnikoff et al., 2014). Also, electrolytic lesions in the mesencephalon performed in cats demonstrated that lesions of catecholamine-containing neurons located in the VTA and substantia nigra were correlated with a decrease in the rostral brain and that dopaminergic neurons of the ventral tegmentum were essential for the maintenance of behavioral arousal (Jones & Beaudet, 1987). The existence of these projections suggests that DA neurons in these nuclei might be intimately involved in maintaining behavioral arousal.

For several decades, the dopaminergic system has been described to be implicated in the modulation of behavior and cognition, and especially in the pathophysiology of neurological (e.g., Parkinson's disease) and neuropsychiatric disorders (e.g., Addiction and Schizophrenia).
More recently, a grown interest has emerged for the dopaminergic system in context of anesthesia and consciousness based on animal experiments testing its relevance in the process of emergence from anesthesia-induced unconsciousness. For instance, methylphenidate and dextroamphetamine, both inhibitors of reuptake for dopamine and norepinephrine, but not atomoxetine, a selective reuptake inhibitor for norepinephrine, restore wake-like behaviors in rodents during continuous isoflurane-, propofol- and sevoflurane-induced anesthesia (Chemali et al., 2012; Kenny et al., 2015; Solt et al., 2011).

Further studies demonstrated that the possible source of arousal-promoting dopamine is primarily the VTA, rather than the substantia nigra. For example, the electrical stimulation of the VTA but not the substantia nigra restored the righting reflex in rats and activated the EEG during continuous sub-clinical concentrations of isoflurane- or propofol-induced anesthesia (Solt et al., 2014). It is important to mention that pain is an important confound in this study, and its discussion is usually neglected.
A subsequent study found that a selective optogenetic stimulation of dopaminergic VTA neurons restores wake-like behaviors in mice anesthetized with isoflurane (Taylor et al., 2016). Additionally, the recovery time after propofol-induced anesthesia in rats increased, however it did not alter the response with isoflurane anesthesia (Zhou et al., 2015). One last study using chemo genetic activation of dopamine neurons in the VTA, but not in the substantia nigra, induced wake-like behavior in rodents, this was completely abolished by pretreatment with dopamine D2/D3 receptor antagonist, but not with antagonists for D1 receptors (Oishi et al., 2017).

Regarding neuroimaging studies, one recent fMRI study in healthy volunteers during propofol sedation and patients with chronic disorders of consciousness studies have demonstrated a reduction of the VTA iFC with specifically the precuneus/posterior cingulate cortex (PCC) relative to wakefulness. Interestingly, this connectivity recovered in patients who behaviorally improved in a follow-up assessment. Furthermore, using a third cohort of patients with traumatic brain injury without disorder of consciousness, the administration of methylphenidate, a dopaminergic and noradrenergic agonist, increased VTA-precuneus/PCC iFC (Spindler et al., 2021).Further fMRI studies assessing ARAS nuclei iFC, including VTA, during anesthesia-induced unconsciousness with sevoflurane and propofol, respectively, demonstrated a reduction of VTA iFC to subcortical areas (Nir et al., 2022) and its recovery during emergence of propofol-induced unconsciousness (Nir et al., 2019).

1.4.2. Cholinergic system, cholinergic basal forebrain, and modulation of arousal and wakefulness

Cholinergic innervation of the brain originates in two main locations, subcortically in the pons, specifically in the laterodorsal and pedunculopontine tegmental nuclei (Jones & Beaudet, 1987), and in the basal forebrain, specifically in four clusters of neurons (Ch1-Ch4), each innervating specific regions with partially overlapping projections (Mesulam et al., 1983; Zaborszky et al., 2015). From these, the Ch4 group corresponds to the nucleus basalis of Meynert, which provides the major source of cholinergic innervation almost to the entire cortex (Mesulam et al., 1983). The rest of the nuclei, Ch1-3, correspond to the neurons of the medial septum (Ch1), the vertical (Ch2) and horizontal (Ch3) limb of the diagonal band of Broca (Mesulam et al., 1983), which projections target predominantly to the hippocampus and centro-medial cortical regions (Fritz et al., 2019; Mesulam et al., 1983; Zaborszky et al., 2015). ACh exerts its action via muscarinic and nicotinic receptors located presynaptically and postsynaptically in both pyramidal glutamatergic projections and local GABA-ergic neurons. Due to its multiple sites of action, ACh affects the signal-to-noise ratio during sensory processing and modulates synchronization of neuronal networks (Benarroch, 2010).

There is an extensive body of evidence linking the basal forebrain cholinergic system with the modulation of cortical and behavioral arousal, one of the first observations being the association of the discharge rate of the nucleus basalis activity with EEG signatures of an activated cortex (Buzsaki et al., 1988; Detari & Vanderwolf, 1987; Metherate et al., 1992; Phillis & York, 1968; Poulet & Crochet, 2018). Further studies have demonstrated increased cortical ACh concentrations during wakefulness, decreased during slow-wave sleep and increased during rapid eye movement sleep, especially during

conscious experience of dreaming (Lydic & Baghdoyan, 2005). Based on this evidence, it has been suggested the basal forebrain represents the rostral extension of the ARAS system (Buzsaki et al., 1988; Sarter & Bruno, 2000).

Focusing specifically on modulation of arousal during anesthesia-induced unconsciousness: microinjections of nicotine in the midline thalamus restores righting and mobility in rats during continuous administration of sevoflurane, however intra-thalamic pretreatment with nicotinic antagonist, mecamylamine, prevented the nicotine-induced arousal response but did not lower the sevoflurane dose associated with loss of righting reflex (Alkire et al., 2007). Also, administration of carbachol, a cholinergic agonist, in the mPFC but not in the parietal cortex during continuous administration of sevoflurane, led to awake-like behavior in rats (Pal et al., 2018). A recent study demonstrated that propofol and isoflurane inhibit the activity of basal forebrain cholinergic neurons. Furthermore, the study evidenced that causing a lesion on these neurons resulted in an increased potency of the anesthetics (Luo et al., 2020) . Finally, they showed that sensitivity to these agents was reduced after optical stimulation of the basal forebrain cholinergic cells, but it failed to restore wake-like behavior during continuous administration of anesthesia (Luo et al., 2020). This was recently contrasted by Dean and colleagues, where they demonstrated that chemo genetic activation of basal forebrain cholinergic neurons in sevoflurane-anesthetized rats induced a wake-like behavior while at the same time increasing the concentration of ACh in the PFC (Dean et al., 2022).

In humans, the administration of physostigmine, an Ach-cholinesterase (AChE) inhibitor that crosses the blood-brain barrier, reversed loss of consciousness in 9 of 11 subjects sedated with propofol (Meuret et al., 2000) and positron emitted signal imaging (PET) data evidenced a recovery of cerebral blood flow in the thalamus and precuneus being previously reduced during loss of consciousness (Xie et al., 2011). Another study assessing the effect of physostigmine in the recovery of sevoflurane-induced unconsciousness resulted in the recovery of wake-like behavior in 5 out of 8 subjects anesthetized subjects (Leung & Luo, 2021; Plourde et al., 2003). However, a double-blinded study concluded that physostigmine does not enhance recovery after sevoflurane anesthesia (Paraskeva et al., 2002).

Regarding neuroimaging studies, iFC of cholinergic basal forebrain (cBF) has been studied during rs-wakefulness (Fritz et al., 2019; Markello et al., 2018) evidencing that the human cBF can be parcellated into two functionally distinct subdivisions along its anterior-posterior axis, i.e., Ch1-3 or anterior cBF projecting to hippocampus/ventromedial cortex, and Ch4 or posterior cBF projecting preferentially to

lateral cortices (Fritz et al., 2019). Interestingly, the characterization of their iFC profiles with respect to RSNs showed a positive functional connectivity between the anterior cBF (a-CBF) and the medial temporal DMN, and the posterior cBF with the so-called salience network (Fritz et al., 2019). Functional connectivity analyses of cBF during anesthesia-induced unconsciousness are still missing.

1.5. Hypotheses

Based on these premises, we have hypothesized that: *(i)* anesthesia-induced unconsciousness is associated with both a reduced VTA and a-cBF intrinsic functional connectivity and that these reductions, specifically in DMN areas mediates the within-DMN BOLD functional connectivity reduction during anesthesia-induced unconsciousness, *(ii)* beyond DMN static functional connectivity reductions, we propose that transient synchronizations of discrete BOLD events across the DMN measured by the Fano Factor (FF) and its distribution are reduced during anesthesia-induced unconsciousness, and that these reductions are mediated by both VTA-DMN and a-cBF-DMN connectivity, respectively, finally *(iii)* subcortical activity (i.e., brainstem and thalamus) participate in the generation of a burst during burst suppression state, reflected by coherent cortico-subcortical activity prior burst-onset further characterized by the length of the bursting event.

2. Methods

2.1. Static BOLD functional connectivity analysis: seed-based to whole-brain analysis

2.1.1. Anesthesia datasets: propofol and sevoflurane

Both rs-fMRI data sets were derived from two previous simultaneous EEG-fMRI studies about effects of sevoflurane (Ranft et al., 2016) and propofol (Jordan et al., 2013), respectively, on brain activity in healthy adults at the Technical University of Munich, Germany. Both studies were in line with the Declaration of Helsinki and approved by the ethics committee of the medical school of the Technical University Munich. Detailed description can be found in the first publications (Jordan et al., 2013; Ranft et al., 2016).

2.1.1.1. Participants and anesthesia

Sevoflurane study. In brief, 20 healthy adult males aged 20 to 36 years (mean 26 years) were recruited for the study. Combined EEG-fMRI measurements were carried out in 5 consecutive states, namely wakefulness pre-anesthesia (session 1), anesthesia sevoflurane 4vol% (burst-suppression state, session 2), anesthesia sevoflurane 3vol% (session 3), anesthesia sevoflurane 2vol% (session 4) and wakefulness post-anesthesia (session5). Sevoflurane anesthesia was administrated in oxygen via tight-fitting facemask using an MRI-compatible anesthesia machine (Fabius Tiro, Dräger, Germany). Sevoflurane as well as O_2 and CO_2 were measured by a cardiorespiratory monitor (Datex AS/3, General Electric, USA); standard American Society of Anesthesiologists monitoring was performed. Initially, an end-tidal sevoflurane concentration of 0.4% was administered for 5 min, then increased in a stepwise fashion by 0.2 vol% until the participant was unconscious, judged by the loss of responsiveness to the repeatedly spoken command “squeeze my hand” two consecutive times (corresponding to Ramsay sedation scale score of 6). After loss of responsiveness, the sevoflurane concentration was increased to reach an end-tidal concentration of 3% to insert a laryngeal mask (i-gel, Intersurgical, United Kingdom). Sevoflurane concentration was increased further until the simultaneously recorded EEG showed suppression periods of at least 1000 ms and about 50% suppression, reached at approximately 4vol% (burst suppression). Data from two further states were acquired for at least 10

more minutes: steady levels of 3vol% ('anesthesia 3vol%' state) and 2vol% ('anesthesia 2vol%' state). 45 min after recovery, 'awake post-anesthesia' state was recorded.
The current study focuses on the rs-fMRI recordings from states awake pre-/post-anesthesia and states of anesthesia 2vol% and 3 vol%. Burst suppression state (session 2) was not included and will be analyzed independently as this is an extreme case of unconsciousness. Data from 15 participants we included, each providing 350 complete and high-quality fMRI volumes. Four participants had missing fMRI data due to technical problems of scanning for at least one state of measurement, one participant had corrupted data quality after preprocessing (see below).

Propofol study. The propofol study was performed in 15 male subjects (21-32y, mean 25.8y), from which combined EEG-fMRI measurements were recorded in three sessions, wakefulness pre-anesthesia (session 1), propofol deep anesthesia (session 2) and propofol light anesthesia (session 3). Propofol was administered using a target-controlled infusion pump (Open TCI; Space infusion system; Braun Medical, Melsungen, Germany). Beginning at 1.2 µg/ml, propofol concentration was increased in 0.4 µg/ml steps until the participant stopped responding to the verbal command 'squeeze my hand' (corresponding to Ramsay sedation scale score of 5-6). This concentration was maintained for 10 min to guarantee equilibrium of the estimated effect-site concentration. After reaching this point, a 10 min-long recording was performed, which is referred here as 'propofol-induced unconsciousness'. This was followed by a second session recorded with 50% of the propofol concentration, however it was discarded due to movement artifacts. It is noteworthy to mention that clinically the sedation depth from this cohort was lesser than the one performed in the sevoflurane experiments (Ramsay sedation scale score of 6). For our study, we included 12 subjects, each providing 300 rs-fMRI volumes for 2 states, namely awake pre-anesthesia and anesthesia propofol. Three participants had excessive head motion during scanning (see below).

2.1.1.2. Imaging and preprocessing

Imaging. Briefly, data acquisition for both experiments, sevoflurane and propofol, were performed on a 3T whole body MRI scanner (Achieva Quasar Dual 3.0T 16CH, The Netherlands) with an eight channel, phased-array head coil. A gradient echo planar imaging sequence was performed with following parameters: echo time = 30ms, repetition time 2s, flip angel = 75°, field of view = 220 x 220mm, matrix = 72x72, 32 slices, acquisition order interleaved odd first, slice thickness = 3mm, and 1mm interslice gap. High-resolution (1x1x1mm voxel size) T1-weighted anatomical images were acquired before fMRI.

Preprocessing. Brainstem analysis requires extended preprocessing of fMRI data: *(i)* To account for physiology-induced artifacts (e.g. heart beat), we performed physiological noise regression using Physiologic Estimation by Temporal Independent Component Analysis (PESTICA, http://www.nitrc.org/projects/pestica/); PESTICA implements temporal independent component analysis to estimate time courses related to cardiac and respiratory fluctuations that were used for both image and voxel-wise physiological noise correction (Glover et al., 2000). *(ii)* To account for motion-induced artifacts particularly in the brainstem (e.g. vessel movements), we performed motion correction using Slice Oriented Motion Correction (SLOMOCO, http://www.nitrc.org/projects/pestica); SLOMOCO regresses out slice-wise rigid body motion parameters according to a second order-voxel and a slice-specific motion regression model (Beall & Lowe, 2014).

Next preprocessing steps and subsequent seed-based FC analyses were performed using the Data Processing Assistant for Resting-State fMRI (DPARSF, http://rfmri.org/DPARSF) (Chao-Gan & Yu-Feng, 2010) based on Statistical Parametric Mapping (SPM12, htttp://www.fil.ion.ucl.ac.uk/spm) and the toolbox for Data Processing & Analysis of Brain Imaging (DPABI, htttp://rfmri.org/DPABI) (Yan et al., 2016). Preprocessing steps included discarding of first 8 volumes, re-alignment, slice-time correction, head motion correction using the Friston 24-parameter model, co-registration, wavelet-based despiking (Patel et al., 2014), CSF and white matter regression, normalization using Diffeomorphic Anatomical Registration Based on Exponentiated Lie Algebra (DARTEL, neurometrika.org/) (Ashburner, 2007), linear detrending, bandpass filtering (0.01-0.1Hz) and smoothing with 6x6x6mm Gaussian kernel. All participants' head motion in the sevoflurane dataset remained under the threshold for exclusion, defined as a mean framewise displacement >0.2. Three subjects were discarded from the propofol data set due to excessive motion.

2.1.2. Seed-based iFC analysis during wakefulness and anesthesia-induced unconsciousness

This consists in extracting the mean averaged time course across all voxels within a seed (or ROI) and correlate it with the time course of each other voxel in the brain, respectively, via voxel-wise bivariate Pearson correlation analysis. This will generate a correlation coefficient map per subject, per state in the sevoflurane (i.e., 4 states) and propofol (i.e., 2 states) experiments. Each correlation coefficient map will be converted into a z-value map by using Fisher´s r-to-z transformation to enable across voxel

and across subject comparisons, which is represented by state-wise and seed-wise iFC outcome map per subject .

2.1.2.2. DMN FC

The DMN seed was defined as the collection of 34 spherical (i.e., 5mm diameter) region of interest (ROI), which were derived from Dosenbach and colleagues (Dosenbach et al., 2010) available in the DPARSF toolbox. A standard DMN template was derived from Yeo and colleagues (Yeo et al., 2011), which was used to validate DMN iFC results and to define our variables for the mediation analyses.

We derived two main connectivity outcomes from the DMN, *(i)* within DMN average connectivity (DMN iFC), which was calculated by the arithmetic mean of z-values from the DMN-based FC analysis across the DMN mask of Yeo and colleagues (Yeo et al., 2011), and *(ii)* VTA-DMN iFC, where the averaged FC connectivity was repeated but using the z-values from the VTA-based FC analyses.

2.1.2.3. VTA FC and VTA 'SRCC' FC

VTA and further brainstem nuclei masks (used for VTA iFC 'SRCC' control analyses, see below) such as: DR, MR, PPN, LC, were derived from the Harvard Ascending Arousal Network Atlas (Edlow et al., 2012).

To control for specificity and to eliminate potential partial volume effects of neighboring neuromodulatory nuclei surrounding VTA, we performed so-called small region confound correction (SRCC) procedure by regression time courses of overlapping nuclei as described by Krimmel and colleagues (Krimmel et al., 2019). The aim of the approach is to determine the overlap between a dilated VTA 6mm and the above-mentioned brainstem nuclei at least 3 mm away from the original VTA mask (**Fig. 3 A**) and use BOLD time courses derived from these resulting areas as regressors of control. To do so, we started by dilating the original ventral tegmental area mask to 6mm using the FSLUTILS, the image calculator tool from FSL (FMRIB´s Software Library, https://fsl.fmrib.ox.ac.uk/fsl/fslwiki/). Next, the dilated ventral tegmental area mask was overlapped with the neighboring nuclei of interest. The overlapping voxels, i.e., shared voxels between dilated ventral tegmental area and the rest of the nuclei, separated 3mm from the original ventral tegmental area mask were defined as a region of interest. A time course was derived from this area (**Fig. 3 A**, *region in white*) and regressed out from the brainstem time courses along with the previously described nuisance covariates, e.g., Friston 24-parameter model, white matter, or cerebral spinal

fluid. The residuals from this analysis were further detrended, filtered and smoothed. Using these 'corrected' brainstem-time series we extracted a VTA corrected mean time course and used in a whole-brain seed-based FC analysis (**Fig. 3 B)**. These VTA corrected FC maps were used to control our sevoflurane mediation analysis for anatomical specificity (*See Mediation analysis).*

2.1.2.4. a-cBF FC

Cholinergic basal forebrain seed, specifically a-cBF (Ch1-3) was derived from (Fritz et al., 2019).

2.1.3. Statistical analysis

2.1.3.1. FC analyses

For testing significance of FC at certain states (e.g., pre-anesthesia wakefulness) and connectivity differences between states (e.g., pre-anesthesia wakefulness vs sevoflurane 3vol%), we performed one-tailed one-sample and one-tailed paired t-tests, respectively, using IBM SPSS Version 26 (IBM Corp., Armonk, NY, USA) for average connectivity scores and Statistical Parametric Mapping (SPM12, Welcome Trust Centre for Neuroimaging, UK, htttp://www.fil.ion.ucl.ac.uk/spm) for voxel-wise connectivity z-maps. Concerning average connectivity tests, significance threshold was set $p<0.05$, for paired-t-tests effect size was measured by Cohen's d corrected for small sample size (Lakens, 2013)**;** concerning voxel-wise z-map tests, each test was limited to grey matter voxels and significance threshold was set $p<0.05$ FWE cluster-corrected for multiple testing with a single-voxel height threshold of $p<0.005$.

2.1.3.2. Mediation analyses

To evaluate the indirect effect of averaged connectivity between VTA and the DMN for the association between anesthesia and averaged connectivity within DMN, we performed mediation analysis for different combinations of anesthesia (e.g., sevoflurane 3vol% or 2vol%) and wakefulness (e.g., pre-, or post-anesthesia wakefulness) using the PROCESS mediation macro in SPSS (www.processmacro.org) (Hayes & Rockwood, 2017).

To ensure that the sample sizes of both data sets we used in our study were appropriate for a mediation analysis approach to test our second hypothesis, we performed a-priori sample size

estimation for mediation analysis by using Sobel's test (https://webpower.psychstat.org/models/med01/). Although several alternative approaches are also available for sample size estimation of mediation analysis such as approaches based on bootstrapping (Shrout & Bolger, 2002) or Monte Carlo method (Mackinnon et al., 2004), Sobel's test has been demonstrated to provide robust and conservative estimates (Pan et al., 2018). Under the assumptions of both large and consistent effect sizes of anesthesia on functional connectivity, estimates of FC variance and error variance based on Ranft and colleagues study (Ranft et al., 2016), and with a desired statistical power of 0.8, a sample size of 16 was estimated for testing the indirect effect of FC between the VTA and the DMN on FC within the DMN under anesthesia. We interpreted this estimate in a way that both fMRI data sets were appropriate for our mediation analysis approach.

Mediation analysis investigates whether the effect of an independent variable 'X' (e.g., wakefulness or anesthesia-induced unconsciousness) on a dependent variable 'Y' (e.g., within-DMN FC) occurs via a third variable called mediator 'M' (e.g., reduction of between VTA and DMN FC). The relationships between these variables are quantified by regression analyses and can be displayed as path diagrams (**Fig. 11 A3 & B3**). The main outcome measure is the indirect effect *ab*, reflecting the product of X's effect on M (*a*) and M's effect on Y (*b*). The statistical significance of the indirect effect is determined via a nonparametric bootstrapping approach (5,000 iterations) to obtain 95% confidence intervals. We used the mediation analysis to test conditional relationships between anesthesia-induced unconsciousness, between VTA and DMN FC, and within-DMN FC.

To verify that interpretation of potential results is valid, variables of the mediation analysis must fulfill certain assumptions, which largely overlap with those of canonical multiple regression analyses. We verified – by the use of SPSS tool (https://www.spss-tutorials.com/spss-multiple-regression-tutorial/; https://www.open.ac.uk/socialsciences/spsstutorial/files/tutorials/assumptions.pdf) - that variables of subsequent mediation models fulfilled the following criteria, respectively: linearity across variables, absence of multi-collinearity, independence of residuals, homoscedasticity, normal distribution of residuals, and absence of biasing cases.

For the model, three variables were determined: *(i)* The i*ndependent variable* defined as a nominal dichotomous variable with 0 = for awake pre-anesthesia state and 1 = for sevoflurane 3vol% state. *(ii)* The *mediator variable* defined as the average connectivity between the VTA and DMN, once for wakefulness and once for sevoflurane 3vol% anesthesia state. For sevoflurane 3vol%, in order to focus on reduced connectivity within the DMN, voxel-space for average connectivity was restricted to the overlap between the DMN mask of Yeo and the result of the paired t-test of VTA connectivity for the contrast pre-anesthesia wakefulness > sevoflurane 3vol%. To avoid possible bias introduced by

different masks, the values corresponding to wakefulness and sevoflurane 3vol% were demeaned. *(iii)* The *dependent variable* defined as the average connectivity within the DMN, once for wakefulness and once for sevoflurane 3vol% anesthesia state.

We performed the further mediation analyses in an analog way for sevoflurane 2vol%-induction, sevoflurane 3vol%-recovery, and propofol-induction as well as with the a-cBF seed analyses.

2.1.3.3. Analysis of differences: correlation analysis and simple linear regression.

To evaluate the relationship between a-cBF iFC and DMN iFC reduction during anesthesia-induced unconsciousness with respect to wakefulness pre-anesthesia, we calculated a Pearson's correlation and implemented a simple linear regression analysis on the differences (also referred as 'Deltas' in the text) of FC from awake pre-anesthesia state and anesthetized state (i.e., sevoflurane 3vol%, sevoflurane 2vol%, or propofol, respectively) of these two variables. To do so, first, we defined the masks to derive a value per subject: *i) for the a-cBF-DMN mask*, we used the cluster of a-cBF iFC reduction outcome from the paired t-test (e.g., awake pre-anesthesia > sevoflurane 3vol%) and used only the overlapping voxels with the DMN Yeo mask, ii) for the DMN mask, we used the canonical pre-defined DMN mask from Yeo and colleagues (Yeo et al., 2011). Second, we extracted per subject a mean z connectivity value from the defined mask (i.e., a-cBF-anterior DMN) during awake pre-anesthesia state and state of unconsciousness (e.g., sevoflurane 3vol%, sevoflurane 2vol% or propofol, respectively) from the voxel-wise connectivity z-maps from the a-cBF FC analysis. The same procedure was done using the DMN mask but using the voxel-wise connectivity z-maps from the DMN FC analysis (**Fig. 17 A-B left side**). Finally, we subtracted the mean connectivity of the anesthetized state from the ones of the wakefulness pre-anesthesia state. We used these values to calculate a Pearson's correlation coefficient and a simple linear regression analysis to investigate if the a-cBF-anterior DMN FC reduction can predict the reduction of the within-DMN FC reduction during anesthesia-induced state. All analyses were performed using SPSS software version 26 and plotted with MATLAB. One-tailed Pearson's correlations were bootstrapped (n=1000) to conform to 95% CIs.

2.2. Point-process BOLD analysis: Fano Factor analysis

2.2.1. DMN vs. whole-brain and control resting-state networks during wakefulness and anesthesia-induced unconsciousness

2.2.1.1. Brain parcellation and brainstem seeds

A whole-brain parcellation scheme, including cerebellum, was defined as 160 regions of interest (ROIs) (i.e., 5mm diameter spheres) according to Dosenbach's 160 functional regions (Dosenbach et al., 2010); ROIs were grouped according to their functional labels to define resting state networks of interest (i.e., DMN and control networks). For brainstem analyses, VTA and further nuclei (used for 'SRCC' control analyses, see above), namely DR, MR, PPN, LC, were derived from the Harvard Ascending Arousal Network Atlas (Edlow et al., 2012).

2.2.1.2. Fano Factor approach: analysis of large-scale synchronization

Following Hahn and colleagues' approach (Hahn et al., 2021), we calculated the Fano Factor (FF) (i.e., variance of counts over the mean of counts) of discrete fMRI BOLD events. To do this, first, using z-scored time courses derived from the ROIs based on Dosenbach and colleagues (Dosenbach et al., 2010) (160 ROIs for a whole-brain scheme, 34 ROIs for DMN, 21 ROIs for frontoparietal network, 33 ROIs for sensorimotor network), we defined event points, i.e., point process analysis, per ROI and per subject as time course positive peaks which trespassed a threshold of one standard deviation of each time series. Next, we counted the number of the points per timepoint of the acquired time series across ROIs per subject to assess the presence of synchronicity between the selected ROIs. Following this, a sliding-window approach was adopted for calculating the FF by shifting a window of ≈50 seconds (25 TRs) length continuously across the whole time series. This time-window was selected based on Hahn and colleagues (Hahn et al., 2021) previous results. The FF was calculated using the formula: FF= var(counts)/mean(counts) per window. The value of the FF captures higher order correlation and global synchrony of the events within each time window, thus a value of FF ≈ 1 suggests that the events occur independently from each other and resembles more a random process, while greater values FF>>1 suggest the presence of large-scale synchrony. The sliding windows yielded a distribution of FF across time. To quantify the overall level of synchronization, the FF distribution

was fitted to a Gamma distribution (Eden & Kramer, 2010; Hahn et al., 2021), which yielded a shape and a scale parameter per subject and per session. In a gamma probability density function the shape parameter describes the overall envelope of the function, while the scale parameter provides information about the variability of the distribution, i.e., higher values will skew the function to the right and decrease its height.

2.2.2. Seed-based iFC analysis: VTA, VTA 'SRCC' and a-cBF FC

These analyses are the same as for the first experiment (Section 2.1.2.3. VTA FC & VTA 'SRCC' FC).

2.2.3. Statistical analysis

2.2.3.1. Fano Factor

All analyses were performed using MATLAB v.18b (Mathworks, Sherbon, MA, USA) and build-in functions. Boundaries for the FF were calculated in order to assess whether the time increments of the points are more variable than that from a Poisson process ($p<0.05$), which are plotted alongside the actual FF distributions (Eden & Kramer, 2010). For the assumption of a Poisson process for a window length W, the shape factor becomes $(W - 1)/2$ and the scale factor become $2/(W - 1)$ (Eden & Kramer, 2010). To assess whether the distribution of the FF matches Poisson or moves away from it, the scale parameters will be tested against randomness. Additionally, it is estimated whether the center of gravity of the whole FF distribution deviates significantly from a Poisson process (Eden & Kramer, 2010).

For sevoflurane, significance of differences in scale parameters between the states was first assessed via repeated measures ANOVA. Post-hoc tests comparing individual states of anesthesia were evaluated with a two-sided Wilcoxon-Sign test. Systematic grading of the scale parameter in the order (sevoflurane 3vol% < sevoflurane vol% < awake post-anesthesia) was tested for via a non-parametric test of trend, (Page test function for MATLAB Central File Exchange, developed by Dimitri Shvorob, https://www.mathworks.com/matlabcentral/fileexchange/14419-perform-page-test). For propofol the two states were compared by a two-sided Wilcoxon-Sign test.

2.2.3.2. FC analyses

At a group-level, statistical significance of voxel-wise VTA functional connectivity per state (e.g., awake pre-anesthesia) and connectivity differences between states (e.g., awake pre-anesthesia vs sevoflurane 3vol%) was assessed via one-tailed one-sample and paired t-tests, respectively, using Statistical Parametric Mapping (SPM12, Welcome Trust Centre for Neuroimaging, UK, htttp://www.fil.ion.ucl.ac.uk/spm). Significance threshold was set $p<0.05$ FWE cluster-corrected for multiple testing with a single-voxel height threshold of $p<0.005$.

To assess VTA cortical connectivity, more specifically for connectivity between VTA and DMN, we used the 5mm-sphere ROIs assigned to the DMN and overlayed them on top of the group-level statistically significant voxel-wise VTA connectivity result (one-sample); next, we look for matching voxels. The overlapping voxels between the DMN ROIs and the voxel-wise VTA one-sample t-test group result map in wakefulness pre- or post-anesthesia was assigned as the 'spatially-defined cortical areas of expected connectivity between VTA and DMN' (**Fig. 17**) (used for the mediation analysis, see below). These same procedure was applied to the a-cBF and DMN FC.

2.2.3.3. Mediation analysis

To assess the mediating effect of connectivity between VTA and DMN in the association between anesthesia and large-scale transient synchronization within the DMN, we performed a mediation analysis using the combinations between anesthesia-induced state (i.e., sevoflurane 3vol% or 2vol%, respectively) and wakefulness (e.g., awake pre- or post-anesthesia, respectively) using the PROCESS mediation macro in SPSS (www.processmacro.org) (Hayes & Rockwood, 2017). Briefly, in the mediation model testing awake pre-anesthesia and sevoflurane 3vol% anesthesia, resembling induction of anesthesia, three variables were determined: *(i)* The *independent variable* as a nominal dichotomous variable coded with 0 = awake pre-anesthesia state and 1 = sevoflurane-induced anesthesia. *(ii)* The *mediator variable* as the average connectivity between the VTA and DMN per subject, once for wakefulness and once for anesthesia-induced state. The values per subject corresponded to the mean z correlation value extracted from the 'spatially-defined cortical areas of expected connectivity between VTA and DMN' from each participant's voxel-wise VTA connectivity z-map per state (i.e., wakefulness pre-anesthesia, sevoflurane 3vol%, sevoflurane 2vol%, wakefulness post-anesthesia). *(iii)* The *dependent variable* as the scale parameter per subject derived from the DMN FF analysis, once for wakefulness and once for sevoflurane state.

We performed the further mediation analyses in an analog way for sevoflurane anesthesia-recovery, and propofol-induction.
These analyses were performed in the same way using a-cBF and DMN FC results.

2.3. Time-resolved BOLD functional connectivity analysis: partial Jackknife correlation approach in burst suppression data

2.3.1. Preprocessing of burst suppression data

The current project focuses only on burst suppression state induced by sevoflurane anesthesia with 4vol% concentration derived from the sevoflurane experiment (session 2). For our purposes, fMRI as well as EEG recordings were utilized in these analyses. Data from 19 subjects were included, one subject was excluded because of missing data in the EEG due to hardware problems during the acquisition.

fMRI. Considering the extreme condition of burst suppression, the preprocessing for these data resembles that for the other sessions, with some modifications: Physiology-induced artifacts (e.g., heartbeat) was accounted using PESTICA, SLOMOCO was not used. Next preprocessing steps included discarding the first 5 volumes, slice-time correction, re-alignment, co-registration, segmentation using DARTEL, normalization, linear detrending, low-pass filtering (0.1Hz), no smoothing or no covariate regression was applied.

EEG. Recordings were performed using an fMRI-compatible, 64-electrode cap and 32-channel EEG. Electrode impedance was kept below 5kΩ using an abrasive gel (Easycap). All signals were recorded at 5 kHz sampling rate. An interface unit (SyncBox; Brain Products) was additionally connected to the amplifiers to reduce timing-related errors in the fMRI artifact correction by synchronizing the clocks of the EEG amplifiers and the fMRI gradients. One of the 64 channels was placed over the chest and registered the electrocardiogram (left anterior axillary line). Quality of EEG data was assessed via detection of signal saturation due to clipping artefacts. The following preprocessing steps were performed using BrainVision Analyzer 2.2.1 Software: *(i)* automatic gradient artifact correction (MR correction) using a template drift detection method (TDC), *(ii)* low pass FIR filter 40 Hz, *(iii)* down-sampling with factor 20, *(iv)* pulse-artefact correction using a semiautomatic mode individualized per

subject (e.g., template searched between 0 and 15 seconds, pulse length average 991 ms, +/- 259ms with the following parameters: coherence trigger= 0.6, minimal amplitude= 0.6, maximal amplitude= 1.2, the identified pulses were marked with R).

Burst-suppression labelling. Using a semi-automatic approach, each fMRI volume was assigned to two categories, i.e., burst or suppression, 1 or 0, according to simultaneously recorded EEG traces (**Fig. 1**). Non-saturated pre-processed EEG data was used for the following approach: *(i)* FFT linear filtering (1-5Hz), *(ii)* amplitude normalization (z-score), *(iii)* calculation of the averaged upper envelope of the sequence using an N-tap Hilbert filter, *(iv)* data points which amplitude trespassed at least 2 standard deviations above the mean were labelled with a 1=burst, everything below was labelled with a 0=suppression (**Fig. 1 B**) *(v)* visual inspection and confirmation of labelling (**Fig. 1 C**).

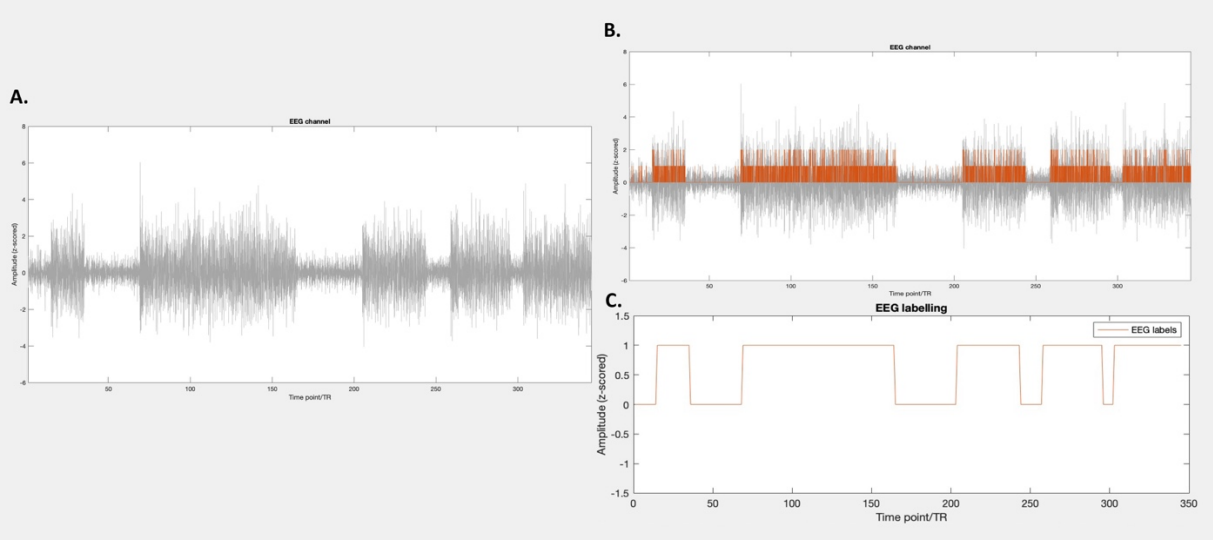

Figure 1. Burst suppression labelling based on EEG pattern.

A. Preprocessed EEG channel. *EEG trace locked to fMRI resolution.* ***B. Burst labeling.*** *In orange is depicted the localization of timepoints where EEG amplitude is higher than 2 standard deviations than mean amplitude, labelled as 'burst=1', rest of timepoints were given a value of 0 =suppression.* ***C. Labels.*** *Trace of burst and suppression (burst=1, suppression=0).*

2.3.2. Time-resolved region-of-interest functional connectivity analysis before a burst event

2.3.2.1. Parcellation scheme and ROI selection

The brain was parcellated in three principal schemes, i.e., whole-brain ('Cortex_BG': cortical regions plus basal ganglia and cerebellum), thalamus, and ARAS nuclei. The thalamus was excluded from the whole-brain parcellation and treated as an independent entity based on previous results from Golkowski and colleagues, who demonstrated that most of grey matter voxels' (except for the thalamus') BOLD signal exhibited a positive correlation with EEG burst suppression signal (Golkowski et al., 2017). For time course extraction all ROIs were transformed into subject space.

Cortex plus basal ganglia. 8 ROIs were derived from the FSL MNI structural (Mazziotta et al., 2001) atlas thresholded to 80% probability, including the frontal lobe, parietal lobe, temporal lobe, occipital lobe, cerebellum, insula, caudate nucleus, and putamen. This parcellation will be referred as '*Cortex_BG*'.

Thalamus. 5 ROIs were derived from the FSL Talairach in MNI space atlas (Lancaster et al., 2000), including anterior nucleus (bilateral grey matter anterior nucleus), mediodorsal nucleus (bilateral grey matter medial dorsal and midline nucleus), ventral nucleus (bilateral grey matter ventral anterior, ventral lateral, ventral posterior lateral and ventral posterior medial nucleus), lateral nucleus (bilateral grey matter lateral dorsal and lateral posterior nucleus), posterior nucleus (bilateral grey matter pulvinar nucleus).

ARAS. 9 ROIs were derived from the Harvard atlas for brainstem arousal nuclei (Edlow et al., 2012), including VTA, DR, MRF, PBC, PO, PPN, LC and PAG.

Grey matter and CSF masks. Probability tissue class images created during segmentation and customed to the subject space using the modelling diffeomorphic method DARTEL (Ashburner, 2007) for grey matter (GM, thresholded to 50%) and CSF (thresholded to 99%) were created.

2.3.2.2. Partial Jackknife correlation approach

We applied a variation of the so-called 'jackknife correlation approach' (JC) on the normalized (z score) ROI's time courses, namely a partial jackknife correlation approach (PJC), consisting of a repetitive re-estimation of the partial pair-wise correlation value between two time courses after the removal of a timepoint. Therefore, average correlation between time courses is not assessed. A time point contributing strongly to the correlation would cause a reduction of correlation when omitted. This means a sign inversion occurs because a negative deviation of PJC correlation at a given time point implies a positive deviation of the correlation at that time point and vice versa.

The jackknife correlation (JC) between two signals x and y at time t is calculated as described by (Thompson et al., 2018): $JC_t = -\left(\frac{\Sigma_i^T (x_i - \bar{x}_t)(y_i - \bar{y}_t)}{\Sigma_i^T (x_i - \bar{x}_t)^2 (y_i - \bar{y}_t)^2}\right), i \neq t$, i.e., just the Pearson correlation with t left out of the computation, where $\bar{x}_t$ and $\bar{y}_t$ are equivalent to the expected values $\frac{1}{T-1} \Sigma_i^T x_i, i \neq t$, and $\frac{1}{T-1} \Sigma_i^T y_i, i \neq t$, respectively. The minus sign is included to correct for the sign inversion of the method. For calculation of the PJC, the Pearson correlation is replaced with the partial correlation matrix Θ_t. In general, given signals of length T from p brain regions, the $x, y - th$ entry of $\Theta \sqsubseteq \mathbf{R^{pxp}}$, represents the conditional dependence of regions x and y, given the other $p - 2$ regions, and is equivalent to the partial correlation between x and y (Peng et al., 2009). To compute Θ, the precision matrix $\Sigma^{-1} \sqsubseteq \mathbf{R^{pxp}}$ is calculated, which can be done efficiently by a Cholesky decomposition of the lower triangular part of the covariance matrix $\Sigma \sqsubseteq \mathbf{R^{pxp}}$. Then, $\Theta = \frac{-\Sigma^{-1}}{\sqrt{\mathrm{diag}(\Sigma^{-1})\mathrm{diag}(\Sigma^{-1})^T}}$, and $PJC_t = -(\Theta_t(x, y))$, where the PJC between regions x and y is computed on p time series of length $T - 1$, with t left out of the calculations. Global signal (averaged time course derived from each subject's GM mask) and CSF (averaged time course derived from each subject's CSF mask) was included as a covariate of no interest.

To assess whether results depended on the length of the bursting event, analyses were done in three different variations: *(i)* using all subjects and all events, *(ii)* using events with a minimal length of 20TRs, which will be referred as 'long' bursts, and *(iii)* using events with a maximal length of 10 TRs, referred as 'short' bursts.

2.3.3. Statistical analysis

2.3.3.1. Partial Jackknife correlation approach

To reconstruct a time-resolved connectivity trajectory before the start of the burst event and to make results more robust, we averaged the dynamic PJC correlations across parcels (within and between parcels) per time point , i.e., in steps of 1 TR until -9 TRs before the start of the burst. Statistical significance was based on paired t-tests testing each average connectivity against average of the rest of the timepoints, p threshold was set to 0.05.

2.3.2.3. General lineal model analysis

To complement the PJC analyses and to assess regional BOLD activations (i.e., signal amplitude analysis), we performed a general lineal model (GLM) analysis following (Golkowski et al., 2017) but artificially varying the start of a burst (Moeller et al., 2008) in steps of 1 TR until 9 TRs before the start of the event (the length of the burst was always conserved). At a single subject level, we used a binary regressor (1 for burst and 0 for suppression) and convoluted it with the canonical hemodynamic response function (HRF) implemented in SPM12. Global signal was included as a nuisance regressor to focus on particularities of regional activity shadowed by the global burst and suppression pattern. Movement parameters were not included in the model as covariates, first, because realignment was successfully performed during preprocessing, and second, because linear motion and rotation parameters were highly correlated to the burst suppression pattern and the global signal is already included in the model. For group analyses, we used a one sample t-test per analysis of varying burst-start (in total 10 GLM analysis). Significance threshold was set to $p<0.05$ FWE cluster-corrected for multiple testing with a single-voxel height threshold of $p<0.005$.

Additionally, to compare individual t-values per ROI and avoid partial volume confounding effects from neighboring voxels, we derived the maximum t-value from of each ROI per parcel (8 ROIs from parcel cortex, 5 ROIs from parcel thalamus, 9 ROIs from parcel ARAS) from the group one sample t-test t-maps.

In line with our PJC analyses, the GLMs were performed in three different variations: *(i)* using all bursts events and all subjects, *(ii)* using only bursts with a minimal length of 20 TRs, which will be referred as 'long' bursts, and *(iii)* using only bursts with a maximal length of 10 TRs, which will be referred as 'short' bursts. If the subject included in the analysis were to provide only a selected event, a second regressor was included in the first level analysis accounting for non-included bursts.

Finally, using the 'Event-related responses' function of SPM12 (htttp://www.fil.ion.ucl.ac.uk/spm) we assessed regional activity, specifically on cortical and thalamus ROIs, extracting a mean peri-stimulus time histogram (PSTH) of adjusted data and fitted response across peri-stimulus time. Responses were derived from the voxel with the maximum t-value within the ROI and averaged across subjects per timepoint (height p threshold $p<0.01$).

3. Results

3.1. VTA and a-cBF are related to DMN BOLD functional connectivity reduction during anesthesia-induced unconsciousness

3.1.1. Anesthesia-induced unconsciousness is related to VTA-DMN functional connectivity reductions

Main result: sevoflurane 3vol%. During wakefulness pre-anesthesia, average VTA-DMN connectivity was significant with mean z= 0.03 (SD 0.03; p<0.05). Voxel-wise VTA connectivity was significant to ACC, PCC, parahippocampus, medial frontal gyrus, cerebellum, brainstem, thalamus, basal ganglia, and amygdala (**Fig. 1 B1, Tab. 1**); 86% of these voxels overlapped with the default mode network (**Tab. 2**); and this pattern resembles that of previous studies on VTA connectivity, supporting the reliability of our approach (Murty et al., 2014; Nir et al., 2019; Zhang et al., 2016). During sevoflurane 3vol%-induced anesthesia, VTA-DMN average connectivity was mean z=-0.01 (SD 0.02; p<0.05), corresponding to a significant connectivity reduction of 140% with a Cohen's d=0.90; voxel-wise connectivity was reduced in PCC, precuneus, ACC, and cerebellum, with 84% overlap with the default mode network, including its cerebellar part of crus I and II (**Fig. 1 B2, Tab. 1-2**). This result indicates that connectivity between VTA and DMN is reduced by sevoflurane 3vol% anesthesia.

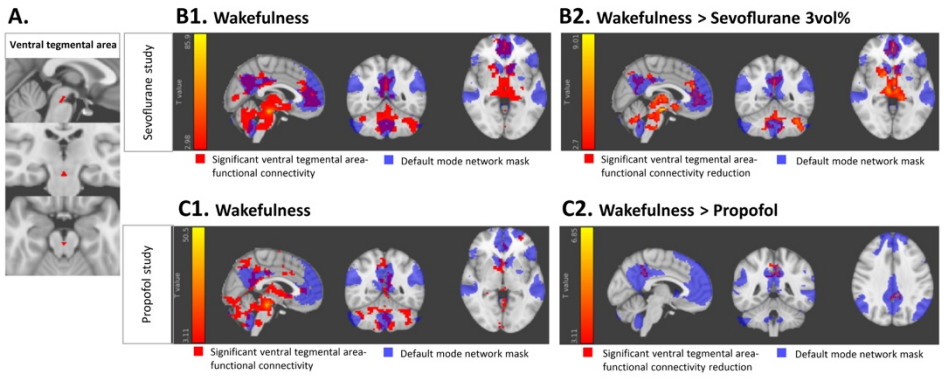

Figure 2. Anesthesia-induced unconsciousness is associated with a reduced VTA iFC.

A. VTA mask for seed-based functional connectivity analysis. *The mask is derived from Harvard Ascending Arousal Network Atlas (Edlow et al., 2012).* *B. Sevoflurane study.* ***B1. VTA connectivity during wakefulness pre-anesthesia.*** *Voxel-wise one-sample t-test on z-maps of VTA iFC during wakefulness, p<0.05 FWE cluster level*

corrected: significant connectivity in red-to-yellow, DMN mask derived from Yeo and colleagues (Yeo et al., 2011) in blue. ***B2. VTA connectivity reduction for the contrast wakefulness pre-anesthesia > sevoflurane 3vol%.*** *Voxel-wise paired t-test on z-maps of VTA iFC during wakefulness and sevoflurane 3vol%, p<0.05 FWE cluster level corrected: significant connectivity in red-to-yellow, DMN mask in blue.* ***C. Propofol study. C1. VTA connectivity during wakefulness pre-anesthesia.*** *Voxel-wise one-sample t-test on z-maps of VTA iFC during wakefulness, p<0.05 FWE cluster level corrected: significant connectivity in red-to-yellow, DMN mask in blue.* ***C2. VTA connectivity reduction for the contrast wakefulness pre-anesthesia > propofol.*** *Voxel-wise paired t-test on z-maps of VTA iFC during wakefulness and propofol, p<0.05 FWE cluster level corrected: significant connectivity in red-to-yellow, DMN mask in blue.*

Regions	*Hemisphere*	*MNI Coordinates [x;y;z]*	*Z value*	*Cluster size*	*P value*
Sevoflurane study					
1) Pre-anesthesia wakefulness – average functional connectivity and one-sample t-test					
VTA-DMN	*L/R*	*Average*	*0.03 (SD 0.03)*		*0.002*
2) Pre-anesthesia wakefulness – voxel-wise connectivity and one sample t-test					
Brainstem	*L*	*[0;-24;-18]*	*>10*	*4330*	*<0.001*
Cerebellum	*R*	*[9;-54;-33]*	*5.54*		
Thalamus	*L*	*[-6;-24;0]*	*5.45*		
ACC	*L*	*[-3;39;12]*	*5.01*	*745*	*<0.001*
Paracingulate gyrus	*R*	*[6;42;-3]*	*4.68*		
Lingual gyrus	*R*	*[6;-57;6]*	*4.67*	*842*	*<0.001*
Precuneus	*L*	*[-6;-57;9]*	*4.38*		
3) Reduction of connectivity during sevoflurane 3vol% - average connectivity and paired t-test					
VTA-DMN	*R/L*	*Average*	*Reduction 140% Cohen's d=0.90*		*0.0015*
4) Reduction of connectivity during sevoflurane 3vol% - voxel-wise connectivity and paired t-test					
Brainstem	*R*	*[3;-15;-15]*	*6.69*	*818*	*<0.001*
Thalamus	*L*	*[-9;-24;6]*	*5.53*		
Caudate nucleus	*R*	*[12;9;0]*	*5.38*		
Paracingulate gyrus	*R*	*[3;39;24]*	*5.58*	*278*	*<0.001*
Cerebellum	*L*	*[-36;-57;-33]*	*5.37*	*78*	*0.001*
PCC	*R*	*[9;-51;33]*	*3.70*	*55*	*0.008*
Precuneus	*L*	*[-3;-60;18]*	*3.66*		
Propofol study					
1) Pre-anesthesia wakefulness – average connectivity and one-sample t-test					
VTA-DMN	*R/L*	*Average*	*0.14 (SD 0.03)*		*<0.001*
2) Pre-anesthesia wakefulness – voxel-wise connectivity and one sample t-test					
Brainstem	*L*	*[0;-24;-18]*	*7.63*	*3020*	*<0.001*
Cerebellum	*L*	*[-27;-66;-33]*	*5.78*		
Cerebellum	*L*	*[-6;-54;-45]*	*4.98*		

PCC	*L*	*[-6;-36;30]*	*4.90*		
Parahippocampus	*L*	*[-24;-27;-18]*	*4.80*		
Hippocampus	*L*	*[-18;-18;-21]*	*4.50*		
Brainstem	*R*	*[3;-39;-27]*	*4.29*		
Prahippocampus	*R*	*[18;-30;-21]*	*4.21*		
Thalamus	*R*	*[3;-18;15]*	*4.20*		
Hippocampus	*R*	*[24;-24;-15]*	*4.09*		
3) Reduction of connectivity during propofol-induced anesthesia - average functional connectivity and paired t-test					
VTA-DMN	*R/L*	*Average*	*Reduction 139% Cohen's d=2,36*		*<0.001*
4) Reduction of connectivity during propofol-induced anesthesia - voxel-wise functional connectivity and paired t-test					
PCC	*L*	*[-6;-42;33]*	*4.19*	*97*	*0.015*
Precuneus	*L*	*[-9;-45;42]*	*4.03*		
PCC	*R*	*[3;-36;45]*	*3.12*		

Table 1. Reduced VTA iFC during anesthesia-induced unconsciousness.

For average functional connectivity: one-sample and paired t-test, one-tailed p<0.05. For voxel-wise functional connectivity: one sample and paired t-test, one-tailed p<0.05, FWE cluster-based corrected for multiple testing. Cohen's d is corrected for small sample size.

	Sevoflurane study					**Propofol study**	
	Awake pre	*Awake pre > Sevoflurane 3vol%*	*Awake pre > Sevoflurane 3vol% 'corrected'*	*Awake pre > Sevoflurane 2vol%*	*Awake post > Sevoflurane 3vol%*	*Awake pre*	*Awake pre > Propofol*
Number of significant voxels in the whole brain	2248,00	1768,00	1073,00	784,00	363,00	773,00	97,00
Number of voxels overlapping the DMN in PFC-cerebellum-precuneus/PCC	1932,00	1473,00	667,00	675,00	162,00	679,00	97,00
% Voxels	85,94	83,31	62,16	86,10	44,63	87,84	100,00
Overlap with main regions of the DMN: cerebellum, PFC and retrosplenial cortex							
Number of significant voxels in the cerebellum	1201,00	692,00	220,00	347,00	0,00	512,00	0,00
Number of voxels overlapping the cerebellum DMN	241,00	21,00	28,00	53,00	0,00	64,00	0,00
% Overlap	20,07	3,03	12,73	15,27	0,00	12,50	0,00
Number of significant voxels in the PFC	434,00	441,00	180,00	315,00	162,00	0,00	0,00

Number of voxels overlapping the PFC - DMN	356,00	219,00	153,00	255,00	144,00	0,00	0,00
% Overlap	82,03	49,66	85,00	80,95	88,89	0,00	0,00
Number of voxels in the precuneus/PCC	297,00	340,00	0,00	13,00	0,00	167,00	97,00
Number of voxels overlapping the precuneus/PCC - DMN	220,00	50,00	0,00	0,00	0,00	95,00	73,00
% Overlap	74,07	14,71	0,00	0,00	0,00	56,89	75,26

Table 2. VTA iFC: overlap with DMN mask from Yeo and colleagues.

Control analyses: partial volume effects. Due to potential confounding partial volume effects of neighboring neuromodulatory brainstem nuclei on VTA-seed time courses and limited spatial resolution of rs-fMRI, we performed two control analyses. *(i) VTA-DMN 'SRCC' FC.* We applied the so-called small region confound correction approach (SRCC) to control directly for partial volume effects of surrounding neuromodulatory nuclei, specifically DR, MR, LC, and PPN on VTA seed time course (**Fig. 2 A**). This resulted in a 'corrected' VTA time course by regression of confounding neuromodulatory nuclei time courses (**Fig. 2 B1, Tab. 3**). During wakefulness pre-anesthesia, the average VTA-DMN corrected connectivity was significant with mean z= 0.02 (SD 0.03; $p<0.05$). Voxel-wise connectivity was significant for ACC, superior frontal gyrus, parahippocampus, cerebellum, and caudate nucleus (**Fig. 2 B1, Tab. 3**). During sevoflurane 3vol%-induced anesthesia, average corrected connectivity was mean z=-0.02 (SD 0.03 ; $p<0.05$), corresponding to a significant connectivity reduction of 195% with a Cohen's d=0.89; voxel-wise connectivity was reduced with the ACC, with 62% overlap with the DMN (**Fig. 2 B2, Tab. 2-3**). These results match our finding of the canonical approach, suggesting that the connectivity reduction between VTA and DMN during sevoflurane 3 vol% is not confounded by brainstem neuromodulatory nuclei effects. *(ii) Changing seeds of seed-based functional connectivity: DMN iFC towards the VTA* to verify the independence of connectivity between the VTA and DMN from seed definition. During wakefulness pre-anesthesia, voxel-wise DMN-based iFC included – beyond canonical DMN regions - also the VTA (**Fig. 3, Tab. 4**). During sevoflurane 3vol%-induced anesthesia, voxel-wise connectivity between the DMN and VTA was diminished (**Fig. 3 B, Tab. 4**). This result indicates that choice of seed does not influence the reducing effect of sevoflurane 3vol% on seed-based functional connectivity between DMN and VTA.

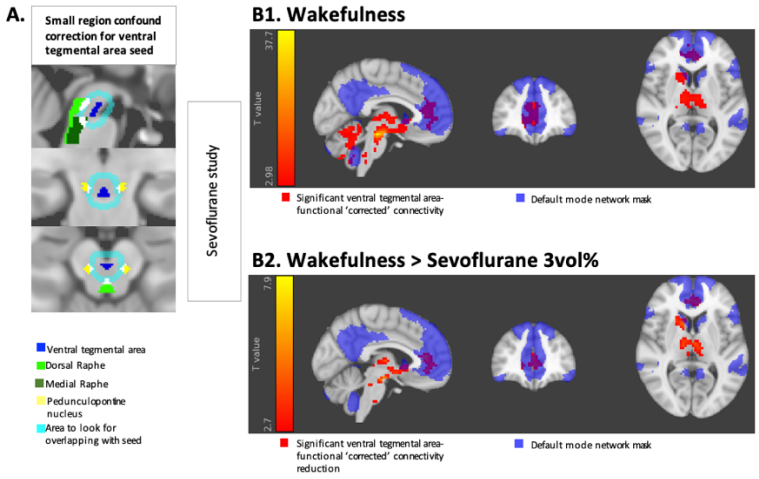

Figure 3. Control analysis. Sevoflurane decreases VTA 'corrected' FC.

A. VTA 'corrected' for seed-based iFC analysis*: All masks are derived from Harvard Ascending Arousal Network Atlas (Edlow et al., 2012): (blue) VTA mask, (cyan) VTA area 3mm away from mask, (light green) DR, (dark green) MR, (yellow) PPN, (white) overlapping VTA with neuromodulatory nuclei used for SRCC approach.* ***B1. VTA 'corrected' connectivity during wakefulness pre-anesthesia:*** *Voxel-wise one-sample t-test on z-maps of VTA 'corrected' connectivity during wakefulness, p<0.05 FWE cluster level corrected: significant connectivity in red-to-yellow, DMN mask derived from Yeo and colleagues (Yeo et al., 2011) in blue.* ***B2. VTA 'corrected' connectivity reduction for the contrast wakefulness pre-anesthesia > sevoflurane 3vol%.*** *Voxel-wise paired t-test on z-maps of VTA 'corrected' connectivity during wakefulness and sevoflurane 3vol%, p<0.05 FWE cluster level corrected: significant connectivity in red-to-yellow, DMN mask in blue.*

Regions	*Hemisphere*	*MNI Coordinates [x;y;z]*	*Z value*	*Cluster size*	*P value*
Sevoflurane study					
1) Pre-anesthesia wakefulness – average 'corrected' VTA iFC and one-sample t-test					
VTA-DMN	R/L	Average	0.02 (SD 0.03)		0.002
2) Pre-anesthesia wakefulness – voxel-wise 'corrected' VTA iFC and one-sample t-test					
Brainstem	R	[3;-18;-18]	>10	2055	<0.001
Brainstem	L	[-3;-24;-18]	7.77		
ACC	L	[-3;39;6]	4.81	333	<0.001
Paracingulate gyrus	R	[6;42;21]	3.62		
3) Reduction of 'corrected' VTA iFC during sevoflurane 3vol% - average connectivity and paired t-test					
VTA-DMN	R/L	Average	Reduction 195% Cohen's d= 0.89		0.0015
4) Reduction of 'corrected' VTA iFC during sevoflurane 3vol% - voxel-wise connectivity and paired t-test					
Thalamus	R	[3;-15;-15]	6.15	605	<0.001
Cerebellum	L	[-12;-36;-27]	4.39		

Brainstem	R	[12;-18;-15]	4.36		
Cerebellum	L	[-36;-57;-33]	5.14	118	0.010
Paracingulate gyrus	R	[3;39;24]	3.86	169	0.001
ACC	L	[-3;39;12]	3.80		

Table 3. Reduced VTA iFC during anesthesia-induced unconsciousness.

For average functional connectivity: one-sample and paired t-test, one-tailed p<0.05. For voxel-wise functional connectivity: one sample and paired t-test, one-tailed p<0.05, FWE cluster-based corrected for multiple testing. Cohen's d is corrected for small sample size.

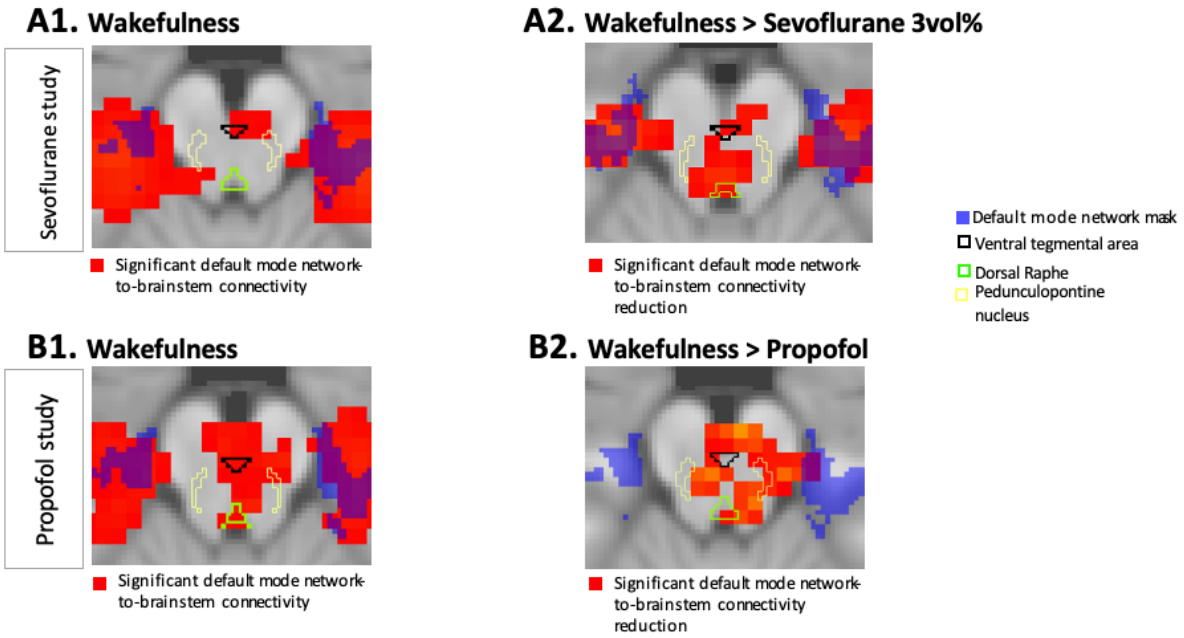

Figure 4. Control analysis. Sevoflurane 3vol% decreases DMN-VTA FC.

A. DMN-to-brainstem FC (close-up): A. Sevoflurane study. A1. Within-DMN iFC during wakefulness pre-anesthesia. *Voxel-wise one-sample t-test on z-maps of DMN iFC during wakefulness, p<0.001: significant connectivity in red-to-yellow, DMN mask derived from Yeo and colleagues (Yeo et al., 2011) in blue.* ***A2. Within-DMN iFC reduction for the contrast wakefulness pre-anesthesia > sevoflurane 3vol%.*** *Voxel-wise paired t-test on z-maps of DMN iFC during wakefulness and sevoflurane 3vol%, p<0.05 FWE cluster level corrected: significant connectivity in red-to-yellow, DMN mask in blue.* ***B. Propofol study. B1. Within-DMN iFC during wakefulness pre-anesthesia.*** *Voxel-wise one-sample t-test on z-maps of DMN iFC during wakefulness, p<0.05 FWE cluster level corrected: significant connectivity in red-to-yellow, DMN mask in blue.* ***B2. Within-DMN iFC reduction for the contrast wakefulness pre-anesthesia > propofol.*** *Voxel-wise paired t-test on z-maps of DMN iFC during wakefulness and propofol, p<0.05 FWE cluster level corrected: significant connectivity in red-to-yellow, DMN mask in blue.*

Regions	*Hemisphere*	*MNI Coordinates [x;y;z]*	*Z value*	*Cluster size*	*P value*
Sevoflurane study					
1) Pre-anesthesia wakefulness – average functional connectivity and one-sample t-test					
Within-DMN	R/L	Average	0.24 (SD 0.03)		<0.001
2) Pre-anesthesia wakefulness – voxel-wise connectivity and one-sample t-test					
Angular gyrus	R	[45;-63;39]	>10	1940	<0.001
Precuneus	L	[-6;-60;33]	>10	9975	<0.001
Brainstem	R	[0;-24;-18]	3.90		
Anterior basal forebrain	L	[-6;0;-12]	3.30		
Cerebellum	R	[45;-69;-39]	5.94	622	<0.001
Cerebellum	L	[-42;-72;-39]	5.70	750	<0.001
3) Reduction of connectivity during sevoflurane 3vol% - average connectivity and paired t-test					
Within-DMN	R/L	Average	Reduction 39% Cohen's d= 1.97		<0.001
4) Reduction of connectivity during sevoflurane 3vol% - voxel-wise connectivity and paired-test					
Precuneus	L	[-3;-63;33]	7.31	1386	<0.001
PCC	R	[6;-45;24]	6.87		
Cerebellum	R	[42;-72;-36]	6.81	499	<0.001
Superior frontal gyrus	R	[18;33;42]	6.65	1953	<0.001
Middle frontal gyrus	L	[-24;36;42]	5.92		
Angular gyrus	R	[45;-63;36]	5.87	356	<0.001
Middle temporal gyrus	L	[-63;-21;-15]	5.83	180	0.001
Parahippocampus	R	[27;-30;-15]	4.87	164	0.003
Brainstem	R	[6;-30;-12]	3.95		
Brainstem	L	[0;-33;-21]	3.50		
Hippocampus	L	[-27;-27;-18]	4.32	144	0.006

Table 4. Reduced DMN iFC during sevoflurane 3vol%.

For average functional connectivity: one-sample and paired t-test, one-tailed p<0.05. For voxel-wise functional connectivity: one sample and paired t-test, one-tailed p<0.05, FWE cluster-based corrected for multiple testing. Cohen's d is corrected for small sample size.

Regions	*Hemisphere*	*MNI Coordinates [x;y;z]*	*Z value*	*Cluster size*	*P value*
Propofol study					
1) Pre-anesthesia wakefulness – average functional connectivity and one-sample t-test					
Within-DMN iFC	R/L	Average	0.37 (SD 0.06)		<0.001
2) Pre-anesthesia wakefulness – voxel-wise functional connectivity and one-sample t-test					
Precuneus	R	[9;-54;18]	6.77	3226	<0.001
PCC	L	[-9;-48;27]	6.60		
ACC	L	[-3;-15;30]	4.55		
Brainstem	L	[0;-33;-24]	4.52		
Parahippocampus	R	[21;-18;-27]	4.52		
Angular gyrus	L	[-45;-66;36]	6.24	771	<0.001
Middle temporal gyrus	L	[-63;-9;-24]	6.23	678	<0.001
Medial frontal gyrus	R	[9;57;-12]	5.86	2938	<0.001
Superior frontal gyrus	L	[-21;36;45]	5.60		
Middle temporal gyrus	R	[54;-69;30]	5.73	658	<0.001
Cerebellum	R	[30;-87;-30]	5.07	1056	<0.001
3) Reduction of connectivity during propofol-induced anesthesia – average connectivity and paired t-test					
Within-DMN iFC	R/L	Average	Reduction 30% Cohen's d= 1.40		<0.001
4) Reduction of connectivity during propofol-induced anesthesia – voxel-wise connectivity and paired t-test					
Inferior temporal gyrus	R	[51;-3;-36]	4.18	192	<0.001
Brainstem	L	[-3;-18;-21]	4.05	111	0.008
Parahippocampus	L	[-15;-30;-15]	3.78		
PCC	L	[0;-54;24]	4.02	237	<0.001
Lingual gyrus	R	[3;-69;-3]	3.73		
Paracingulate gyrus	R	[0;45;9]	3.94	279	<0.001
Medial frontal gyrus	R	[15;60;-12]	3.94		

Table 5. Reduced DMN iFC during propofol-induced anesthesia.

For average functional connectivity: one-sample and paired t-test, one-tailed p<0.05. For voxel-wise functional connectivity: one sample and paired t-test, one-tailed p<0.05, FWE cluster-based corrected for multiple testing. Cohen's d is corrected for small sample size.

Control for different anesthetic: Propofol. During wakefulness pre-anesthesia, average connectivity between the VTA and DMN was significant with mean z= 0.14 (SD 0.03 p<0.05). Voxel-wise connectivity was significant for PCC, precuneus, parahippocampus, basal ganglia, thalamus, upper brainstem, amygdala, and cerebellum, with 88% overlap with the DMN (**Fig. 1 C1, Tab. 1-2**). This connectivity pattern resembles VTA connectivity maps of both the sevoflurane data set above and previous studies (Murty et al., 2014; Spindler et al., 2021; Zhang et al., 2016), supporting further the reliability of our approach. During propofol-induced anesthesia, VTA-DMN average connectivity was mean z=-0.05 (SD 0.08; p<0.05), corresponding to a significant connectivity reduction of 139% with a Cohen's d=2.36. Voxel-wise connectivity was reduced in the PCC and precuneus, with 100% overlap with the DMN (**Fig. 1 C2, Tab. 1-2**). This result indicates that the reduction in connectivity during anesthesia is caused independently from the anesthetic agent and its molecular mechanism of action.

Control for different sevoflurane concentration: sevoflurane 2vol%. Next, we controlled for potential concentration effects of the anesthetic agent, namely sevoflurane 3vol%. During sevoflurane 2vol%-induced anesthesia, VTA-DMN average connectivity was mean z=-0.02 (SD 0.07; p<0.05), corresponding to a significant connectivity reduction of 151% as compared with wakefulness pre-anesthesia with a Cohen's d=0.54; voxel-wise connectivity was reduced in the ACC, with 86% overlap with the DMN (**Fig. 4, Tab. 2 & 6**). This result indicates that the VTA connectivity reduction during sevoflurane is independent from sevoflurane concentration.

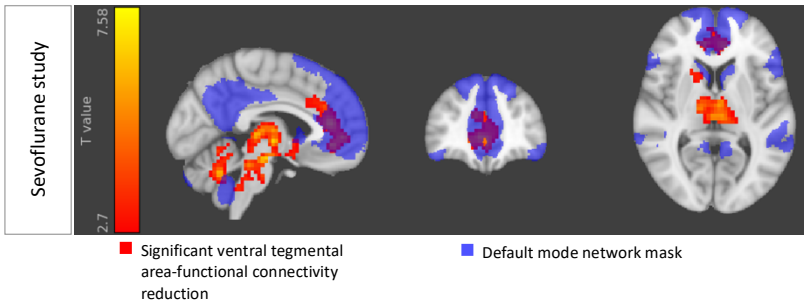

Figure 5. Control analysis. Sevoflurane 2vol% decreases VTA iFC.

***VTA iFC** reduction for the contrast wakefulness pre-anesthesia > sevoflurane 2vol%. Voxel-wise paired t-test on z-maps of VTA iFC during wakefulness and sevoflurane 2vol%, p<0.05 FWE cluster level corrected: significant connectivity in red-to-yellow, DMN mask in blue.*

Regions	*Hemisphere*	*MNI Coordinates [x;y;z]*	*Z value*	*Cluster size*	*P value*
Sevoflurane study					
1) Reduction of VTA iFC during sevoflurane 2vol% - average connectivity and paired t-test					
VTA-DMN	R/L	Average	Reduction 151% Cohen's d= 0.54		0.024
2) Reduction of VTA iFC during sevoflurane 2vol% - voxel-wise connectivity and paired t-test					
Cerebellum	L	[-39;-54;-36]	5.99	1905	<0.001
Brainstem	R	[6;-12;-15]	5.96		
Thalamus	L	[-3;-12;-3]	5.48		
Paracingulate gyrus	R	[3;39;24]	5.14	534	<0.001
ACC	L	[-3;39;12]	4.64		

Table 6. Reduced VTA iFC during sevoflurane 2vol%.

For average functional connectivity: one-sample and paired t-test, one-tailed p<0.05. For voxel-wise functional connectivity: one sample and paired t-test, one-tailed p<0.05, FWE cluster-based corrected for multiple testing. Cohen's d is corrected for small sample size.

Control for contrast: sevoflurane 3vol% relative to wakefulness post-anesthesia. Finally, we controlled for potential contrast effects of the anesthetics, namely induction of versus recovery from sevoflurane-induced anesthesia. During sevoflurane 3vol%-induced anesthesia relative to wakefulness post-anesthesia, VTA-DMN average connectivity during wakefulness post-anesthesia was mean z=0.03 (SD 0.03; p<0.05), corresponding to a significant connectivity reduction of 139% during 3vol% as compared with wakefulness post-anesthesia with a Cohen's d=0.91; voxel-wise connectivity was reduced in the ACC, with 46% overlap with the DMN (**Fig. 5, Tab. 2 & 7**). This result overlaps with that of sevoflurane 3vol%-induced VTA connectivity reduction relative to wakefulness pre-anesthesia, indicating that this connectivity reduction is independent from anesthesia contrast.

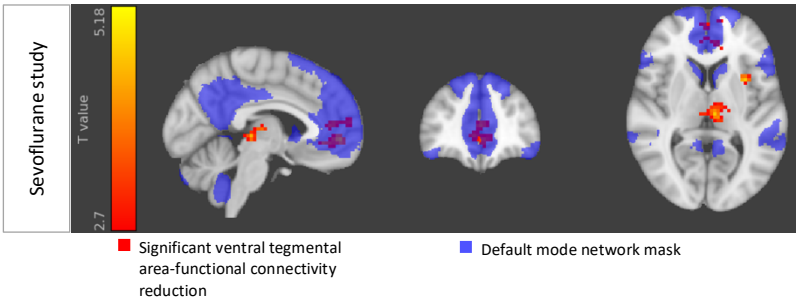

Figure 6. Control analysis. Sevoflurane 3vol% decreases VTA iFC relative to wakefulness post-anesthesia.

VTA iFC reduction for the contrast wakefulness post-anesthesia > sevoflurane 3vol%. Voxel-wise paired t-test on z-maps of VTA iFC during wakefulness post-anesthesia and sevoflurane 3vol%, p<0.05 FWE cluster level corrected: significant connectivity in red-to-yellow, DMN mask in blue.

Regions	*Hemisphere*	*MNI Coordinates [x;y;z]*	*Z value*	*Cluster size*	*P value*
Sevoflurane study					
1) Reduction VTA iFC during sevoflurane 3vol% relative to wakefulness post-anesthesia - average connectivity and paired t-test					
VTA-DMN	R/L	Average	Reduction 139% Cohen's d= 0.91		0.0015
2) Reduction of VTA iFC during sevoflurane 3vol% relative to wakefulness post-anesthesia - voxel-wise connectivity and paired t-test					
Insula	R	[36;15;-6]	4.53	95	0.034
Insula	L	[-39;9;-6]	4.18	106	0.020
Thalamus	R	[6;-24;-3]	4.17	114	0.013
Paracingulate gyrus	L	[-3;51;-3]	3.95	160	0.002
Superior frontal gyrus	R	[3;57;9]	3.54		

Table 7. Reduced VTA iFC during sevoflurane 3vol% relative to wakefulness post-anesthesia.

For average functional connectivity: one-sample and paired t-test, one-tailed p<0.05. For voxel-wise functional connectivity: one sample and paired t-test, one-tailed p<0.05, FWE cluster-based corrected for multiple testing. Cohen's d is corrected for small sample size.

3.1.2. Anesthesia-induced unconsciousness is related to a-cBF (Ch1-Ch3) functional connectivity reductions

Main result: sevoflurane 3vol%. During wakefulness pre-anesthesia, voxel-wise a-cBF connectivity was significant to caudate nucleus, thalamus, olfactory gyrus, nucleus accumbens, hippocampus, ACC,

insula, and frontal medial cortex (**Fig. 6 B1, Tab. 8**), mainly overlapping with anterior portions of the DMN. This pattern partially resembles that of previous studies on a-cBF connectivity, we did not find significant positive connectivity to the PCC/precuneus areas as previous reports (Fritz et al., 2019), however connectivity to anterior areas in the forebrain was successfully replicated. From these voxels, 61% overlapped with the anterior portion of the DMN (**Tab. 9**). Average a-cBF to anterior DMN connectivity was significant with mean z= 0.19 (SD 0.08; p<0.05). During sevoflurane 3vol%-induced anesthesia, a-cBF to anterior DMN average connectivity was mean z=0.06 (SD 0.04; p<0.05), corresponding to a significant connectivity reduction of 66% with a Cohen's d=0.73; voxel-wise connectivity was reduced principally to the ACC and mPFC, with 76% overlap with anterior portion of the DMN (**Fig. 6 B2, Tab. 8-9**). This result indicates that connectivity between a-cBF with anterior DMN is reduced by sevoflurane 3vol% anesthesia.

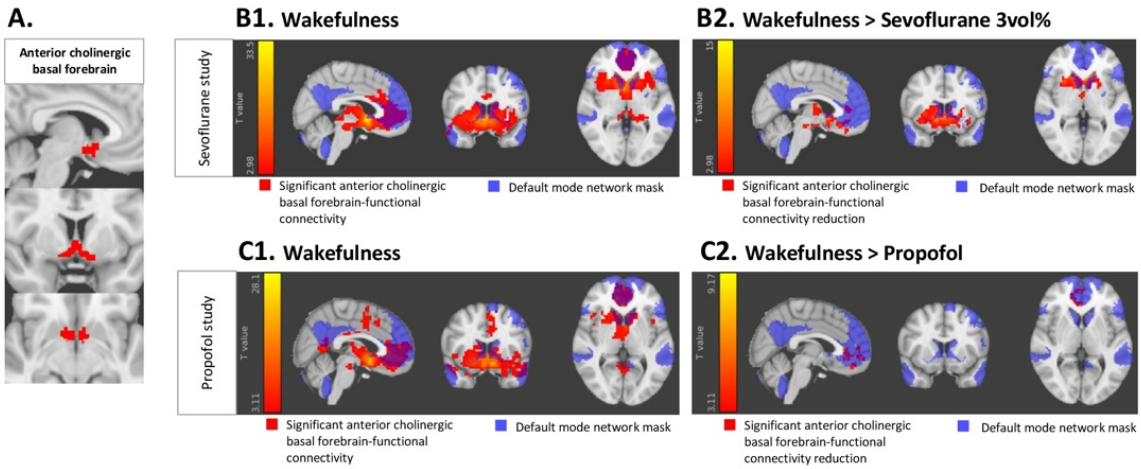

Figure 7. Anesthesia-induced unconsciousness is associated with a reduced a-cBF iFC.

A. a-cBF mask for seed-based functional connectivity analysis. *The mask is derived from (Fritz et al., 2019).* ***B. Sevoflurane study. B1. a-cBF connectivity during wakefulness pre-anesthesia.*** *Voxel-wise one-sample t-test on z-maps of a-cBF iFC during wakefulness, p<0.05 FWE cluster level corrected: significant connectivity in red-to-yellow, DMN mask derived from Yeo and colleagues (Yeo et al., 2011) in blue.* ***B2. a-cBF connectivity reduction for the contrast wakefulness pre-anesthesia > sevoflurane 3vol%****. Voxel-wise paired t-test on z-maps of a-cBF iFC during wakefulness and sevoflurane 3vol%, p<0.05 FWE cluster level corrected: significant connectivity in red-to-yellow, DMN mask in blue.* ***C. Propofol study. C1. a-cBF connectivity during wakefulness pre-anesthesia.*** *Voxel-wise one-sample t-test on z-maps of a-cBF iFC during wakefulness, p<0.05 FWE cluster level corrected: significant connectivity in red-to-yellow, DMN mask derived from Yeo and colleagues (Yeo et al., 2011) in blue.* ***C2. a-cBF connectivity reduction for the contrast wakefulness pre-anesthesia > propofol****. Voxel-wise paired t-test on z-maps of a-cBF iFC during wakefulness and propofol anesthesia, p<0.05 FWE cluster level corrected: significant connectivity in red-to-yellow, DMN mask in blue.*

Regions	*Hemisphere*	*MNI Coordinates [x;y;z]*	*Z value*	*Cluster size*	*P value*
Sevoflurane study					
1) Pre-anesthesia wakefulness – average functional connectivity and one-sample t-test					
a-CBF-anterior DMN	*L/R*	*Average*	*0.19 (SD 0.08)*		*<0.001*
2) Pre-anesthesia wakefulness – voxel-wise connectivity and one sample t-test					
Subcallosal cortex	*R*	*[3;6;-6]*	*7.75*	*4629*	*<0.001*
Accumbens	*R*	*[15;18;-6]*	*6.88*		
ACC	*R*	*[9;39;9]*	*5.70*		
3) Reduction of connectivity during sevoflurane 3vol% - average connectivity and paired t-test					
a-CBF-anterior DMN	*L/R*	*Average*	*Reduction 66% Cohen's d=0.73*		*0.0058*
4) Reduction of connectivity during sevoflurane 3vol% - voxel-wise connectivity and paired t-test					
Accumbens	*R*	*[15;18;-6]*	*6.22*	*1403*	*<0.005*
Subcallosal cortex	*R*	*[0;15;-3]*	*5.77*		
Caudate nucleus	*L*	*[-15;21;-3]*	*5.29*		
Propofol study					
1) Pre-anesthesia wakefulness – average functional connectivity and one-sample t-test					
a-cBF-anterior DMN	*L/R*	*Average*	*0.21 (SD 0.07)*		*<0.001*
2) Pre-anesthesia wakefulness – voxel-wise connectivity and one sample t-test					
Subcallosal cortex	*L*	[-3;6;-9]	6.76	3478	*<0.001*
Caudate nucleus	*L*	[-12;18;-3]	6.18		
Paracingulate gyrus	*L*	[-3;9;54]	4.52	411	*<0.001*
Superior frontal gyrus	*L*	[-24;3;57]	4.32		
ACC	*L*	[-6;9;30]	4.29		
Lingual gyrus	*L*	[0;-57;6]	4.03	88	*0.019*
Precuneus	*R*	[3;-54;18]	3.37		
Precentral gyrus	*L*	[-51;-3;42]	4.01	92	*0.015*
Postcentral gyrus	*L*	[-51;-15;36]	3.34		
Fusiform gyrus	*L*	[-33;-63;-21]	3.47	84	*0.024*
Cerebellum	*L*	[-30;-54;-27]	3.46		
3) Reduction of connectivity during propofol-induced anesthesia - average connectivity and paired t-test					
a-cBF-anterior DMN	*L/R*	*Average*	*Reduction 98% Cohen's d=1.83*		
4) Reduction of connectivity during propofol-induced anesthesia - voxel-wise connectivity and paired t-test					
ACC	*R*	*[6;36;-6]*	*4.78*	*288*	*<0.001*
Paracingulate gyrus	*R*	*[12;48;-3]*	*4.06*		
ACC	*L*	*[-6;36;-6]*	*3.77*		

Table 8. Reduced a-cBF iFC during anesthesia-induced unconsciousness.

For average functional connectivity: one-sample and paired t-test, one-tailed p<0.05. For voxel-wise functional connectivity: one sample and paired t-test, one-tailed p<0.05, FWE cluster-based corrected for multiple testing. Cohen's d is corrected for small sample size.

	Sevoflurane study				**Propofol study**	
	Awake pre	*Awake pre>sevoflurane 3vol%*	*Awake pre>sevoflurane 2vol%*	*Awake post>sevofluane 3vol%*	*Awake pre*	*Awake pre>propofol*
# Significant Voxels	4629,00	1403	323,00	737,00	4173,00	288,00
# Voxels only in prefrontal cortex-cerebellum-precuneus/posterior cingulate cortex	1140,00	172,00	87,00	48,00	1593,00	281,00
% Voxels	24,63	12,26	26,93	6,51	38,17	97,57
# Voxels from all significant clusters only in cerebellum	0,00	0,00	0,00	0,00	67,00	0,00
# Voxels overlapping with template	0,00	0,00	0,00	0,00	0,00	0,00
% Overlap	0,00	0,00	0,00	0,00	0,00	0,00
# Voxels from all significant clusters only in prefrontal cortex	1140,00	172,00	87,00	48,00	1402,00	281,00
# Voxels overlapping with template	697,00	130,00	36,00	48,00	731,00	229,00
% Overlap	61,14	75,58	41,38	100,00	52,14	81,49
# Voxels from all significant clusters only in precuneus/posterior cingulate cortex	0,00	0,00	0,00	0,00	124,00	0,00
# Voxels overlapping with template	0,00	0,00	0,00	0,00	51,00	0,00
% Overlap	0,00	0,00	0,00	0,00	41,13	0,00

Table 9. a-cBF iFC: overlap with DMN mask from Yeo and colleagues.

Control analyses: (ii) Changing seeds of seed-based functional connectivity: DMN iFC towards the a-cBF to verify the independence of connectivity between the a-cBF and DMN from seed definition. During wakefulness pre-anesthesia, voxel-wise DMN-based functional connectivity included – beyond canonical DMN regions - also the a-cBF (**Fig. 8**). During sevoflurane 3vol%-induced anesthesia, voxel-wise connectivity between the DMN and a-cBF showed only a trend towards reduction (single-voxel height threshold of p<0.005, uncorrected for multiple comparisons) (**Fig. 8**). This result partially supports the idea that sevoflurane 3vol% reduces a-cBF to anterior DMN connectivity.

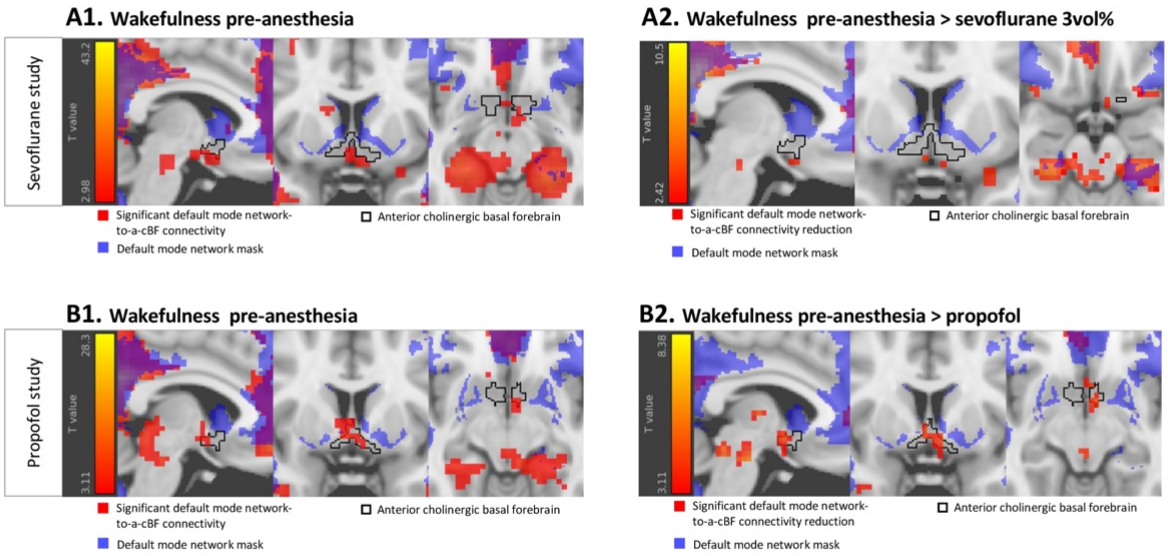

Figure 8. Control analysis. Sevoflurane 3vol% decreases DMN-a-cBF FC.

A. DMN-to-a-cBF FC (close-up): A. Sevoflurane study. A1. Within-DMN iFC during wakefulness pre-anesthesia. *Voxel-wise one-sample t-test on z-maps of DMN iFC during wakefulness, p<0.005 uncorrected: significant connectivity in red-to-yellow, DMN mask derived from Yeo and colleagues (Yeo et al., 2011) in blue, a-cBF mask delineated in black.* ***A2. Within-DMN iFC reduction for the contrast wakefulness pre-anesthesia > sevoflurane 3vol%.*** *Voxel-wise paired t-test on z-maps of DMN iFC during wakefulness and sevoflurane 3vol%, p<0.01 uncorrected: significant connectivity in red-to-yellow, DMN mask in blue, a-cBF mask delineated in black.* ***B. Propofol study. B1. Within-DMN iFC during wakefulness pre-anesthesia.*** *Voxel-wise one-sample t-test on z-maps of DMN iFC during wakefulness, p<0.005 uncorrected: significant connectivity in red-to-yellow, DMN mask in blue, a-cBF mask delineated in black.* ***B2. Within-DMN iFC reduction for the contrast wakefulness pre-anesthesia > propofol.*** *Voxel-wise paired t-test on z-maps of DMN iFC during wakefulness and propofol, p<0.005 uncorrected: significant connectivity in red-to-yellow, DMN mask in blue, a-cBF mask delineated in black.*

Control for different anesthetic: Propofol. During wakefulness pre-anesthesia, average connectivity between the a-cBF and anterior DMN was significant with mean z= 0.21 (SD 0.07 p<0.05). Voxel-wise connectivity was significant for prefrontal areas in ACC, paracingulate gyrus, superior frontal gyrus, subcortical areas such as thalamus, basal ganglia, ventral brainstem, and posterior cortical areas such as PCC/precuneus, with 52% overlap with the anterior portion of the DMN and 51% with the posterior portion of the DMN, such as PCC/precuneus (**Fig. 7 C1, Tab. 9**). This connectivity pattern resembles a-cBF connectivity maps of both the sevoflurane data set above and previous studies (Fritz et al., 2019) supporting further the reliability of our approach. During propofol-induced anesthesia, a-cBF to anterior DMN showed a significant connectivity reduction of 98% with a Cohen's d=1.83. Voxel-wise connectivity was reduced in principally the ACC, with 81% overlap with the anterior DMN (**Fig. 7 C2, Tab. 9**). This result indicates that the reduction in connectivity during anesthesia is caused independently from the anesthetic agent and its molecular mechanism of action.

Control for different sevoflurane concentration: sevoflurane 2vol%. Next, we controlled for potential concentration effects of the anesthetic agent. During sevoflurane 2vol%-induced anesthesia, reduction of a-cBF iFC showed a trend of reduction in the anterior portion of the DMN, in average connectivity was mean z=-0.07 (SD 0.15; p<0.05), this corresponds to a 59% (p<0.1) of reduction as compared with wakefulness pre-anesthesia with a Cohen's d=0.36; voxel-wise connectivity was reduced in the brainstem and ACC (single-voxel height threshold of p<0.01, FWE corrected) with 41% overlap with the anterior portion of the DMN (**Fig. 9, Tab. 9-10)**. This result supports only partially the idea that sevoflurane 2vol% influences a-cBF to anterior DMN connectivity.

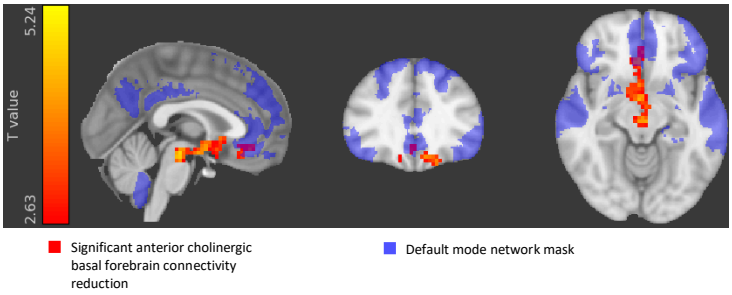

Figure 9. Control analysis. Sevoflurane 2vol% decreases a-cBF iFC.

a-cBF iFC reduction for the contrast wakefulness pre-anesthesia > sevoflurane 2vol%. Voxel-wise paired t-test on z-maps of a-cBF iFC during wakefulness and sevoflurane 2vol%, single voxel height threshold of p<0.01 p<0.05 FWE cluster level corrected: significant connectivity in red-to-yellow, DMN mask in blue.

Regions	*Hemisphere*	*MNI Coordinates [x;y;z]*	*Z value*	*Cluster size*	*P value*
Sevoflurane study					
1) Reduction of a-cBF iFC during sevoflurane 2vol% - average connectivity and paired t-test					
a-cBF-DMN	R/L	Average	Reduction 59% Cohen's d= 0.36		0.0875
2) Reduction of a-cBF iFC during sevoflurane 2vol% - voxel-wise connectivity and paired t-test					
Frontal orbital cortex	L	[-15;36;-18]	3.83	323	<0.001
Brainstem	R	[0;-21;-15]	3.62		
Subcallosal cortex	L	[3;30;-15]	3.50		

Table 10. Reduced a-cBF iFC during sevoflurane 2vol%.

For average functional connectivity: one-sample and paired t-test, one-tailed p<0.05. For voxel-wise functional connectivity: one sample and paired t-test, one-tailed p<0.05, FWE cluster-based corrected for multiple testing. Cohen's d is corrected for small sample size.

Control for contrast: sevoflurane 3vol% relative to wakefulness post-anesthesia. Finally, we controlled for potential contrast effects of the anesthetics, namely induction of versus recovery from sevoflurane-induced anesthesia. During sevoflurane 3vol%-induced anesthesia relative to wakefulness post-anesthesia, a-cBF to anterior DMN average connectivity during wakefulness post-anesthesia was mean z=0.05 (SD 0.05; p<0.05), corresponding to a significant connectivity reduction of 42% during 3vol% as compared with wakefulness post-anesthesia with a Cohen's d=0.46; voxel-wise connectivity was reduced in the mPFC, with 100% overlap with the anterior portion of the DMN (**Fig. 10, Tab. 9 & 11**). This result overlaps with that of sevoflurane 3vol%-induced VTA connectivity reduction relative to wakefulness pre-anesthesia, indicating that this connectivity reduction is independent from anesthesia contrast.

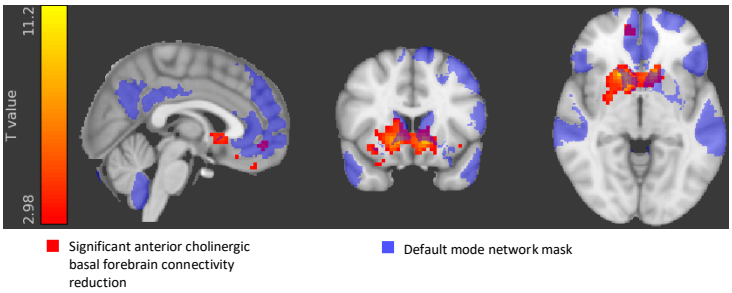

Figure 10. Control analysis. Sevoflurane 3vol% decreases a-cBF iFC relative to wakefulness post-anesthesia.

a-cBF iFC reduction for the contrast wakefulness post-anesthesia > sevoflurane 3vol%. Voxel-wise paired t-test on z-maps of a-cBF iFC during wakefulness post-anesthesia and sevoflurane 3vol%, p<0.05 FWE cluster level corrected: significant connectivity in red-to-yellow, DMN mask in blue.

Regions	*Hemisphere*	*MNI Coordinates [x;y;z]*	*Z value*	*Cluster size*	*P value*
Sevoflurane study					
1) Reduction a-cBF iFC during sevoflurane 3vol% relative to wakefulness post-anesthesia - average connectivity and paired t-test					
a-cBF-DMN	R/L	Average	Reduction 42% Cohen's d= 0.46		0.045
2) Reduction of a-cBF iFC during sevoflurane 3vol% relative to wakefulness post-anesthesia - voxel-wise connectivity and paired t-test					
Accumbens	L	[-12;18;-6]	5.59	645	<0.001
Putamen	R	[18;18;-3]	5.35		
Frontal medial cortex	R	[12;9;-9]	3.72	92	0.014

Table 11. Reduced a-cBF iFC during sevoflurane 3vol% relative to wakefulness post-anesthesia.

For average functional connectivity: one-sample and paired t-test, one-tailed p<0.05. For voxel-wise functional connectivity: one sample and paired t-test, one-tailed p<0.05, FWE cluster-based corrected for multiple testing. Cohen's d is corrected for small sample size.

3.1.3. Reduction of within-DMN BOLD connectivity during anesthesia-induced unconsciousness is mediated by reduction of VTA-DMN connectivity reductions

Main result: sevoflurane 3vol%. To test whether DMN connectivity reduction during anesthesia-induced unconsciousness is mediated by reductions of VTA-DMN connectivity, we performed a mediation analysis. We found a significant indirect effect of average connectivity between VTA-DMN, with partially standardized indirect effect *ab*= -0.48 (95% CI: [-0.88;-0.18]). Standardized *ab* is an estimate of the indirect effect of average connectivity between VTA and DMN on DMN connectivity; it refers to the product of regression coefficients *a* and *b* in the path model divided by the standard deviation of the dependent variable DMN average connectivity; it is significant when it's 95% confidence interval does not include zero. The significant indirect effect *ab* demonstrates that the effect of sevoflurane 3vol% on DMN connectivity can be partially explained by VTA connectivity reduction during the anesthesia (**Fig. 11 A3**).

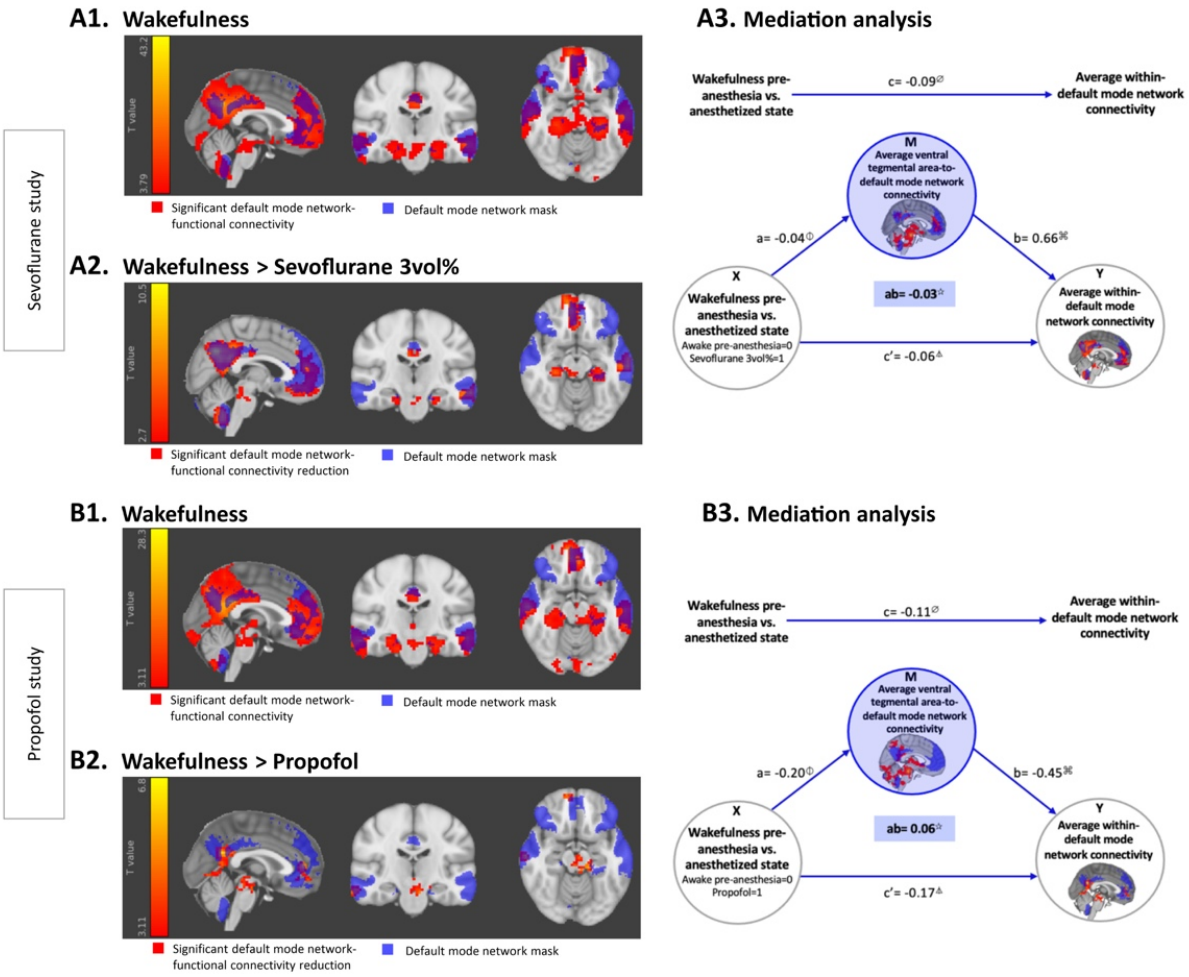

Figure 11. Anesthesia-induced unconsciousness is associated with a reduced within-DMN FC, which is mediated by connectivity reductions between VTA-DMN.

A. Sevoflurane study. A1. DMN iFC during wakefulness pre-anesthesia. *Voxel-wise one-sample t-test on z-maps of DMN iFC during wakefulness, p<0.05 FWE cluster level corrected: significant connectivity in red-to-yellow, DMN mask derived from Yeo and colleagues (Yeo et al., 2011) in blue.* ***A2. DMN iFC reduction for the contrast wakefulness pre-anesthesia > sevoflurane 3vol%.*** *Voxel-wise paired t-test on z-maps of DMN iFC during wakefulness and sevoflurane 3vol%-induced anesthesia, p<0.05 FWE cluster level corrected: significant connectivity in red-to-yellow, DMN mask in blue.* ***A3. Mediation analysis for sevoflurane 3vol%.*** *Reduction of average within-DMN FC during sevoflurane 3vol% is mediated by average VTA-DMN FC, demonstrated by a significant indirect effect* ab *with partially standardized value -0.48 (i.e.,* ab *divided by the standard deviation of the dependent variable), 95% CI: ☆[-0.88;-0.18]. 95% CI for further regression coefficients: ∅[-0.12;-0.07], ♢[-0.06;-0.02], ⌘[0.29;1.03], ⧋[-0.09;-0.04], ☆[-0.05;-0.01].* ***B. Propofol study. B1. DMN iFC during wakefulness pre-anesthesia.*** *Voxel-wise one-sample t-test on z-maps of DMN iFC during wakefulness, p<0.05 family-wise error cluster level corrected: significant connectivity in red-to-yellow, DMN mask in blue.* ***B2. DMN iFC reduction for the contrast wakefulness pre-anesthesia > propofol.*** *Voxel-wise paired t-test on z-maps of DMN iFC during wakefulness and propofol-induced anesthesia, p<0.05 FWE cluster level corrected: significant connectivity in red-to-yellow, DMN mask in blue.* ***B3. Mediation analysis for propofol****. Reduction of average within-DMN FC during propofol is mediated by average VTA-DMN FC, demonstrated by a significant indirect effect* ab *with partially standardized value 0.76, 95% CI: ☆[0.01;1.77]. 95% CI for further regression coefficients: ∅[-0.16;-0.06], ♢[-0.25;-0.14], ⌘[-0.76;+0.12], ⧋[-0.27;-0.07], ☆[0.00;0.15].*

Control analyses: partial volume effects. We confirmed this finding by repeating the mediation analysis with values derived from the 'SRCC' VTA iFC analysis. We found a significant indirect effect of corrected VTA connectivity, with a partially standardized effect *ab*= -0.35 (95% CI: ☆[-0.64;-0.11]) (**Fig. 12**). This indicates that the mediation effect of connectivity between VTA and DMN is not confounded by brainstem neuromodulatory nuclei effects.

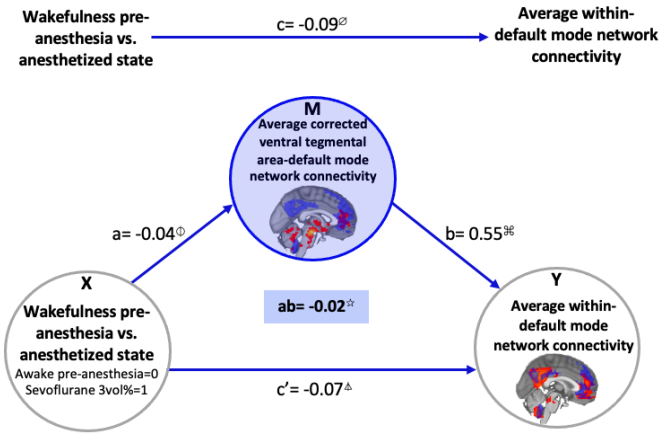

Figure 12. Control analysis. Mediation analysis. Sevoflurane study. Within-DMN FC decrease during sevoflurane 3vol% is mediated by DMN and 'corrected' VTA FC.

Mediation analysis. Reduction of average connectivity within the default mode network during sevoflurane 3vol% is mediated by average 'corrected' connectivity between ventral tegmental area and default mode network, demonstrated by a significant indirect effect ab with partially standardized value -0.35 (i.e., ab divided by the standard deviation of the dependent variable), 95% CI: ☆[-0.64;-0.11]. 95% CI for further regression coefficients: ∅[-0.12;-0.07], ◊[-0.06;-0.01], ⌘[0.16;0.93], △[-0.10;-0.05], ☆[-0.04;-0.01]

Control for different anesthetic: Propofol. Next, we tested whether this mediation effect is dependent on the anesthetic agent. Therefore, we repeated our mediation approach on the propofol data set. We found a significant indirect effect of propofol-induced connectivity reduction between VTA and DMN on DMN connectivity reduction, with partially standardized effect *ab* = 0.76 (95% CI: ☆[0.01;1.77]) (**Fig. 11 B3**). This indicates that the mediation effect does not depend on the anesthetic agent.

Control for different sevoflurane concentration: Sevoflurane 2vol%. To control for possible concentration-dependent effects, we performed the mediation analysis for sevoflurane 2vol%-induced anesthesia. We found a significant indirect effect for sevoflurane 2vol%-induced VTA iFC

reduction, with partially standardized effect *ab*= -0.33 (95% CI: ☆[-0.74;-0.03]) (**Fig. 13 B**). This indicates that the mediation effect does not depend on the anesthetic agent concentration.

A. Wakefulness > Sevoflurane 2vol%.

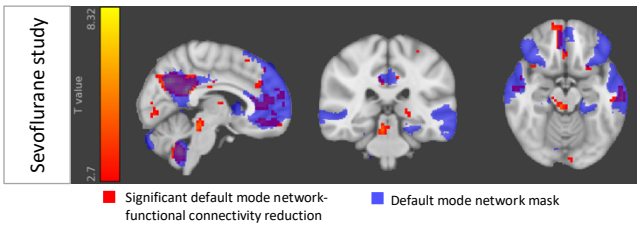

B. Mediation analysis

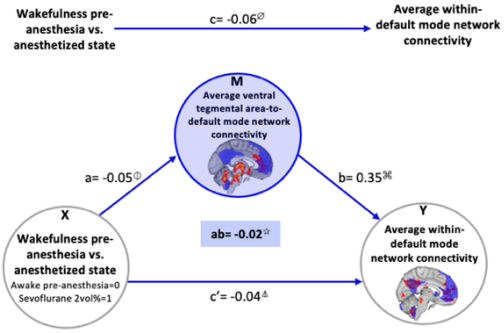

Figure 13. Control analysis. Mediation analysis. Sevoflurane study. Within-DMN FC decreases during sevoflurane 2vol% and is mediated by DMN-VTA FC.

A. Reduction of DMN iFC with sevoflurane 2vol%. *Voxel-wise paired t-test on z-maps of DMN iFC during wakefulness and sevoflurane 2vol%, p<0.05 FWE cluster level corrected: significant connectivity in red-to-yellow, DMN mask in blue.* ***B. Mediation analysis.*** *Reduction of average within-DMN FC during sevoflurane 2vol% is mediated by average VTA-DMN FC, demonstrated by a significant indirect effect ab with partially standardized value -0.33 (i.e., ab divided by the standard deviation of the dependent variable), 95% CI: ☆[-0.74;-0.03]. 95% CI for further regression coefficients: ∅[-0.09;-0.03], Φ[-0.09;-0.004], ⌘[0.11;0.59], Δ[-0.07;- 0.02], ☆[-0.04;-0.001].*

Control for contrast: sevoflurane 3vol% relative to wakefulness post-anesthesia. Finally, we controlled for potential contrast effects, namely induction of versus recovery from sevoflurane-induced anesthesia. Using connectivity z-maps for sevoflurane 3vol% and awake post-anesthesia, we found a significant indirect effect of sevoflurane 3vol% recovery-induced VTA connectivity increase on DMN connectivity increase during wakefulness, with partially standardized effect *ab*) = -0.72 (95% CI: ☆[-1.24;-0.28]) (**Fig. 14 B**). This indicates that the mediation effect does not depend on anesthesia contrast.

B. Wakefulness post-anesthesia> Sevoflurane 3vol%.

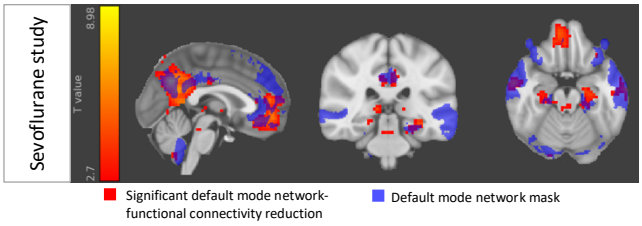

B. Mediation analysis

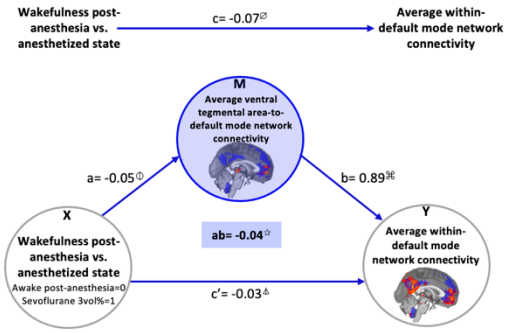

Figure 14. Control analysis. Mediation analysis. Sevoflurane study. Within-DMN FC decreases during sevoflurane 3vol% relative to wakefulness post-anesthesia and is mediated by DMN-VTA FC.

A. Reduction of DMN iFC with sevoflurane 3vol% relative to wakefulness post-anesthesia. *Voxel-wise paired t-test on z-maps of DMN iFC during wakefulness post-anesthesia and sevoflurane 3vol%, p<0.05 FWE cluster level corrected: significant connectivity in red-to-yellow, DMN mask in blue.* ***B. Mediation analysis.*** *Reduction of average within-DMN FC during sevoflurane 3vol% is mediated by average VTA-DMN FC, demonstrated by a significant indirect effect ab with partially standardized value -0.72 (i.e., ab divided by the standard deviation of the dependent variable), 95% CI: ☆[-1.24;-0.28]. 95% CI for further regression coefficients: ∅[-0.11;-0.04], Φ[-0.07;-0.03], ⌘[0.37;1.40], ≙[-0.07;0.01], ☆[-0.08;-0.01].*

3.1.4. Reduction of within-DMN BOLD connectivity during sevoflurane-induced unconsciousness correlates with the reduction of a-cBF to anterior DMN connectivity reduction

3.1.4.1. Mediation analyses.

Main result: sevoflurane 3vol%. To test whether within-DMN connectivity reduction during anesthesia-induced unconsciousness is mediated by reductions of a-cBF to DMN connectivity, we performed a mediation analysis. We found a non-significant indirect effect of average connectivity between a-cBF to anterior DMN, with partially standardized indirect effect *ab*= -0.03 (95% CI: [-0.48;0.40]). This results shows that a-cBF connectivity to anterior DMN does not mediate reductions of within-DMN connectivity.

Control for different anesthetic: Propofol. Next, we tested whether this mediation effect is dependent on the anesthetic agent. Therefore, we repeated our mediation approach on the propofol data set. We found a non-significant indirect effect of propofol-induced connectivity reduction between a-cBF and anterior DMN on within-DMN connectivity reduction, with partially standardized effect *ab* = -0.27

(95% CI: [-1.36;0.71]). This indicates that a-cBF does not mediate the reduction of DMN under sevoflurane nor propofol-induced anesthesia.

Control for different sevoflurane concentration: Sevoflurane 2vol%. To control for possible concentration-dependent effects, we performed the mediation analysis for sevoflurane 2vol%-induced anesthesia. We found a non-significant indirect effect for sevoflurane 2vol%-induced a-cBF iFC reduction to within-DMN reductions, with partially standardized effect *ab*= -0.02 (95% CI: [-0.52;0.40]). This further indicates that there is no mediation effect between a-cBF to anterior DMN independently from sevoflurane concentration.

Control for contrast: sevoflurane 3vol% relative to wakefulness post-anesthesia. Finally, we controlled for potential contrast effects, namely induction of versus recovery from sevoflurane-induced anesthesia. We found a non-significant indirect effect with partially standardized effect *ab* = -0.02 (95% CI: [-0.79;0.35]). This indicates that the absence of mediation effect does not depend on anesthesia contrast.

3.1.4.2. Analysis of differences.

We have previously demonstrated that a-cBF iFC is reduced with sevoflurane-induced anesthesia independently of its concentration, i.e., 3vol% and 2vol% (**Fig. 15 B2 & B3**), as well as with propofol (**Fig. 15 C2**), and particularly in the anterior forebrain, e.g., ACC, which overlaps with the anterior DMN area (**Fig. 15 B & C**). Furthermore, we have also demonstrated that the within-DMN iFC is reduced with sevoflurane 3- and 2vol% (**Fig. 16 A2 & A3**) and propofol (**Fig. 16 B2**), respectively.

Although the results show that a-cBF to anterior DMN is not a mediator of the within-DMN connectivity for sevoflurane nor for propofol-induced anesthesia (non-significant indirect effect independent of sevoflurane concentration or anesthetic), we calculated a Pearson's correlation coefficient and performed a simple linear regression analysis to test if the a-cBF-anterior DMN FC reduction significantly predicted the within-DMN FC reduction.

Briefly, we calculated the correlation and performed a linear regression using the difference from wakefulness pre-anesthesia state and anesthesia-induced unconsciousness states, e.g., sevoflurane 3vol% or 2vol%, or propofol, of the a-cBF-anterior DMN (values were extracted per subject from the reduction cluster from the paired t-test, e.g., wakefulness pre-anesthesia > sevoflurane 3vol%, overlapping with the DMN mask of Yeo and colleagues from the a-cBF-FC analysis) and within-DMN

connectivity (values were extracted per subject from the whole DMN Yeo mask from the DMN-FC analysis) (**Fig. 17 A-B left side**).

For sevoflurane, the results show that a-cBF-anterior DMN FC reduction significantly explained 28% of the within-DMN FC reduction under sevoflurane 3vol% (p=0.022) (**Fig. 17 A1**), and 18% under sevoflurane 2vol% with a strong trend (p=0.056) (**Fig. 17 A2**) relative to wakefulness pre-anesthesia. For propofol, a-cBF-anterior DMN FC reduction explained only 2% of the within-DMN FC reduction under propofol-induced anesthesia relative to wakefulness pre-anesthesia (**Fig. 17 B**), which was not significant (p=0.349). However, when repeating the analysis focusing only on voxels overlapping the significant reduction of DMN iFC (result from paired t-test awake pre-anesthesia >propofol (**Fig. 16 B2 red map**) with the Yeo mask (**Fig. 18 upper brain cartoon**), we obtain a strong trend of significance (p=0.06) on the power of prediction of the a-cBF-anterior DMN about the reduction of within-DMN iFC during propofol-induced anesthesia (**Fig. 18**). These results evidenced that the relationship between the reduction of a-cBF-anterior DMN and that of the within-DMN FC might be dependent on regional-specific effects of the anesthetic concentration., i.e., sevoflurane 3- and 2vol%, and anesthetic agent, sevoflurane or propofol.

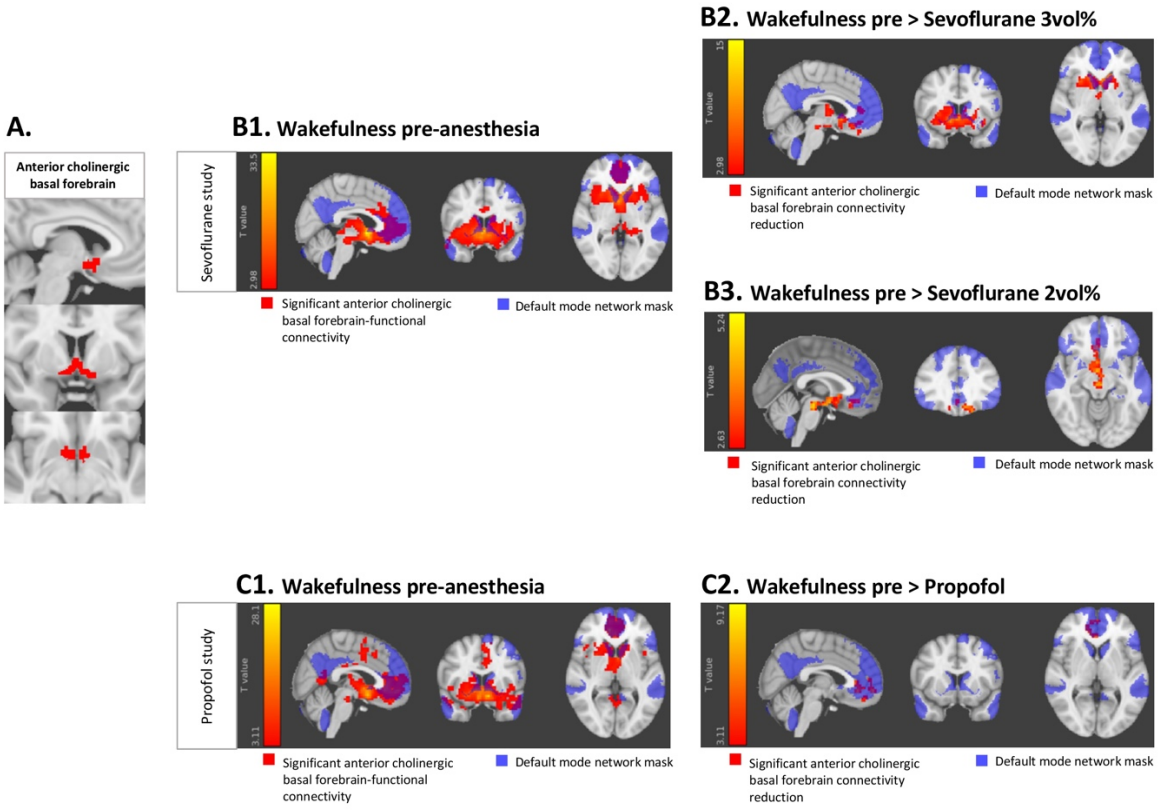

Figure 15. Summary figure: Anesthesia-induced unconsciousness is associated with a reduced a-cBF iFC relative to wakefulness pre-anesthesia.

A. a-cBF mask for seed-based functional connectivity analysis. *The mask is derived from (Fritz et al., 2019).* ***B. Sevoflurane study. B1. a-cBF connectivity during wakefulness pre-anesthesia.*** *Voxel-wise one-sample t-test on z-maps of a-cBF iFC during wakefulness, p<0.05 FWE cluster level corrected: significant connectivity in red-to-yellow, DMN mask derived from Yeo and colleagues (Yeo et al., 2011) in blue.* ***B2. a-cBF connectivity reduction for the contrast wakefulness pre-anesthesia > sevoflurane 3vol%.*** *Voxel-wise paired t-test on z-maps of a-cBF iFC during wakefulness and sevoflurane 3vol%, p<0.05 FWE cluster level corrected: significant connectivity in red-to-yellow, DMN mask in blue.* ***B3. a-cBF connectivity reduction for the contrast wakefulness pre-anesthesia > sevoflurane 2vol%.*** *Voxel-wise paired t-test on z-maps of a-cBF iFC during wakefulness and sevoflurane 2vol%, single voxel height threshold of p<0.01 p<0.05 FWE cluster level corrected: significant connectivity in red-to-yellow, DMN mask in blue.* ***Propofol study. C1. a-cBF connectivity during wakefulness pre-anesthesia.*** *Voxel-wise one-sample t-test on z-maps of a-cBF iFC during wakefulness, p<0.05 FWE cluster level corrected: significant connectivity in red-to-yellow, DMN mask derived from Yeo and colleagues (Yeo et al., 2011) in blue.* ***C2. a-cBF connectivity reduction for the contrast wakefulness pre-anesthesia > propofol.*** *Voxel-wise paired t-test on z-maps of a-cBF iFC during wakefulness and propofol anesthesia, p<0.05 FWE cluster level corrected: significant connectivity in red-to-yellow, DMN mask in blue.*

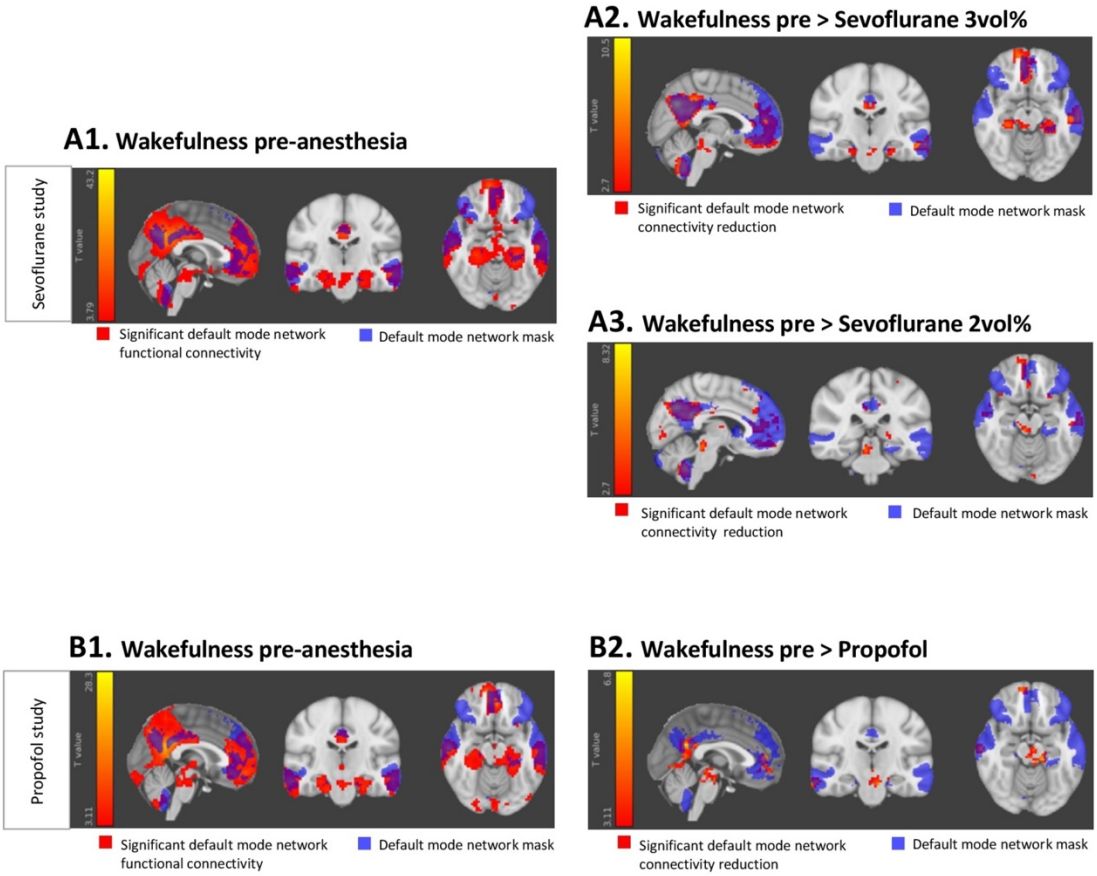

Figure 16. Summary figure: Anesthesia-induced unconsciousness is associated with a reduced within-DMN FC relative to wakefulness pre-anesthesia.

A. Sevoflurane study. A1. DMN iFC during wakefulness pre-anesthesia. *Voxel-wise one-sample t-test on z-maps of DMN iFC during wakefulness, p<0.05 FWE cluster level corrected: significant connectivity in red-to-yellow, DMN mask derived from Yeo and colleagues (Yeo et al., 2011) in blue.* ***A2. DMN iFC reduction for the contrast wakefulness pre-anesthesia > sevoflurane 3vol%.*** *Voxel-wise paired t-test on z-maps of DMN iFC during wakefulness and sevoflurane 3vol%-induced anesthesia, p<0.05 FWE cluster level corrected: significant connectivity in red-to-yellow, DMN mask in blue.* ***A3. DMN iFC reduction for the contrast wakefulness pre-anesthesia > sevoflurane 2vol%.*** *Voxel-wise paired t-test on z-maps of DMN iFC during wakefulness and*

sevoflurane 2vol%, p<0.05 FWE cluster level corrected: significant connectivity in red-to-yellow, DMN mask in blue. ***B. Propofol study. B1. DMN iFC during wakefulness pre-anesthesia.*** *Voxel-wise one-sample t-test on z-maps of DMN iFC during wakefulness, p<0.05 family-wise error cluster level corrected: significant connectivity in red-to-yellow, DMN mask in blue.* ***B2. DMN iFC reduction for the contrast wakefulness pre-anesthesia > propofol.*** *Voxel-wise paired t-test on z-maps of DMN iFC during wakefulness and propofol-induced anesthesia, p<0.05 FWE cluster level corrected: significant connectivity in red-to-yellow, DMN mask in blue.*

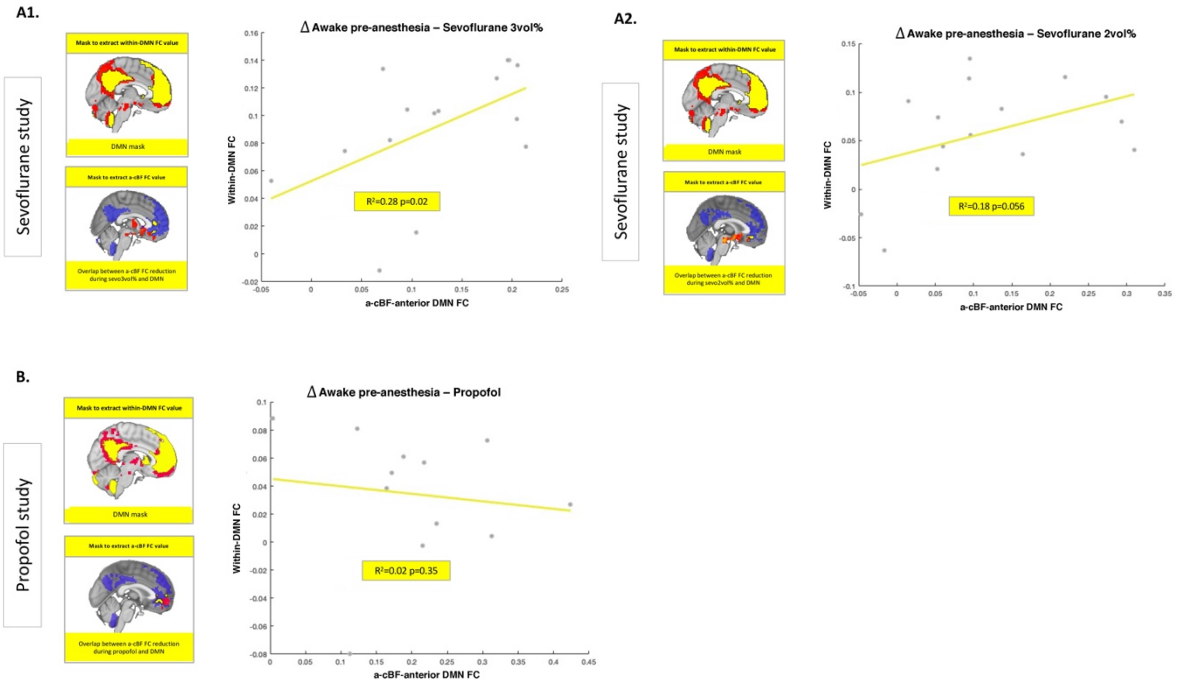

Figure 17. Analysis of differences.

A. Sevoflurane study. A1. Deltas wakefulness pre-anesthesia vs. sevoflurane 3vol%. *a-cBF-anterior DMN FC reduction explained 28% of the within-DMN FC reduction under sevoflurane 3vol% (r= 0.525, R^2=0.28, p=0.022, one-tailed correlations were bootstrapped (n=1000) 95% CI: [0.08;0.89]) relative to wakefulness pre-anesthesia (ANOVA: F(1,13)=4.945, p=0.045). This results were tested at alpha 0.05 level.* ***A2. Deltas wakefulness pre-anesthesia vs. sevoflurane 2vol%.*** *a-cBF-anterior DMN FC reduction explained 18% of the within-DMN FC reduction under sevoflurane 2vol% (r= 0.428, R^2=0.18, p=0.056, one-tailed correlations were bootstrapped (n=1000) 95% CI: [-0.019;0.78]) relative to wakefulness pre-anesthesia (ANOVA: F(1,13)=2.917, p=0.111). This results were tested at alpha 0.05 level.* ***B. Propofol study. Deltas wakefulness pre-anesthesia vs. propofol.*** *a-cBF-anterior DMN FC reduction explained 2% of the within-DMN FC reduction under propofol-induced anesthesia (r= 0.125, R^2=0.016, p=0.349, one-tailed correlations were bootstrapped (n=1000) 95% CI: [-0.74;0.44]) relative to wakefulness pre-anesthesia (ANOVA: F(1,10)=0.159, p=0.698). This results were tested at alpha 0.05 level.*

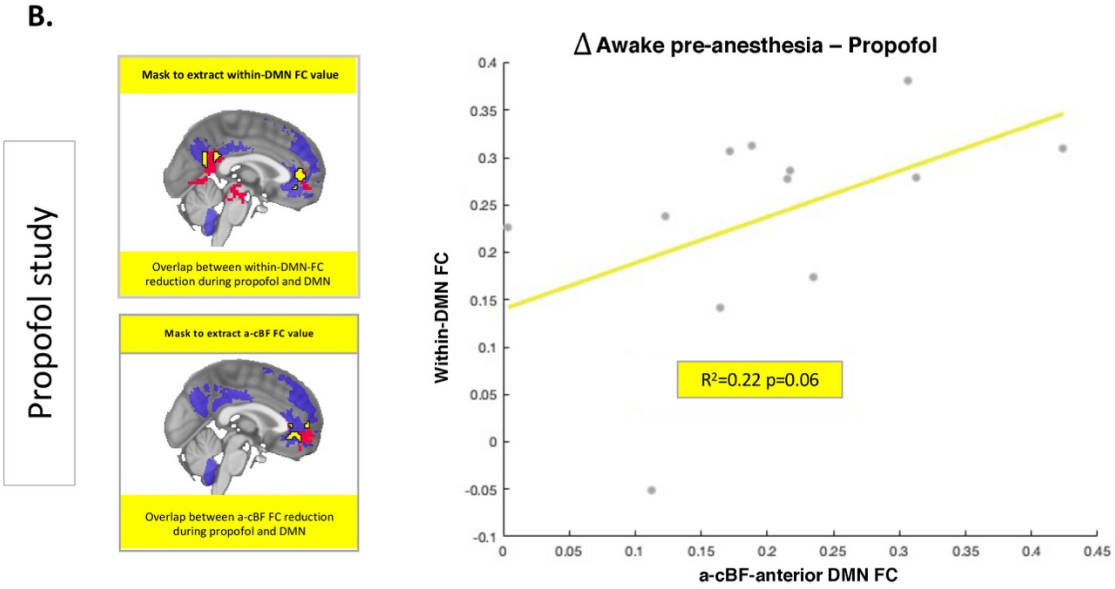

Figure 18. Control Analysis. Analysis of differences. Propofol study.

A. Propofol study Deltas wakefulness pre-anesthesia vs. propofol. *a-cBF-anterior DMN FC reduction explained 22% of the within-DMN FC reduction under propofol-induced anesthesia (r= 0.47, R^2=0.22, p=0.06, one-tailed correlations were bootstrapped (n=1000) 95% CI: [0.05;0.86]) relative to wakefulness pre-anesthesia (ANOVA: F(1,10)=2.82, p=0.199). This results were tested at alpha 0.05 level.*

3.2. Beyond static connectivity analyses: DMN transient global synchronizations are reduced during anesthesia and mediated by VTA

3.2.1. Anesthesia-induced unconsciousness is related to reduced transient large-scale synchronizations across the DMN relative to wakefulness

The impact of anesthesia on transient large-scale BOLD synchronizations across DMN, whole-brain and control networks was tested during anesthesia-induced unconsciousness with sevoflurane 3vol% against the awake states. Anesthetic concentration's effect as well as anesthetic's agent was tested using data from sevoflurane 2vol%- and from propofol-induced unconsciousness, respectively.

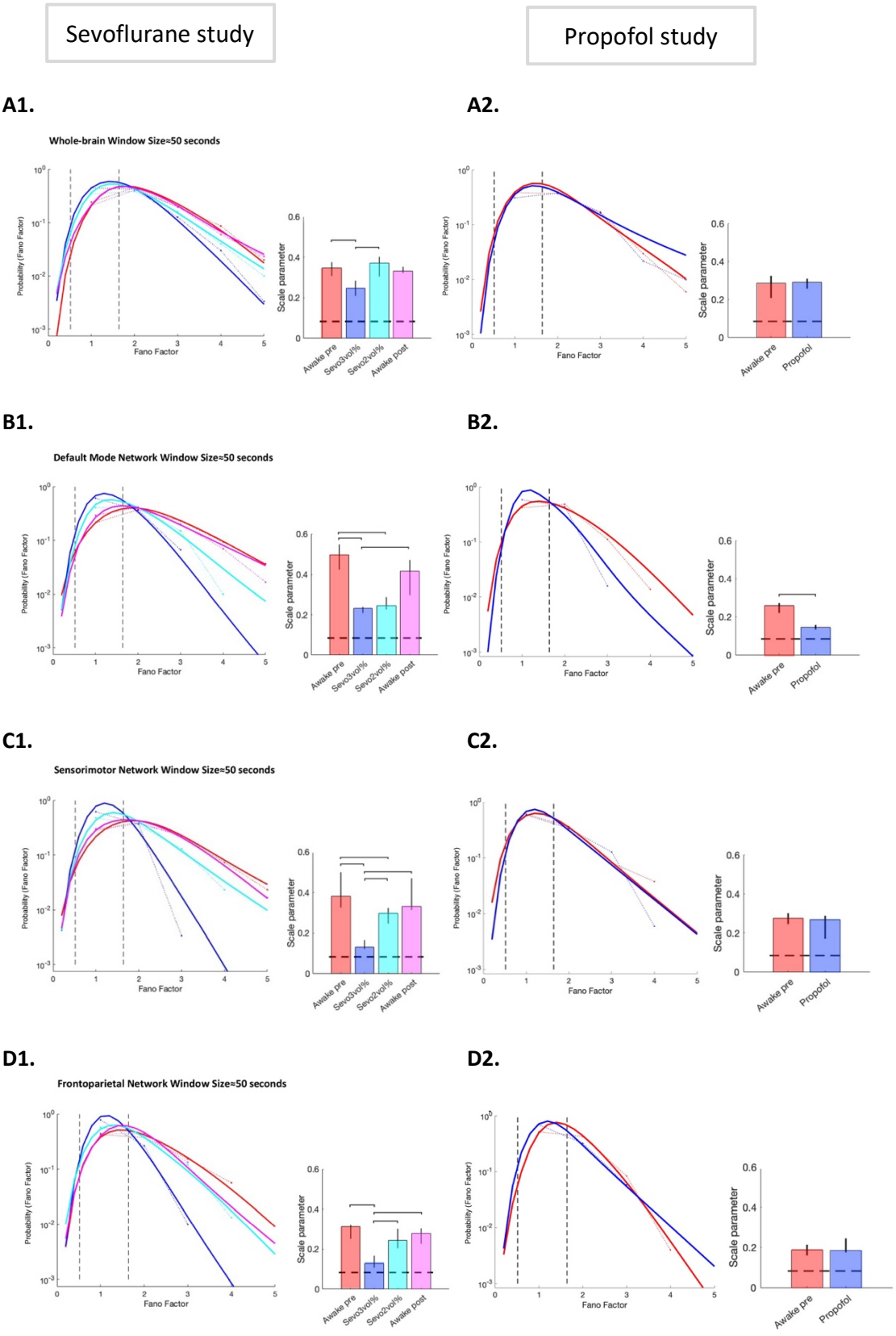

Figure 19. Transient large-scale synchronization of BOLD fluctuations across DMN, whole-brain and control networks in a ≈50 second window size for sevoflurane and propofol.

Distributions of the sizes of transient large-scale synchronizations (Fano Factors) of blood oxygenation level dependent fluctuations across DMN, whole-brain and control networks for sevoflurane and propofol and

distribution fits. Distributions are taken from all ≈50 second time windows within the whole time series. Chance sizes of transient large-scale synchronizations would fall into the interval between the vertical dashed lines. Within the plot, measured data are indicated by dotted lines, while drawn out lines depict the fitted curves. The line colors reflect anesthesia depth as indicated. Scale parameters derived from the fitting procedure to the distribution are shown in the respective bar plots to the right of the distribution plots.

Main result: sevoflurane 3vol%. **Fig. 19** shows the average distribution of the FF across time (within ≈50 seconds) and subjects per state and per network. Results for sevoflurane-induced anesthesia (sevoflurane 3vol% and 2vol%) are shown on the left-hand side. Measured FF distributions were statistically compared against FF distributions arising from a purely random occurrence of events, labelled Poisson process. During wakefulness (pre- or post-anesthesia), distributions significantly deviate from those resulting from a Poisson process regardless the ensemble (i.e., DMN, whole-brain, frontoparietal or sensorimotor network). Thus, when testing their centers of gravity against a value derived for a Poisson process all distributions were significant ($P<0.01$). In contrast, during sevoflurane 3vol%, and only for the networks (i.e., DMN and control networks), the distributions do not contain high FF values and are hardly separable from originating from Poisson processes (DMN: $P=0.062$, frontoparietal network: $P=0.148$, sensorimotor network: $P=0.109$). For the whole-brain, this comparison was significant ($P=0.013$). These differences are reflected in a significant reduction of the scale parameter of the distributions compared to that of wakefulness pre- and post-anesthesia particularly for the DMN and control networks (DMN: $P=<0.001/0.003$, frontoparietal network: $P=<0.001/0.003$, sensorimotor network: $P=<0.001/<0.001$). In the gamma distribution, the scale parameter represents the variability of the FF values. This implies that higher FF values (increased synchronizations) will shift the probability density function to the right while shifting away from the Poisson' derived value range (**Fig. 19** *range between vertical dashed lines*). The reduction of scale parameter for the whole-brain compared to wakefulness pre- and post- anesthesia showed a trend of significance (whole-brain: $P=0.048/0.107$).

Control analysis for concentration of anesthetic: sevoflurane 2vol%. During sevoflurane 2vol%, the FF distributions significantly deviated from a Poisson process in all ensembles $P<0.05$ (DMN: $P=0.008$, whole-brain: $P=0.003$, sensorimotor network: $P=0.008$, frontoparietal network: $P=0.024$). These differences were reflected in a significant reduction of the scale parameter relative to wakefulness pre-anesthesia only in the DMN and sensorimotor network (DMN: $P=0.005$, whole-brain: $P=0.561$, frontoparietal network: $P=0.277$, sensorimotor network: $P=0.026$) (**Fig. 19 A1-D1 left side**). Compared to wakefulness post-anesthesia, sevoflurane 2vol% was not significantly different for any ensemble, for DMN there was a strong trend towards significance $P<0.1$ (DMN: $P=0.064$, whole-brain: $P=0.804$, sensorimotor: $P=0.121$, frontoparietal: $P=0.639$). A Page test was used to test for systematic grading

of the scale factor in the order (sevoflurane 3vol% < sevoflurane 2vol% < awake post-anesthesia) being significant for all networks and the whole-brain ensemble (DMN: P=0.022, whole-brain: P=0.038, sensorimotor: P<0.001, frontoparietal: P=0.012. This suggests that the recovery of transient large-scale BOLD synchronizations within each network is dependent on the depth of the anesthesia, and not solely on the state of consciousness. However, the behavior across DMN regions during anesthetized states compared to wakefulness suggests a more 'binary' nature, i.e., awake states are different than states with anesthesia, however there is this difference is not present between anesthesia-induced states (sevoflurane 3vol% vs. sevoflurane 2vol%).

Control analysis for anesthetic: propofol. During wakefulness pre-anesthesia, distributions significantly deviate from those resulting from a Poisson process, regardless the ensemble (i.e., DMN: P=0.009, whole-brain: P=0.005, frontoparietal: P=0.027, sensorimotor network: P=0.03). During propofol-induced anesthesia the results are mixed, the distributions for DMN and sensorimotor network does not differ from those originating from a Poisson process (DMN: P=0.073, frontoparietal network: P=0.058), indicating loss of transient large-scale synchronicity also reflected in a significant reduction of the scale factor of the distributions particularly for the DMN (DMN: P=0.009, frontoparietal network: P=0.301). The whole-brain and sensorimotor network FF distributions significantly differed from a Poisson distribution also under propofol anesthesia (whole-brain: P=0.001, sensorimotor network: P=0.037), neither was the derived scale factor significantly reduced towards the awake state (whole-brain: P=0.665, sensorimotor network: P=0.064) (**Fig. 19 A2-D2 right side**). This result indicates that propofol affects the transient large-scale synchronization of particularly the DMN.

Summary. In combination the results indicated that transient large-scale synchronizations particularly in the DMN relate to the state of consciousness. A reduction of the scale factor, parametrizing the FF distribution, within the DMN is the most consistent finding in the conscious versus the unconscious state.

3.2.2. VTA- and a-cBF-DMN functional connectivity is reduced during anesthesia-induced unconsciousness: summary of seed-based connectivity results from first project

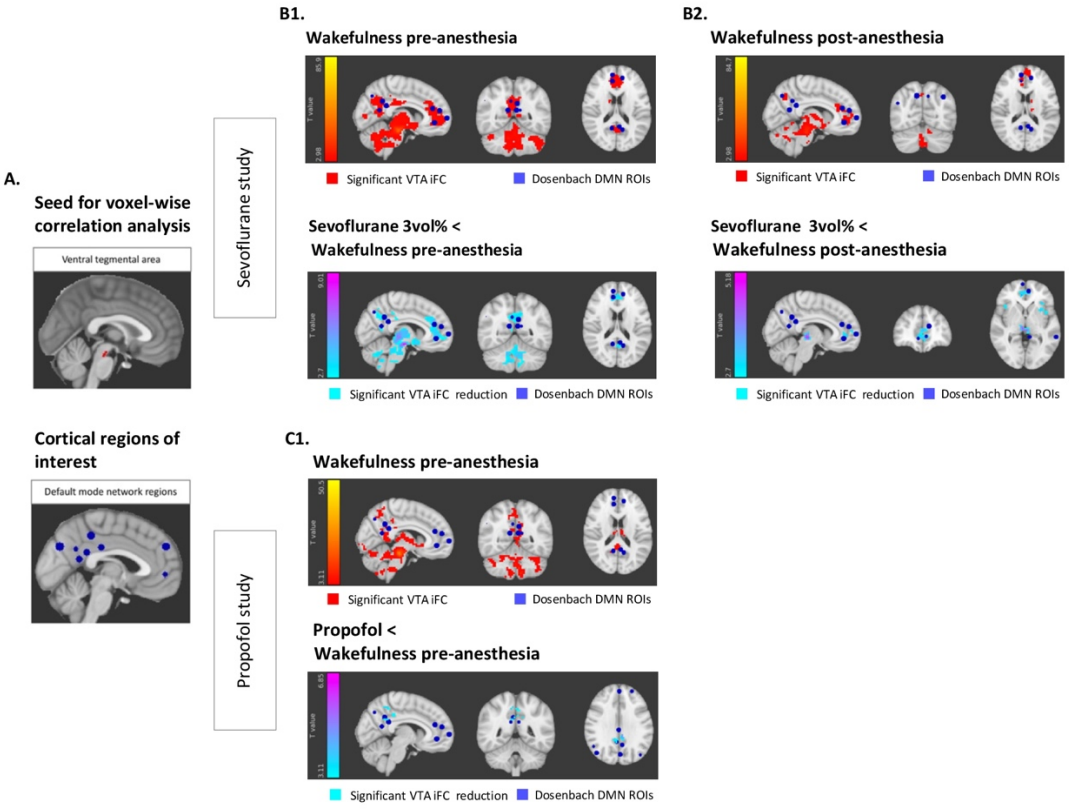

Figure 20. VTA correlated spontaneous BOLD fluctuations during wakefulness and its reduction during sevoflurane 3vol%- and propofol-induced unconsciousness.

A1. VTA mask for seed-based correlation analysis. *The mask is derived from Harvard Ascending Arousal Network Atlas (Edlow et al., 2012).* ***A2. DMN ROIs to compare areas of correlation****. 5-mm spheres derived categorized as DMN derived from Dosenbach and colleagues(Dosenbach et al., 2010)* ***. B. Sevoflurane study. B1. VTA iFC wakefulness pre-anesthesia.*** *Voxel-wise one-sample t-test on z-maps of VTA correlation during wakefulness, p<0.05 FWE cluster level corrected: significant correlation in red-to-yellow, DMN ROIs derived from Dosenbach and colleagues in blue.* ***B2. VTA iFC reduction for the contrast wakefulness pre-anesthesia > sevoflurane 3vol%.*** *Voxel-wise paired t-test on z-maps of VTA correlation during wakefulness and sevoflurane 3vol%, p<0.05 FWE cluster level corrected: significant correlation in red-to-yellow, DMN ROIs derived from Dosenbach and colleagues.* ***B3. VTA iFC during wakefulness post-anesthesia.*** *Voxel-wise one-sample t-test on z-maps of VTA correlation during wakefulness post-intervention, p<0.05 FWE cluster level corrected: significant correlation in red-to-yellow, DMN ROIs derived from Dosenbach and colleagues in blue.* ***B2. VTA iFC reduction for the contrast wakefulness post-anesthesia > sevoflurane 3vol%.*** *Voxel-wise paired t-test on z-maps of VTA correlation during wakefulness post-intervention and sevoflurane 3vol%, p<0.05 FWE cluster level corrected: significant correlation in red-to-yellow, DMN ROIs derived from Dosenbach and colleagues in blue.* ***C. Propofol study. C1. VTA iFC during wakefulness pre-anesthesia.*** *Voxel-wise one-sample t-test on z-maps of VTA correlation during wakefulness, p<0.05 FWE cluster level corrected: significant correlation in red-to-yellow, DMN ROIs derived from Dosenbach and colleagues in blue.* ***B2. VTA iFC reduction for the contrast wakefulness pre-anesthesia > propofol-induced unconsciousness.*** *Voxel-wise paired t-test on z-maps of VTA correlation during*

wakefulness and propofol-induced unresponsiveness, p<0.05 FWE cluster level corrected: significant correlation in red-to-yellow, DMN ROIs derived from Dosenbach and colleagues in blue.

In **Fig. 20** we depicted the summary results from our first project, where we have demonstrated that BOLD fluctuations derived from the VTA correlate with cortical areas in the brain, such as ACC, precuneus/PCC which are classically defined as being part of the DMN, which are significantly reduced with sevoflurane and propofol-induced unconsciousness, respectively.

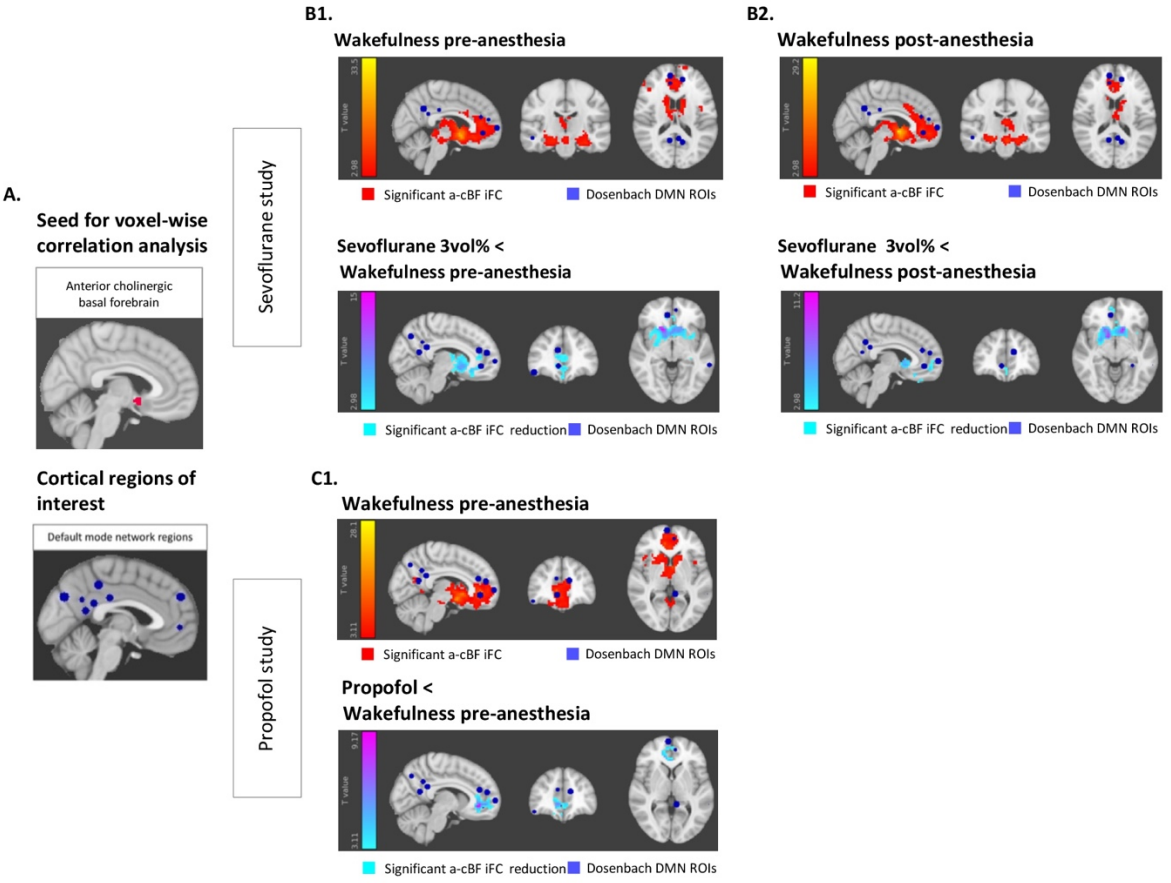

Figure 21. a-cBF correlated spontaneous BOLD fluctuations during wakefulness and its reduction during sevoflurane 3vol%- and propofol-induced unconsciousness.

A1. A-cBF mask for seed-based correlation analysis. *The mask is derived from (Fritz et al., 2019).* ***A2. DMN ROIs to compare areas of correlation****. 5-mm spheres derived categorized as DMN derived from Dosenbach and colleagues(Dosenbach et al., 2010)* ***. B. Sevoflurane study. B1. a-cBF iFC wakefulness pre-anesthesia.*** *Voxel-wise one-sample t-test on z-maps of a-cBF correlation during wakefulness, p<0.05 FWE cluster level corrected: significant correlation in red-to-yellow, DMN ROIs derived from Dosenbach and colleagues in blue.* ***B2. a-cBF iFC reduction for the contrast wakefulness pre-anesthesia > sevoflurane 3vol%.*** *Voxel-wise paired t-test on z-maps of a-cBF correlation during wakefulness and sevoflurane 3vol%, p<0.05 FWE cluster level corrected: significant correlation in red-to-yellow, DMN ROIs derived from Dosenbach and colleagues.* ***B3. a-cBF iFC during wakefulness post-anesthesia.*** *Voxel-wise one-sample t-test on z-maps of a-cBF correlation during wakefulness post-intervention, p<0.05 FWE cluster level corrected: significant correlation in red-to-yellow, DMN ROIs derived from Dosenbach and colleagues in blue.* ***B2. a-cBF iFC reduction for the contrast wakefulness post-anesthesia >***

sevoflurane 3vol%. *Voxel-wise paired t-test on z-maps of a-cBF correlation during wakefulness post-intervention and sevoflurane 3vol%, p<0.05 FWE cluster level corrected: significant correlation in red-to-yellow, DMN ROIs derived from Dosenbach and colleagues in blue.* ***C. Propofol study. C1. a-cBF iFC during wakefulness pre-anesthesia.*** *Voxel-wise one-sample t-test on z-maps of a-cBF correlation during wakefulness, p<0.05 FWE cluster level corrected: significant correlation in red-to-yellow, DMN ROIs derived from Dosenbach and colleagues in blue.* ***B2. a-cBF iFC reduction for the contrast wakefulness pre-anesthesia > propofol-induced unconsciousness.*** *Voxel-wise paired t-test on z-maps of a-cBF correlation during wakefulness and propofol-induced unresponsiveness, p<0.05 FWE cluster level corrected: significant correlation in red-to-yellow, DMN ROIs derived from Dosenbach and colleagues in blue.*

In **Fig. 21** we depicted the summary results from our first project, where we have demonstrated that BOLD fluctuations derived from the a-cBF correlate with cortical areas in the brain, particularly to the anterior part of the DMN, which are significantly reduced with sevoflurane and propofol-induced unconsciousness, respectively.

3.2.3. Reduction of transient large-scale BOLD synchronizations across the DMN is mediated by reduced VTA-DMN functional connectivity during anesthesia-induced unconsciousness

Main result: sevoflurane 3vol%. To test whether altered connectivity between VTA and DMN during anesthesia-induced unconsciousness (tested in the first project) mediates the reduction in large-scale synchronicity within the DMN, we performed a mediation analysis. Testing for effect of sevoflurane 3vol%-induced anesthesia compared to wakefulness pre-anesthesia, we found a non-significant indirect effect with partially standardized value *ab*= -0.39 (95% CI: [-0.88;0.40]) (**Fig. 23 A1**). Standardized *ab* is an estimate of the mediation effect of reduction in connectivity between VTA and DMN on reduction of large-scale synchronicity within the DMN; it refers to the product of regression coefficients *a* and *b* in the path model divided by the standard deviation of the dependent variable large-scale synchronization within DMN; it is significant when it's 95% confidence interval does not include zero. In contrast, testing for effect of sevoflurane 3vol%-induced anesthesia compared to wakefulness post-anesthesia, we found a significant indirect effect with a partially standardized value *ab*= -0.60 (95% CI: [-1.09;-0.09]) (**Fig. 23 A2**). This result indicates that changes in connectivity between VTA and DMN during sevoflurane 3vol%-induced anesthesia compared to wakefulness post-anesthesia mediate the recovery of large-scale synchronicity within the DMN upon emergence. Control analyses for further RSN were not performed due to lack of overlapping voxels between VTA iFC and ROIs from sensorimotor or frontoparietal network (**Fig. 22**).

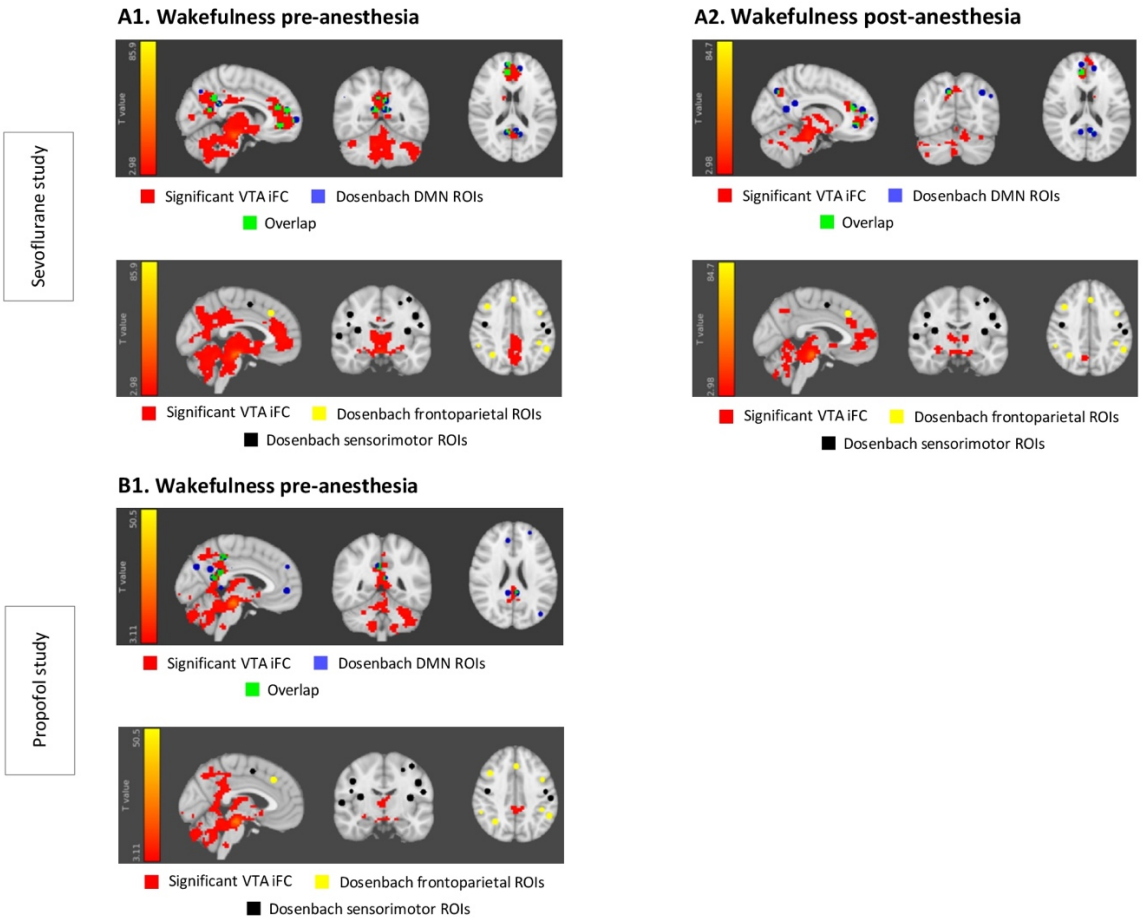

Figure 22. Definition of VTA-DMN mediator variable to test.

A. Sevoflurane study. A1. Overlap between VTA correlated spontaneous BOLD fluctuations during wakefulness pre-anesthesia and DMN ROIs. *Overlap depicted in green. Control RSN do not overlap with VTA iFC.* ***A2. Overlap between VTA correlated spontaneous BOLD fluctuations during wakefulness post-anesthesia and DMN ROIs.*** *Overlap depicted in green. Control RSN do not overlap with VTA iFC.* ***A. Propofol study. B1. Overlap between VTA correlated spontaneous BOLD fluctuations during wakefulness pre-anesthesia and DMN ROIs.*** *Overlap depicted in green. Control RSN do not overlap with VTA iFC.*

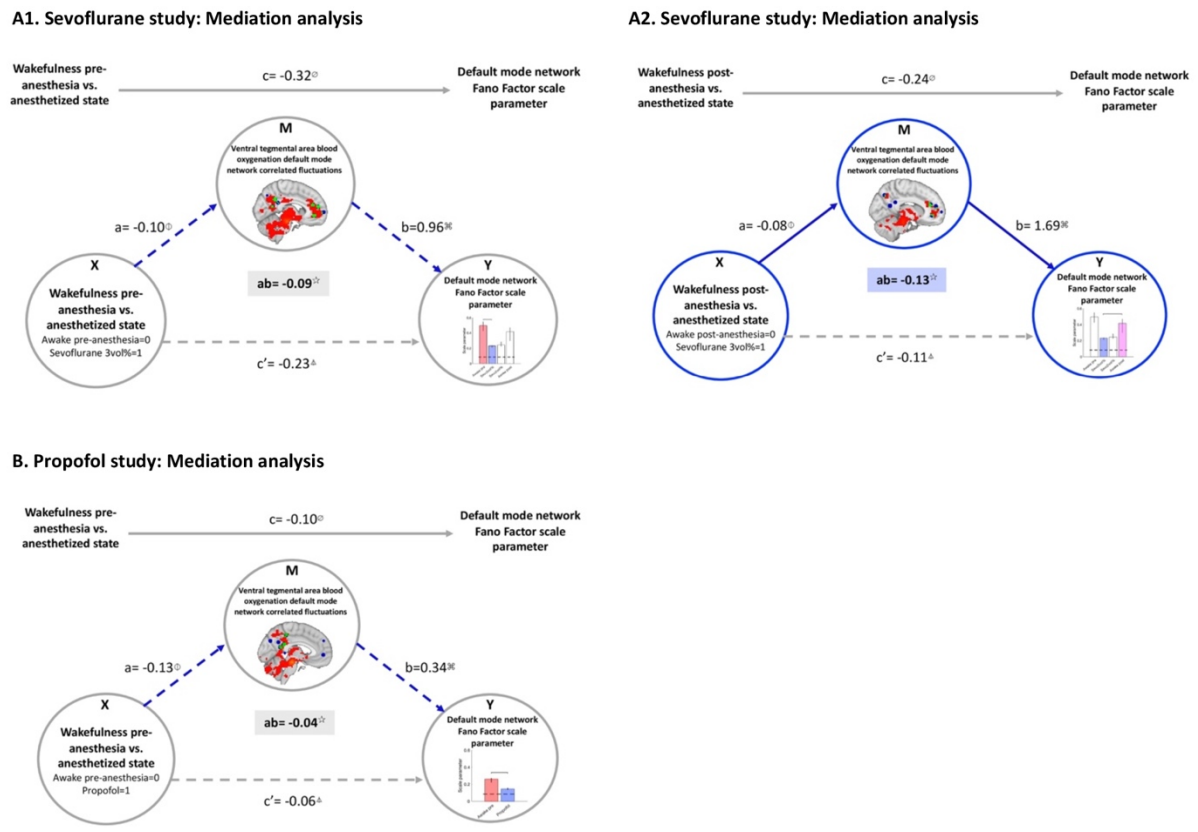

Figure 23. Testing for cortical correlated fluctuations between VTA and DMN influence on DMN transient large-scale synchronized BOLD fluctuations during induction of and emergence from anesthesia-induced unresponsiveness.

A1. Sevoflurane study. Mediation analysis. *Reduction of cortical correlated fluctuations between VTA and DMN during sevoflurane 3vol%-induced unresponsiveness does not mediate the effect of the anesthetic agent during sevoflurane 3vol%-induced unconsciousness on the BOLD transient large-scale synchronization within the DMN. This is demonstrated by the non-significant indirect effect ab with partially standardized value -0.39 (i.e., ab divided by the standard deviation of the dependent variable), 95% CI: [-0.88;0.40]. 95% CI for further regression coefficients: ∅[-0.46;-0.19], ◊[-0.14;-0.06], ⌘[-0.38;2.30], ▵[-0.42;-0.04], ☆[-0.22;0.08].* ***A2. Sevoflurane study: Mediation analysis.*** *Reduction of cortical correlated fluctuations between VTA and DMN during sevoflurane 3vol%-induced unresponsiveness mediates the recovery of effect of the anesthetic agent during sevoflurane 3vol%-induced unresponsiveness in wakefulness post-intervention on the transient large-scale synchronization of the blood oxygenation level dependent fluctuations within the DMN. This is demonstrated by the significant indirect effect ab with partially standardized value -0.60 (i.e., ab divided by the standard deviation of the dependent variable), 95% CI: ☆[-1.11;-0.15]. 95% CI for further regression coefficients: ∅[-0.34;-0.06], ◊[-0.10;-0.03], ⌘[0.57;3.44], ▵[-0.22;0.10], ☆[-0.26;-0.03].* ***B. Propofol study: Mediation analysis.*** *Reduction of cortical correlated fluctuations between VTA and DMN during propofol-induced unresponsiveness does not mediate the effect of the anesthetic agent during propofol-induced unresponsiveness on the transient large-scale synchronization of the blood oxygenation level dependent fluctuations within the DMN. This is demonstrated. By the non-significant indirect effect ab with partially standardized value -0.60 (i.e., ab divided by the standard deviation of the dependent variable), 95% CI: [-1.08;-0.09]. 95% CI for further regression coefficients: ∅[-0.38;-0.11], ◊[-0.11;-0.04], ⌘[0.30;3.07], ▵[-0.23;0.05], ☆[-0.27;-0.02].*

Control analyses: partial volume effects. We confirmed this finding about the mediating effect of VTA-DMN connectivity during sevoflurane 3vol%-induced anesthesia compared to wakefulness post-anesthesia on the recovery of large-scale BOLD synchronizations within the DMN, by repeating the mediation analysis with values derived from the 'SRCC' VTA iFC but conserving the VTA-DMN mask from the non-corrected analyses. We found a significant indirect effect of corrected VTA connectivity, with a partially standardized effect *ab*= -0.64 (90% CI: [-1.17;-0.09]). This indicates that the mediation effect of connectivity between VTA and DMN is not confounded by brainstem neuromodulatory nuclei effects.

Control analysis for concentration of anesthetic: sevoflurane 2vol%. We repeated the mediation analyses with sevoflurane 2vol% derived values. Relative to wakefulness pre-anesthesia or post-anesthesia the indirect effect was not significant with a partially standardized value *ab*= -0.43 (95% CI: [-0.93;0.23]) / *ab*= -0.52 (95% CI: [-1.23;0.30]). This results indicates that the reduction of large-scale BOLD synchronizations within-DMN during sevoflurane 2vol%-induced anesthesia cannot be explained through the reductions in connectivity between VTA and DMN during this anesthesia-induced state.

Control for anesthetic: Propofol. To test for effects of propofol on the large-scale synchronization of the DMN and the role of the change of connectivity between VTA and DMN as mediator, we repeated the mediation analysis. We found a non-significant indirect effect with partially standardized value *ab*= -0.34 (95% CI: [-1.22;0.30]) (**Fig. 23 B**). This result indicates that the reduction of large-scale synchronization within the DMN during propofol-induced anesthesia is not mediated by the change in connectivity between VTA and DMN.

3.2.5. Reduction of transient large-scale BOLD synchronizations across the DMN is not mediated by reduced a-cBF-DMN functional connectivity during anesthesia-induced unconsciousness

Main result: sevoflurane 3vol%. To test whether altered connectivity between a-cBF and DMN during anesthesia-induced unconsciousness (tested in the first project) mediates the reduction in large-scale synchronicity within the DMN, we performed a mediation analysis. Testing for effect of sevoflurane 3vol%-induced anesthesia compared to wakefulness pre-anesthesia, we found a non-significant indirect effect with partially standardized value *ab*= 0.21 (95% CI: [-0.20;0.83]). Standardized *ab* is an estimate of the mediation effect of reduction in connectivity between VTA and DMN on reduction of

large-scale synchronicity within the DMN; it refers to the product of regression coefficients *a* and *b* in the path model divided by the standard deviation of the dependent variable large-scale synchronization within DMN; it is significant when it's 95% confidence interval does not include zero. To test the dependency on the contrast, i.e., wakefulness pre-anesthesia vs. wakefulness post-anesthesia, we found a non-significant indirect effect as well, with a partially standardized value *ab*= 0.26 (95% CI: [-0.31;0.66]). This result indicates that changes in connectivity between a-cBF and DMN during sevoflurane 3vol%-induced anesthesia compared to wakefulness pre-anesthesia or post-anesthesia do not mediate the change in large-scale synchronicity within the DMN during anesthesia-induced unconsciousness.

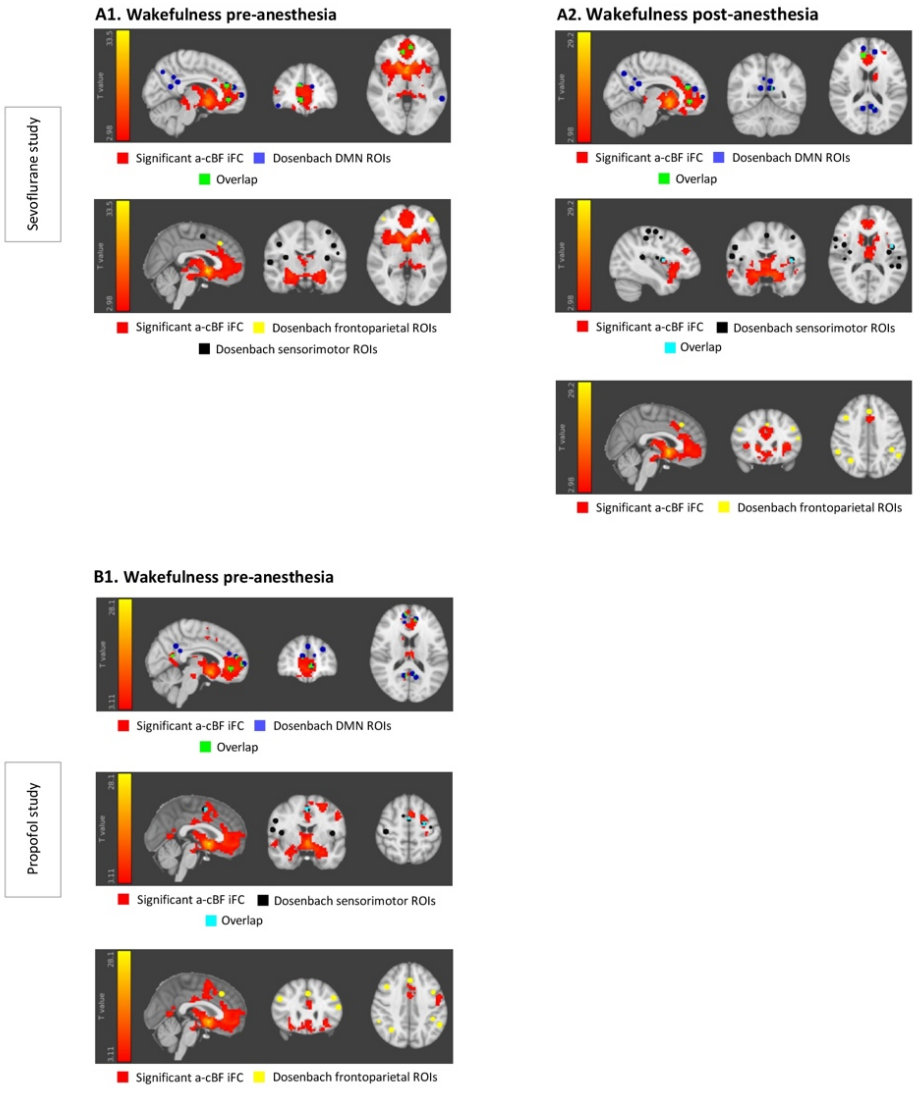

Figure 24. Definition of a-cBF-DMN mediator variable to test.

A. Sevoflurane study. A1. Overlap between a-cBF correlated spontaneous BOLD fluctuations during wakefulness pre-anesthesia and DMN ROIs. *Overlap depicted in green. Control RSN do not overlap with a-cBF*

iFC. ***A2. Overlap between a-cBF correlated spontaneous BOLD fluctuations during wakefulness post-anesthesia and DMN ROIs.*** *Overlap depicted in green. Control RSN: overlap between a-cBF spontaneous BOLD fluctuations and sensorimotor network depicted in cyan. There is no overlap with frontoparietal network.* ***A. Propofol study. A1. Overlap between a-cBF correlated spontaneous BOLD fluctuations during wakefulness pre-anesthesia and DMN ROIs.*** *Overlap depicted in green. Control RSN: overlap between a-cBF spontaneous BOLD fluctuations and sensorimotor network depicted in cyan. There is no overlap with frontoparietal network.*

Control analysis for different RSN: sensorimotor network. We found an overlap between a-cBF iFC and sensorimotor ROIs during wakefulness post-anesthesia (**Fig. 24 A2)**, therefore we repeated the mediation analyses with values derived from the scale parameters from this control network. The analyses using sevoflurane 3vol% or 2vol% showed a non-significant indirect effect with a partially standardized value *ab*= 0.24 (95% CI: [-0.04;0.66]) / *ab*= 0.01 (95% CI: [-0.12;0.37]). This results indicates that the reduction of large-scale BOLD synchronizations within the sensorimotor network during sevoflurane 3vol%- or 2vol%-induced anesthesia cannot be explained through the reductions in connectivity between a-cBF and DMN during this anesthesia-induced state, respectively.

Control analysis for concentration of anesthetic: sevoflurane 2vol%. We repeated the mediation analyses with sevoflurane 2vol% derived values. Relative to wakefulness pre-anesthesia or post-anesthesia the indirect effect was not significant with a partially standardized value *ab*= 0.04 (95% CI: [-0.15;0.47]) / *ab*= 0.19 (95% CI: [-0.34;0.38]). This results indicates that the reduction of large-scale BOLD synchronizations within-DMN during sevoflurane 2vol%-induced anesthesia cannot be explained through the reductions in connectivity between a-cBF and DMN during this anesthesia-induced state.

Control for anesthetic: Propofol. To test for effects of propofol on the large-scale synchronization of the DMN and the role of the change of connectivity between a-cBF and DMN as mediator, we repeated the mediation analysis. We found a non-significant indirect effect with partially standardized value *ab*= 0.25 (95% CI: [-0.54;1.26]). We repeated the analyses to evaluate the sensorimotor network as a control network due to overlap with ROIs from this network (**Fig. 24 B1**), where we found a non-significant indirect effect with partially standardized value *ab*=-0.07 (95% CI: [-0.65;0.59]). This result indicates that the reduction of large-scale synchronization within the DMN nor somatosensory network during propofol-induced anesthesia is not mediated by the change in connectivity between a-cBF and the respective network.

3.3. Subcortical activity in period prior burst-onset during sevoflurane-induced burst suppression state

3.3.1. Period prior burst-onset is associated to increased subcortical-cortical functional connectivity

3.3.1.1. All events included.

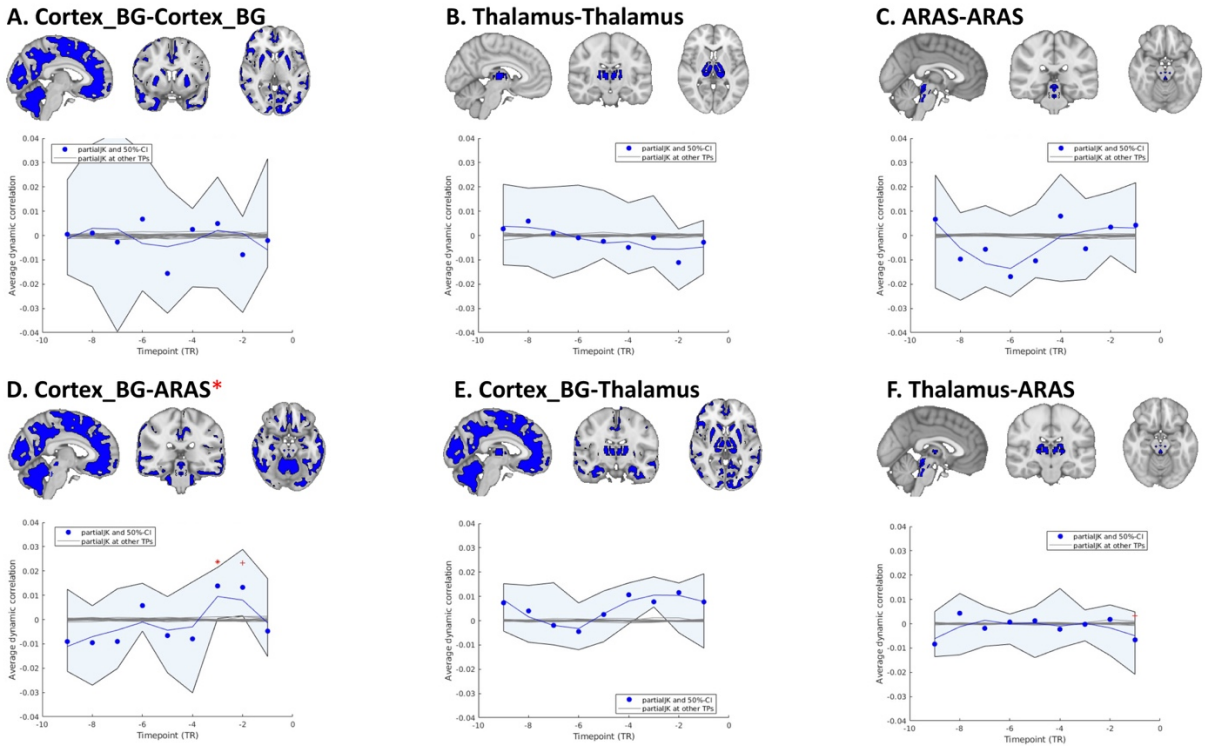

Figure 25. Average dynamic correlation between different parcels of the brain prior to burst-onset for all bursts independent of length.

A-F. Pre-burst correlation within and between parcels. *Average correlation per time timepoint (blue dots), median (blue trace), average correlation from other timepoints (grey traces), 50% CI (light blue shaded area), ROIs from each parcel displayed in brain cartoon (blue) to indicate different combinations, significant average connectivity compared to the rest of timepoints displayed with an asterisk (*p<0.05) and a plus (+p<0.1).*

All bursts included. **Fig. 25** shows the time-resolved averaged dynamic connectivity between Cortex_BG and ARAS parcels showing a significantly increase in connectivity at timepoint -3 TRs ($p<0.05$), i.e., around 6 seconds before the start of a burst; timepoint -2 TRs showed only a trend of significance ($p<0.1$). Thalamus to Cortex_BG parcel showed an increased connectivity before the event

start; however, this was not significant (**Fig. 25 D**). No other combination of parcels showed significantly increased connectivity before the start of the bursting event. Our results indicate that just before an event there is coherent activity between midbrain nuclei and cortical and subcortical areas excluding the thalamus, which might support the idea that brainstem areas area causal in the generation of individual bursts in sevoflurane anesthesia.

3.3.1.2. Short and long bursts analysis.

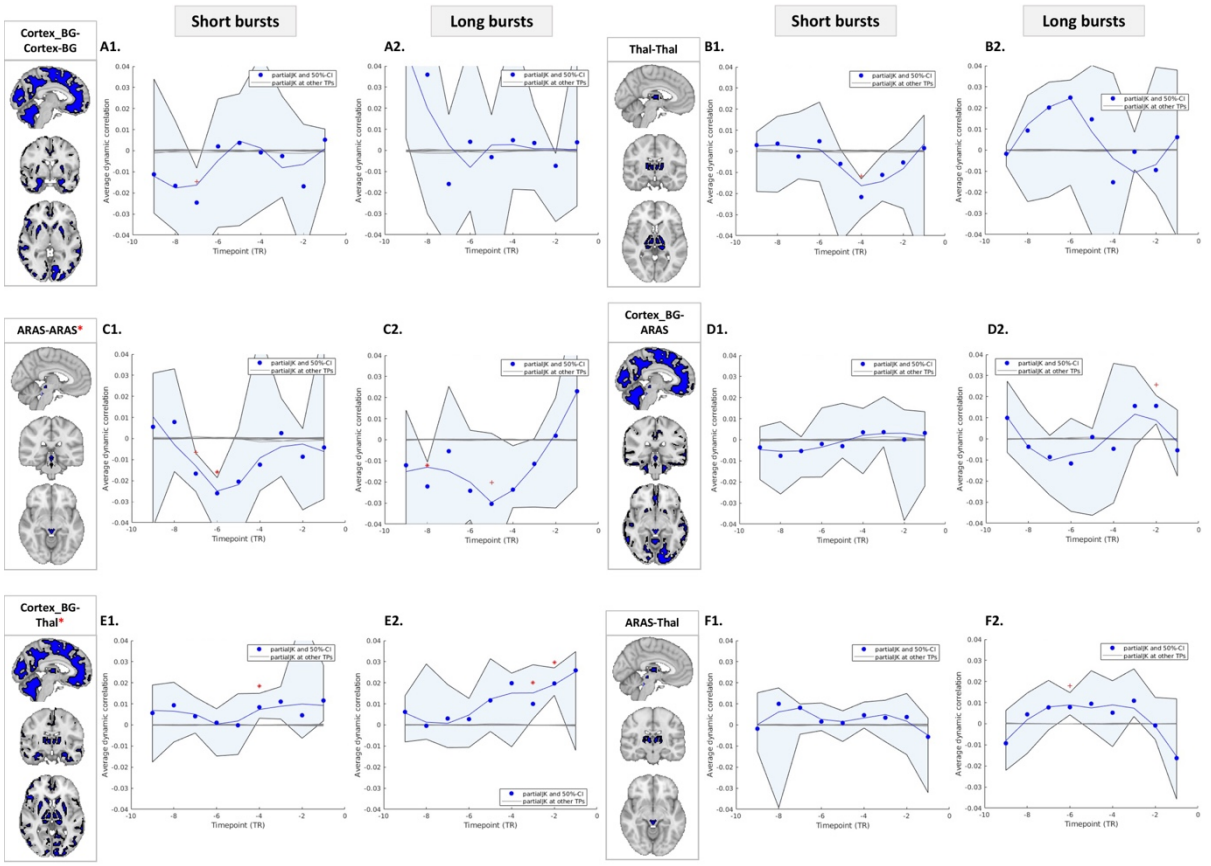

Figure 26. Average dynamic correlation between different parcels of the brain prior to burst-onset for short and long bursts.

A-F. Pre-burst correlation within and between parcels of short bursts (left side) and long bursts (right side). *Average correlation per time timepoint (blue dots), median (blue trace), average correlation from other timepoints (grey traces), 50% CI (light blue shaded area), ROIs from each parcel displayed in brain cartoon (blue) to indicate different combinations, significant average connectivity compared to the rest of timepoints displayed with an asterisk (*p<0.05) and a plus (+p<0.1).*

'Short' bursts. **Fig. 26 left side** shows the average dynamic correlation for the 'short' bursts showed a significant increase in connectivity between Cortex_BG-Thalamus parcels at time point -4 TR ($p<0.05$),

i.e., around 8 seconds before the start of a burst (**Fig. 26 E1**). A decrease in connectivity was evidenced around timepoint -7 TR for Cortex_BG-Cortex_BG ($p<0.1$) (**Fig. 26 A1**), for ARAS-ARAS (-7 TR: $p<0.1$, -6 TR: $p<0.05$) (**Fig. 26 C1**), as well as for Thalamus-Thalamus (-4 TR: $p<0.1$) (**Fig. 26 B1**). No other combination of parcels showed significant increased connectivity before the start of event.

'*Long' bursts*. **Fig. 26 right side** shows the average dynamic correlation for the 'long' bursts showed a significant increase in connectivity between Cortex_BG-Thalamus parcels at timepoint -3 TR and timepoint -2 TR ($p<0.05$) (**Fig. 26 E2**), i.e., around 6 seconds before the start of the burst. This connectivity seems to start to increase at timepoint -7 TR. Cortex_BG-ARAS (-2 TR: $p<0.1$) (**Fig. 26 D2**) and ARAS-Thalamus (-6 TR: $p<0.1$) (**Fig. 26 F2**) showed a trend of increased connectivity before the event start. A decrease in connectivity was evidenced in timepoint -8 TR ($p<0.05$) and timepoint -5 ($p<0.1$) for ARAS-ARAS (**Fig. 26 C2**). No other combination of parcels showed significant increased connectivity before the start of event.

Summary. Overall, these results suggest that there might be a common feature of all bursting events independently of their length, which is a coherent ARAS-Cortex_BG activity before the burst-onset, while thalamic-cortical coherent activity might be dependent on the length of the burst.

3.3.2. Period prior burst-onset is associated to increased subcortical BOLD activations: GLM analyses.

3.3.2.1. All bursts included.

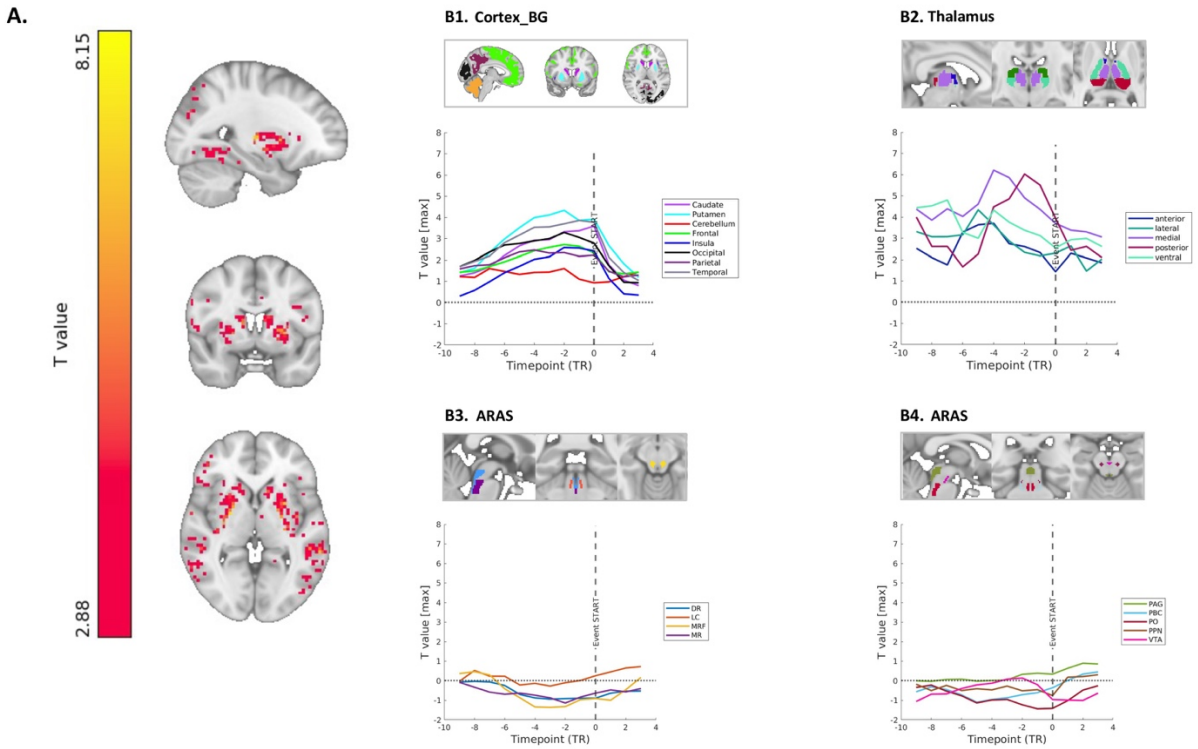

Figure 27. GLM analyses and summary of maximum t-values per ROI per timepoint.

A. Significant positive co-activations with electrophysiological signal of bursts in the brain. *Group statistics shown as a voxel-wise t-values of a GLM modeling burst on the EEG as regressor of interest (height p threshold 0.005 FWE cluster corrected for multiple comparisons).* ***B1-B4. Summary plots from GLM modeling burst modifying start of event: maximum t-value per ROI per timepoint.*** *Maximum t-values were extracted from the group statistics t-maps result from a GLM modeling burst on the EEG as a regressor of interest modifying the start of the burst in consecutive steps of 1 TR back to 9 TRs; zero line corresponds to the real start of the event as defined by the EEG signal. Significant t-value starts at around t=2. Color in traces correspond to same colors in the brain cartoons for each ROI. ARAS ROIs are displayed in different plots for a better overview.*

Regions	*Hemisphere*	*MNI Coordinates [x;y;z]*	*Z value*	*Cluster size*	*P value*
Burst suppression: all events included					
1) Original					
Superior temporal gyrus	L	*[-60;-37;5]*	5.21	201	<0.001
Caudate nucleus	L	*[-15;11;14]*	5.14	261	<0.001
Pallidum	R	[24;-4;2]	4.9	260	<0.001
Inferior frontal gyrus	L	[-39;2;26]	4.46	39	<0.001
Inferior temporal gyrus	R	[48;-49;-19]	4.37	84	<0.001
Fusiform gyrus	L	[-24;-61;-13]	4.22	186	<0.001
Inferior frontal gyrus	R	[45;35;14]	4.05	45	<0.001
Lingual gyrus	R	[33;-43;-10]	4.03	85	<0.001
Middle temporal gyrus	R	[57;-52;5]	3.99	133	<0.001

Precentral gyrus	R	[60;2;11]	3.46	28	0.001
2) Minus 1					
Pallidum	L	[-24;-7;2]	4.91	242	<0.001
Putamen	R	[21;2;2]	4.66	228	<0.001
Lingual gyrus	L	[-18;-67;-10]	4.41	107	<0.001
Superior temporal gyrus	L	[-51;-37;2]	4.34	313	<0.001
Inferior frontal gyrus	R	[45;35;14]	4.14	55	<0.001
Supramarginal gyrus	R	[57;-43;11]	4.06	70	<0.001
PCC	R	[6;-49;14]	3.97	31	<0.001
Middle temporal gyrus	R	[54;-52;5]	3.88	26	0.001
Precuneus	L	[-15;-64;23]	3.87	20	<0.001
Inferior temporal gyrus	R	[45;-64;-4]	3.85	32	<0.001
Fusiform gyrus	R	[24;-55;-10]	3.77	36	<0.001
Lingual gyrus	R	[27;-73;-13]	3.55	18	0.01
3) Minus 2					
Pallidum	R	[21;2;2]	5.18	247	<0.001
Putamen	L	[-27;-16;5]	4.69	247	<0.001
Supramarginal gyrus	R	[51;-37;11]	4.59	105	<0.001
Lingual gyrus	L	[-18;-67;-10]	4.54	465	<0.001
Inferior frontal gyrus	L	[-39;17;23]	4.48	49	<0.001
Precuneus	L	[-15;-64;23]	4.36	26	0.001
Angular gyrus	R	[54;-52;5]	4.14	23	0.002
PCC	R	[6;-49;26]	4.13	14	0.003
Fusiform gyrus	R	[24;-55;-10]	4.12	47	<0.001
Inferior frontal gyrus	R	[45;35;14]	4.06	51	<0.001
Precuneus	R	[15;-67;32]	4.03	22	<0.001
Fusiform gyrus	R	[42;-52;-13]	3.97	51	<0.001
Lingual gyrus	R	[21;-70;-1]	3.87	17	0.001
Precuneus	R	[21;-52;5]	3.64	17	0.001
Operculum	L	[-45;-37;23]	3.64	31	<0.001
Middle temporal gyrus	R	[51;-64;5]	3.64	16	0.001
Postcentral gyrus	R	[60;-19;20]	3.33	21	<0.001
4) Minus 3					
Putamen	R	[24;-7;5]	4.77	141	<0.001
Superior temporal gyrus	R	[48;-28;-7]	4.76	30	<0.001
Pallidum	L	[-21;-4;5]	4.43	188	<0.001
Inferior temporal gyrus	L	[-48;-64;-13]	4.30	48	<0.001
Supramarginal gyrus	R	[57;-43;11]	4.04	34	<0.001
Precuneus	L	[-15;-61;23]	3.99	17	0.012
Inferior frontal gyrus	L	[-39;17;23]	3.88	25	0.001
Middle temporal gyrus	R	[54;-55;8]	3.85	16	<0.001

Superior temporal gyrus	L	[-51;-31;-1]	3.80	160	<0.001
Fusiform gyrus	L	[-18;-67;-10]	3.73	69	<0.001
Inferior frontal gyrus	R	[51;35;8]	3.69	27	<0.001
Lingual gyrus	R	[24;-55;-10]	3.63	29	<0.001
Precuneus	R	[15;-67;29]	3.60	25	0.001
5) Minus 4					
Insula	L	[-30;-25;11]	4.75	121	<0.001
Putamen	R	[24;-4;5]	4.68	138	<0.001
Caudate nucleus	L	[-9;8;14]	4.04	44	<0.001
Heschl's gyrus	R	[48;-19;-10]	4.01	31	<0.001
Fusiform gyrus	L	[-33;-64;-13]	3.95	127	<0.001
Precuneus	R	[15;-70;38]	3.85	28	<0.001
Middle temporal gyrus	R	[60;-46;8]	3.84	29	<0.001
Postcentral gyrus	L	[-63;-7;14]	3.59	21	0.002
Inferior frontal gyrus	R	[42;29;17]	3.55	27	<0.001
Precuneus	L	[-6;-52;14]	3.44	25	0.001
Precentral gyrus	L	[-42;8;29]	3.40	24	0.001
Fusiform gyrus	R	[24;-55;-13]	3.30	22	0.002
6) Minus 5					
Insula	L	[-33;-25;5]	4.49	15	0.026
Putamen	R	[24;-4;5]	4.32	117	<0.001
Precuneus	R	[21;-58;26]	4.10	22	0.002
Middle temporal gyrus	L	[-54;-16;-13]	3.97	14	0.039
Caudate nucleus	L	[-9;-1;17]	3.89	38	<0.001
Fusiform gyrus	L	[-27;-52;-7]	3.85	39	<0.001
Pallidum	L	[-24;-7;2]	3.77	56	<0.001
Superior temporal gyrus	L	[-54;-34;-1]	3.72	60	<0.001
Fusiform gyrus	L	[-33;-64;-13]	3.71	32	<0.001
Middle temporal gyrus	R	[48;-16;-10]	3.61	18	0.008
Inferior temporal gyrus	L	[-48;-64;-13]	3.37	27	<0.001
7) Minus 6					
Putamen	R	[27;-7;-1]	4.16	79	<0.001
Lingual gyrus	L	[-27;-52;-7]	4.05	35	<0.001
Precuneus	R	[21;-58;26]	3.99	19	0.005
Middle temporal gyrus	L	[-54;-34;-1]	3.56	20	0.001
Putamen	L	[-27;-1;8]	3.50	17	0.012
Fusiform gyrus	L	[-39;-67;-16]	3.50	31	<0.001
8) Minus 7					
Lingual gyrus	L	[-27;-52;-7]	3.38	20	0.005
9) Minus 8					
No voxel survived to FWE					
10) Minus 9					

No voxel survived to FWE					

Table 12. Regional BOLD co-activations with electrophysiologic burst during burst suppression state per timepoint.

Group results from GLM modelling burst EEG signal as a regressor of interest, one sample t-test height p threshold 0.005 FWE cluster-based corrected for multiple testing.

Group analysis revealed that BOLD activity positively increased in association with bursts occurrence on the EEG specifically in subcortical areas, such as basal ganglia, and cortical areas such as inferior temporal and frontal gyrus (**Fig. 27 A**, **Tab. 12** ***Original***); voxels in the thalamus did not survive the cluster correction. This result goes in line with the original publication of Golkowski and colleagues (Golkowski et al., 2017).

Briefly, to study BOLD activity per region before the start of a burst, we have modeled a GLM in single subjects with appearance of burst (burst=1, suppression=0) alternating the start of the event back in time in consecutive steps of 1 TR back to 9 TRs. **Fig. 27 B1-B4** depicts the summary region-resolved activation plots showing the maximum t-value resolved per timepoint. Activations in cortical ROIs follows a progressive increase until reaching timepoint 0, i.e., where the burst starts defined by EEG (**Fig. 27 B1**), suggesting that the GLM modelling of these regions' BOLD response fits better at the burst-onset time. This was confirmed by plotting the fitted and adjusted BOLD event-related responses of a cortical ROI, e.g., the temporal cortex, resolved in time, where the ROI's BOLD fitted response appears to match best the HRF when approaching the burst-onset (**Fig. 29 A**). On the contrary, thalamus activity shows an evident peak around -4 and -2 TRs before the burst event in voxels from the medial and posterior thalamus (**Fig. 27 B2**). ARAS regions do not show a clear pattern of activity, most of them evidencing t-values around zero before the start of the event (**Fig. 27 B3-4**).

3.3.2.2. 'Short' and 'long' bursts analyses.

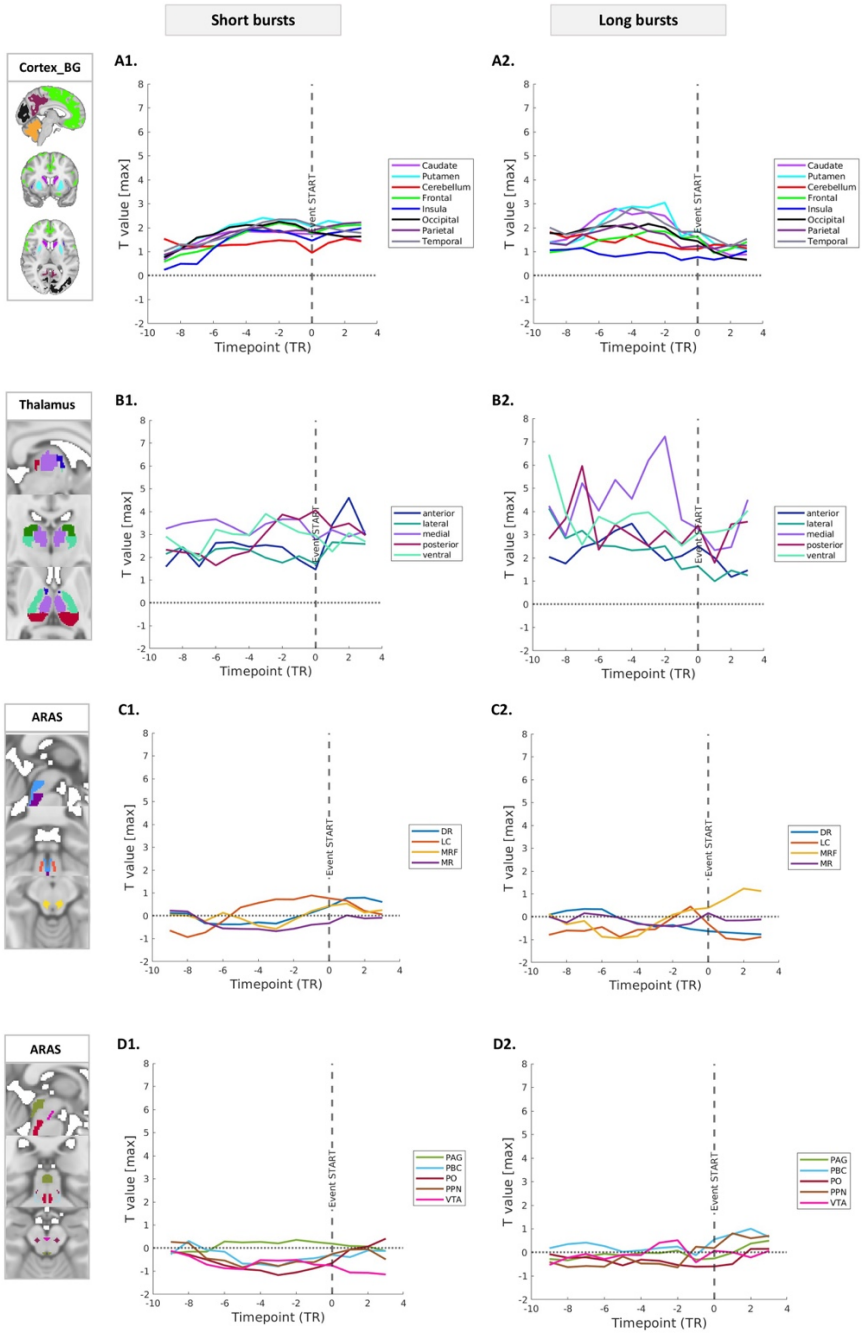

Figure 28. GLM analyses and summary of maximum t-values per ROI per timepoint.

A-D. Summary plots from GLM modeling burst modifying start of event: maximum t-value per ROI per timepoint for short bursts (left side) and long bursts (right side). *Maximum t-values were extracted from the group statistics t-maps result from a GLM modeling burst on the EEG as a regressor of interest modifying the start of the burst in consecutive steps of 1 TR back to 9 TRs; zero line corresponds to the real start of the event as defined by the EEG signal. Significant t-value starts at around t=2. Color in traces correspond to same colors in the brain cartoons for each ROI. ARAS ROIs are displayed in different plots for a better overview.*

To study whether the length of the bursting event is related to specific region activity, we have repeated our GLM analyses using only 'short' bursts (length= max 10 TRs), and 'long' bursts (length= min 20 TRs).

'Short' bursts. Pattern of activations in cortical and thalamic ROIs appears to be flattened in comparison to the analysis including all events. More specifically, for Cortex_BG ROIs, the pattern follows a less pronounced increase of activations during the period before the start of the burst in comparison to the analysis including all the bursts (**Fig. 28 A1**). Concerning thalamus activity, the pattern looks homogenous and none of the ROIs show a sudden increase of activations as suggested by the analysis including all the bursts (**Fig. 28 B1**). ARAS regions do not show a clear pattern of activity, most of them evidencing t-values around zero before the start of the event (**Fig. 28 C1 & D1**).

'Long' bursts. Activations in cortical ROIs follows a different pattern as expected, activations increase in a progressive manner until timepoint -2 TRs, which flattens afterwards, confirming that the best GLM modelling fit improves while reaching the burst-onset (**Fig. 28 A2**). Interestingly, in the thalamus, there is a peak of activation within the medial thalamus at timepoint -2 TR (**Fig. 28 B2**) and in the posterior thalamus at timepoint -7 TRs (**Fig. 28 B2**). Event-related responses of the medial and posterior thalamus are shown in **Fig. 29 B-C *Long bursts***; responses from anterior thalamus were included as a control region (**Fig. 29 D**). These plots show that medial thalamus as well as the posterior thalamus follow the expected BOLD response function (HRF), specifically medial thalamus in timepoint -4 TRs and the posterior thalamus in timepoint -7 TRs for the long bursts. ARAS regions do not show a clear pattern of activity, most of them evidencing t-values around zero before the start of the event (**Fig. 28 C2 & D2**).

Summary. Overall, these results confirm previous studies showing a positive correlation of cortical and basal ganglia BOLD activity with EEG signal at the burst-onset and depicts evidence of subcortical thalamic activity before the burst-onset.

A.

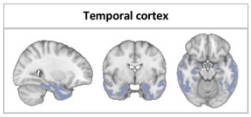

All bursts

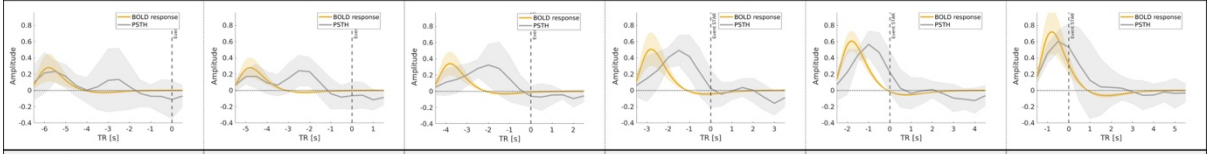

-7 TRs (~14 seconds) | *-6 TRs (~12 seconds)* | *-5 TRs (~10 seconds)* | *-4 TRs (~8 seconds)* | *-3 TRs (~6 seconds)* | *-2 TRs (~4 seconds)*

B.

Short bursts

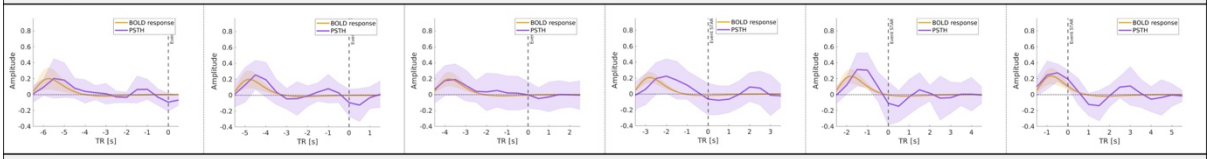

Long bursts

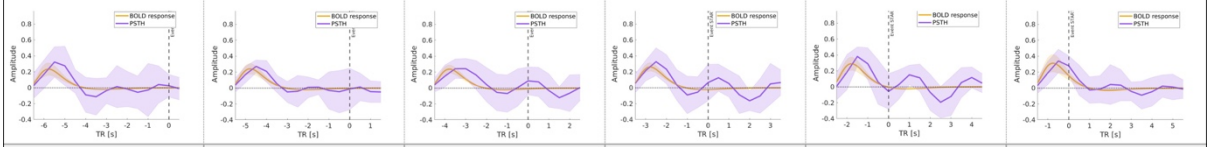

-7 TRs (~14 seconds) | *-6 TRs (~12 seconds)* | *-5 TRs (~10 seconds)* | *-4 TRs (~8 seconds)* | *-3 TRs (~6 seconds)* | *-2 TRs (~4 seconds)*

C.

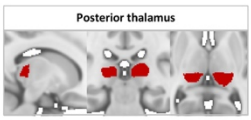

Short bursts

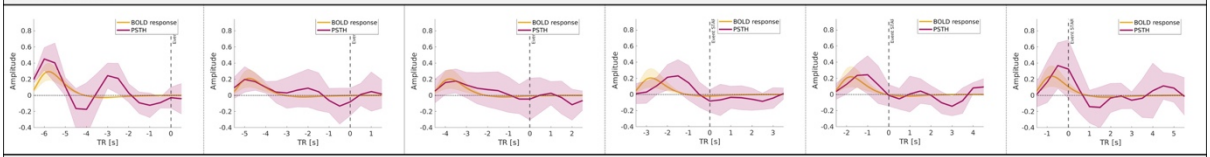

Long bursts

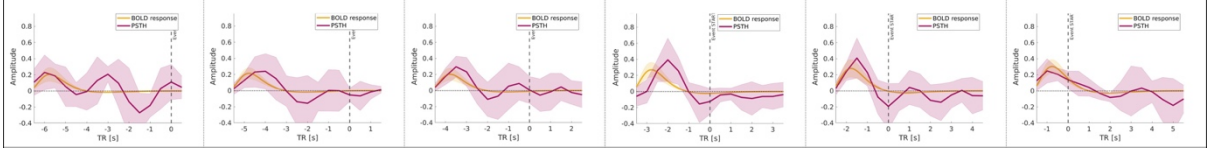

-7 TRs (~14 seconds) | *-6 TRs (~12 seconds)* | *-5 TRs (~10 seconds)* | *-4 TRs (~8 seconds)* | *-3 TRs (~6 seconds)* | *-2 TRs (~4 seconds)*

D.

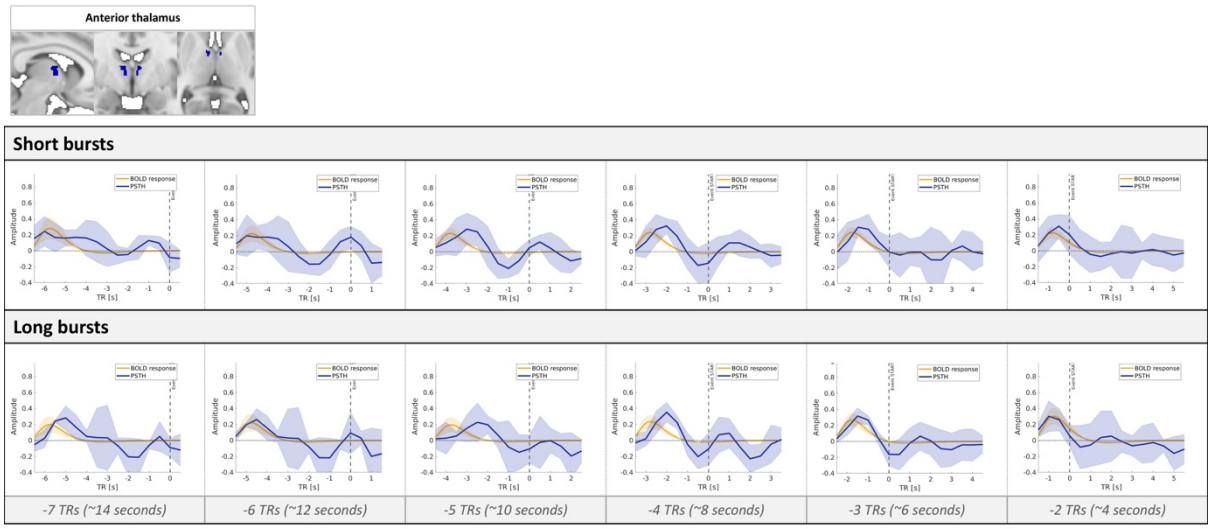

Figure 29. Event-related response time course extraction.

A-D. Mean peri-stimulus time histogram (PSTH) of adjusted data and fitted response across peri-stimulus time. *Summary plots from PSTH of adjusted BOLD response with respect to burst-modeled-BOLD response.* ***A.*** *summary plots in temporal cortex including all events per time point.* ***B-D****. summary plots for medial, anterior, and posterior thalamus per timepoint for short and long bursts. Responses were derived from the voxel with the maximum t-value within the ROI and averaged across subjects per timepoint (height p threshold p<0.01). The burst-onset is indicated in each plot for reference. Traces are color coded according to thalamus ROI (lila=medial thalamus, dark blue= anterior thalamus, dark red= posterior thalamus, yellow= peri-stimulus hemodynamic response function, shaded area= SD across subjects).*

4. Discussion

4.1. VTA and a-cBF are related to DMN BOLD functional connectivity reductions during anesthesia-induced unconsciousness

Using two independent fMRI data sets of healthy controls during wakefulness and anesthesia-induced unconsciousness with sevoflurane and propofol, respectively, we found that anesthetized states are characterized by a reduced VTA and a-cBF iFC, and that this reduction occurs in areas associated with the DMN. Particularly for VTA, this reduction regionally overlaps posterior and anterior hubs of the DMN, while for the a-cBF, the reduction targets mainly the anterior DMN. Furthermore, results from the mediation analysis showed that the reduction of the within-DMN FC independently from anesthetic, anesthetic concentration, or from anesthesia contrast, is mediated by the reduction of VTA-DMN FC. On the contrary, reduction of a-cBF-anterior DMN FC did not mediate the within-DMN FC during anesthetized states for either of the study samples, however the reduction of a-cBF-anterior DMN FC predicted the reduction of the within-DMN FC, especially for sevoflurane-induced anesthesia relative to wakefulness pre-anesthesia. This finding is, possibly, consistent with the model that an alteration between coherent activity between neuromodulatory systems, such as the dopaminergic (represented by VTA iFC) or cholinergic (represented by a-cBF iFC), and cortical DMN is intrinsically related with within-coherent activity in the DMN during anesthesia-induced unconsciousness.

4.1.1. Anesthesia-induced unconsciousness is related to VTA-DMN functional connectivity reductions

We demonstrated that connectivity between the VTA and DMN, including both forebrain and cerebellar regions, is reduced during anesthetized states (**Fig. 2 & Table 2**). This result was not confounded by neuromodulatory brainstem nuclei effects, others than VTA, and choice of seed in seed-based functional connectivity analysis (**Fig. 4**). Its generality for anesthesia-induced unconsciousness is based on consistent reductions of FC between VTA and DMN across different anesthetic agents (**Fig. 2 B & C**), anesthetic concentrations (**Fig. 5**), and anesthesia contrasts (**Fig. 6**). Our finding of reduced VTA iFC during anesthesia-induced unconsciousness is in line with recently reported reduced subcortical nuclei connectivity, including the VTA, during propofol (Nir et al., 2019; Spindler et al., 2021) and sevoflurane (Nir et al., 2022). Furthermore, it fits several animal studies,

demonstrating that direct stimulation of the VTA induces arousal behavior during continuous administration of anesthesia (Solt et al., 2014; Taylor et al., 2016).

Although not directly studied, we suggest that VTA-DMN FC reduction might reflect changes in neuromodulatory input from the brainstem towards the DMN, most probably dependent on dopamine, induced by the anesthetic agent. This interpretation is based on previous findings: first, VTA iFC resembles anatomical dopaminergic projections (Fallon & Moore, 1978; Garcia-Cabezas et al., 2009; Morales & Margolis, 2017; Yetnikoff et al., 2014); second, this pattern of connectivity can be modulated by externally administered dopamine levels (Cole et al., 2013; Kelly et al., 2009; Kohno et al., 2016; Shafiei et al., 2019); third, it can be affected by VTA-deep brain stimulation-evoked dopamine release in swine, demonstrating a correlation between stimulation amplitude and fMRI-BOLD amplitude changes (Settell et al., 2017); and fourth, in a recent publication it was demonstrated that methylphenidate, a dopamine reuptake inhibitor, increased VTA-DMN connectivity in patients with chronic disorders of consciousness (Spindler et al., 2021).

However, there are three limitations to acknowledge: First, definitive direct evidence for dopaminergic manipulation leading to VTA BOLD FC reduction, (as it has been demonstrated for cBF lesions and related connectivity changes in monkeys (Drew et al., 2020)), is still missing. Second, dopamine-related changes induced by propofol, or halogenated ethers are mixed (for a Review on this topic, see (Hao et al., 2020)). For instance, presynaptic dopamine release in isolated nerve terminals is inhibited by isoflurane, while in striatal slices this anesthetic causes an increase in the basal release of dopamine (Hao et al., 2020). Furthermore, propofol increases dopamine release in the somatosensory cortex (Shyr et al., 1997) but decreases dopamine concentrations in the nucleus accumbens (Schulte et al., 2000) and in the mPFC (Wang et al., 2016). Such findings suggest that these anesthetic agents alter the normal physiology of dopaminergic neurotransmission in the brain, however, they do this in a heterogenous way. It is also unclear whether these alterations result from a direct effect of the anesthetic agent on dopaminergic VTA cells and/or at dopaminergic synapses in the projection target regions, or from an indirect effect of the anesthetics on different mechanisms controlling VTA activity, e.g., enhancement of GABA-mediated inhibitory neurons in the VTA (Lee et al., 2001). Third, our measure of FC does not allow inferences about the direction of connectivity changes. Therefore, due to reciprocal structural connections between VTA and cortical forebrain, FC changes might be also induced by changes in the cortical DMN due to anesthesia effects. Future effective connectivity analyses might solve this problem of directed connectivity (Sabaroedin et al., 2022).

4.1.2. Anesthesia-induced unconsciousness is related to a-cBF (Ch1-Ch3) functional connectivity reductions

To the best of our knowledge, this is the first study assessing effects of anesthesia on a-cBF-DMN FC in humans. Our results showed that a-cBF to anterior DMN FC is significantly reduced during anesthetized states (**Fig. 7 & Table 8**), independently of anesthetic agent, i.e., sevoflurane or propofol (**Fig. 7 B & C**), anesthetic concentrations, i.e., sevoflurane 3- and 2vol%, (**Fig. 9**), and anesthesia contrasts., i.e., wakefulness pre- and post-anesthesia (**Fig. 10**).

Although not directly studied, this result might reflect the direct effect of anesthesia on cholinergic forebrain input to DMN anterior hubs associated with modulation of wakefulness. This interpretation is grounded through previous reports: first, rs-FC mapping of cBF, including a region-specific a-cBF map, has been demonstrated in healthy controls (Fritz et al., 2019; Markello et al., 2018); second, areas of FC reduction were largely consistent through the analyses, principally localized in the medial frontal and anterior cingulate cortices, which goes in line with the origin of its cholinergic innervation coming from rostromedially cholinergic cellular groups (Ch1-Ch3) (Bloem et al., 2014; Ghashghaei & Barbas, 2001; Luiten et al., 1987); third, cBF FC has been used to assess cholinergic dysfunction in patients with cognitive impairment disorders, e.g., mild cognitive impairment (Byun et al., 2022; Meng et al., 2018), neuropsychiatric diseases, such as, Parkinson's disease (Gargouri et al., 2019), and diseases directly related with a dysfunction of sleep-wake cycle, such as Insomnia (Ma et al., 2021), or vigilance, like in temporal lobe epilepsy (Fan et al., 2022); and fourth, experiments in rodents have demonstrated that the administration propofol and sevoflurane, respectively, are associated with a decreased ACh release in the frontal cortex (Gamou et al., 2010; Kikuchi et al., 1998; Nemoto et al., 2013; Shichino et al., 1998; Shichino et al., 1997), as well as with reduced neuronal activity in the cBF (Luo et al., 2020).

If our results, a-cBF-anterior DMN FC reduction, reflect any aspect of cholinergic downregulation through anesthesia, there are some limitations to consider. First, the amount of neurons within the a-cBF (Ch1-Ch3) is considerably reduced in comparison to the Ch4: from ~200 000 cholinergic neurons per hemisphere, only ~5% where identified as Ch1-Ch3 groups (Arendt et al., 1985); also the proportion of cholinergic to non-cholinergic neurons varies within these cell groups: ~90% of neurons are cholinergic in the Ch4, while only 10% in the Ch1, 70% in the Ch2, and 1% in the Ch3 group (Mesulam et al., 1983). Thus, is not clear whether the observed effect depends solely on cholinergic input. Second, although there is experimental evidence in primates demonstrating that cBF lesions affect ipsilateral global fMRI fluctuations as well as RSN-within FC, the tested cBF regions were

specifically, subregions of Ch4 (Turchi et al., 2018). Studies addressing more anterior regions of the cBF, i.e., Ch1-Ch3 are still missing. Third, as mentioned before, our FC measure does not allow inferences about the directionality of connectivity changes. Hence, the observed effect could emerge as well from direct effects of anesthesia on anterior-DMN FC affecting a-cBF iFC. Future effective connectivity analyses might solve this problem of directed connectivity (Sabaroedin et al., 2022).

4.1.3. Reduction of within-DMN BOLD connectivity during anesthesia-induced unconsciousness is mediated by reduction of VTA-DMN connectivity reductions

The main motivation of this study was to explain the effect of sevoflurane- and propofol-induced anesthesia, respectively, on DMN FC via connectivity changes between VTA and DMN. To do so, we replicated DMN FC reductions during anesthesia-induced unconsciousness for both sevoflurane and propofol (**Fig. 11 A2 & B2**), and we demonstrated that this reduction is mediated by VTA-DMN FC reduction. This was evidenced independently of anesthetic agent (**Fig. 11 A3 & B3**), anesthetic agent concentration (Fig. S6), confounds of ventral tegmental area nearby neuromodulatory nuclei (**Fig. 13**), and anesthesia contrast (**Fig. 14**). This finding fits recent evidence showing that alteration in dopaminergic neuromodulation within the precuneus/PCC area might explain both DMN FC reduction and consciousness modulation (Spindler et al., 2021). While these results focused on the posterior hub of the DMN, we could also observe that the reduction of VTA FC towards the *anterior* parts of the DMN, namely the ACC, might be of comparable importance. Concretely, we found for mediation analyses of both sevoflurane 2vol% anesthesia induction and sevoflurane 3vol% anesthesia recovery (**Fig. 13-14**), that specifically VTA FC reduction towards the mPFC is a mediator of the anesthetic´s effect on DMN FC. These results are consistent with recent experiments in rodents showing that a pharmacologically induced inactivation of the mPFC facilitates induction of anesthesia-induced unconsciousness, and that this inactivation delayed emergence from sevoflurane-induced unresponsiveness (Huels et al., 2021). These results suggest that FC reduction between VTA and anterior DMN is a comparable mediator of anesthesia-induced DMN FC reduction as VTA FC reduction towards the posterior DMN.

Even when assuming that these VTA FC mediation effects on DMN FC during anesthesia are influenced by dopaminergic effects (see discussion above), it is worth to mention that the mechanisms by which dopaminergic modulation eventually affects BOLD-based DMN FC are still poorly understood. One reason is that the specific nature of the effect which translates into a reduction of correlated BOLD signals is unclear, e.g., is the target of modulatory dopamine vessel cells that control directly cerebral

blood flow or/and neuronal populations that control blood flow indirectly (Bruinsma et al., 2018). Future studies such as those separating neuronal (e.g., EEG-derived measures) from neuro-vascular coupling outcomes (e.g., HRF) with respect to VTA FC are necessary to address these topics.

4.1.4. Reduction of within-DMN BOLD connectivity during sevoflurane-induced unconsciousness correlates with reduction of a-cBF to anterior DMN connectivity reduction

The goal of this study was to determine the association between the effect of sevoflurane- and propofol-induced anesthesia, respectively, on DMN FC and changes between a-cBF to anterior DMN FC. Using our mediation analysis approach, we could not demonstrate that a-cBF-anterior DMN FC reductions mediated the within-DMN FC reductions, independently of anesthetic agent, i.e., sevoflurane or propofol, anesthetic agent concentration, i.e., sevoflurane 3- or 2vol%, or anesthesia contrast, i.e., wakefulness pre- or post-anesthesia. Based on the extensive body of literature suggesting the importance of the cholinergic system in the modulation of wakefulness, we conclude that that our model is not suitable to explain the relationship between these variables.

Results from our correlation analyses demonstrated that a-cBF-anterior DMN FC reductions significantly predicted the within-DMN FC during sevoflurane 3vol%-induced anesthesia (**Fig. 17 A1**), whereas during sevoflurane 2-vol%-induced anesthesia, we only found a strong trend of significance (**Fig. 17 A2**). During propofol-induced anesthesia, the analysis showed that the definition of the DMN FC affected the results, for instance, the statistical power of the correlation between a-cBF-anterior DMN FC and within-DMN FC reductions improved after focusing strictly on voxels of significant reduction of the within-DMN FC (from a p value of 0.3 to 0.06) (**Fig. 17 A3 & Fig. 18**), but still only showing a strong trend of significance. These results suggest, that although the effect of anesthesia on a-cBF iFC, i.e., significant reduction in anterior DMN forebrain areas (**Fig. 15**), as well as the effect on within-DMN FC, i.e., significant reduction in posterior as well as anterior hubs (**Fig. 16**), is largely consistent between studies, the relationship between a-cBF-anterior DMN FC and within-DMN FC reduction could be specific for anesthetic concentrations or anesthetic agent. For instance, experiments in rodents have shown that both, sevoflurane and propofol, decrease concentrations of ACh in the frontal cortex, however with sevoflurane there is also a decrease in the striatum, whereas for propofol this is not the case (Nemoto et al., 2013; Shichino et al., 1998; Shichino et al., 1997). This is also evidenced in our results comparing anesthetized-states vs. wakefulness pre-anesthesia, e.g., the reduction of a-cBF iFC during sevoflurane 3vol% include subcortical areas such as basal ganglia

(**Fig. 15 B2**), while this is not the case during sevoflurane 2vol% (**Fig. 15 B3**) or propofol (**Fig. 15 C2**). Alternatively, there might be a regional-specific effect dependent on anesthetic concentration or anesthetic agent on ACC/frontal cortex (e.g., Brodmann areas 24, 25 or 32) which could better explain the reduction of DMN iFC during anesthesia-induced unconsciousness during this specific states. Particularly considering that these cortical areas have their own unique receptor fingerprint (Palomero-Gallagher et al., 2008), hence these might be affected in different ways dependent on anesthetic or anesthetic concentration.

If we consider that our findings might reflect cholinergic changes under anesthesia, we were able to demonstrate that the effect of sevoflurane on cholinergic input to the ACC/medial frontal cortex predicts the reduction of the within-DMN, which is consistent with the idea that cholinergic neuromodulation of PFC plays a critical role in the modulation of consciousness (Mashour et al., 2022; Pal et al., 2018). However, it is important to mention that the mechanisms by which cholinergic modulation affects BOLD-based DMN FC are not yet completely understood. More specifically, it is not clear yet how a cholinergic activity disruption translates into reduction of correlated BOLD signals. Future experiments determining quantitative relationships between neural activity, BOLD and cerebral blood flow with cholinergic modulation is still needed.

4.1.5. Limitations

First, while BOLD 3-Tesla fMRI enables brain-wide analysis of brain activity, it is clearly limited in both its spatial-temporal resolution particularly in the brainstem and its specificity of signal nature. These resolution and specificity limitations prevent not only more detailed analysis of cellular underpinnings (e.g., dopaminergic nature of VTA FC or cholinergic nature of a-cBF iFC) but also – at a larger scale – exact regional delineations of our seeds with potentially confounding effects of neighboring nuclei. For the later problem, 7-Tesla MRI approaches might be useful. Beyond partial volume effects from neighboring structures, further regions such as direct projections from the PFC to or striatal inhibitory influences on the analyzed seeds, might confound connectivity the connectivity patterns and its associated role with the DMN. Second, as our study is only based on two rather small cohorts, statistical power of results is limited. However, a-priori power calculations under the assumption of large and consistent effect size of anesthesia on FC confirmed chosen sample sizes for both state comparison and mediation analysis (see Methods). Furthermore, results were replicated across cohorts, suggesting further reliability of findings. Third, our study is restricted to males. Therefore, generalization of results to females should be evaluated carefully. Fourth, our experimental and

analytic approach prevent a process analysis of anesthesia effects in terms of cause/effect and event-based resolution. Instead, it is based on averaged outcomes across large brain areas as well as across prolonged periods of time, which, together with the mediation analysis approach, restricts us to an analysis of conditional factors of anesthesia-induced unconsciousness. Fifth, although results of reduced VTA-DMN as well as a-cBF-anterior DMN and its association with reduced within-DMN FC are consistent across samples, findings might not be the same with agents acting through other mechanisms (e.g., ketamine, dexmedetomidine). Future experiments with those anesthetics are necessary.

4.1.5. Conclusion

Our findings demonstrate that the reduction of VTA-DMN FC mediates the within-DMN FC during anesthesia-induced unconsciousness with sevoflurane and propofol anesthesia, and that the reduction of a-cBF-anterior DMN FC predicts the reduction of within-DMN FC during sevoflurane-induced anesthesia.

4.2. Beyond static connectivity analyses: DMN transient global synchronizations are reduced during anesthesia and mediated by VTA

We demonstrated that first, during anesthesia-induced unconsciousness with sevoflurane and propofol, respectively, transient large-scale BOLD synchronizations across the DMN are reduced relative to wakefulness states, and second, that the effect of sevoflurane on transient large-scale synchronizations across the DMN is mediated by the change in correlated activity between VTA and DMN upon wakefulness post-anesthesia. We did not find any mediating effect of a-cBF and DMN correlated activity on the change of transient large-scale synchronizations across the DMN nor across further control networks. These findings suggest that: first, a pattern of reduced BOLD synchronizations in the DMN could be a signature of anesthesia-induced unconsciousness, with sevoflurane and propofol respectively; and second, that a coherent VTA-DMN functional connectivity is crucial for reestablishing structured synchronization pattern in the DMN.

4.2.1. Anesthesia-induced unconsciousness is related to reduced transient large-scale synchronizations across the DMN relative to wakefulness

Our results showed a significant reduction of transient large-scale synchronizations across the DMN, but not in the whole-brain, independent of anesthetic concentration, i.e., sevoflurane 3- and 2vol%, or anesthetic, i.e., sevoflurane or propofol, compared to wakefulness pre-anesthesia. Relative to wakefulness post-anesthesia, this reduction was significant across DMN during sevoflurane 3vol%; there was a strong trend of significance compared to sevoflurane 2vol%-induced state (**Fig. 19 A1-2 & B1-2**). To control for specificity, we tested further RSNs, i.e., sensorimotor and frontoparietal network, where we found a significant reduction of synchronizations, however only during sevoflurane-induced states (**Fig. 19 C1-2 & D1-2**).

This finding demonstrates that among the tested ensembles, the DMN showed the pattern of large-scale synchronizations most sensitive to discern between wakefulness and anesthetized states across anesthetics, hence suggesting that a structured synchronization pattern within the DMN could be a neural correlate of anesthesia-induced unconsciousness (independent on anesthetic concentration, but on the presence or absence of responsiveness). This interpretation is based on the following evidence: first, disrupted large-scale synchrony among neural processes has been suggested as a potential mechanism of anesthesia-induced unconsciousness (Alkire et al., 2008; Barttfeld et al., 2015; Demertzi et al., 2019; Mashour & Hudetz, 2018); second, studies of ongoing BOLD fMRI fluctuations suggest that physiologically-, e.g., deep sleep, or pharmacologically-induced unconsciousness, e.g., propofol sedation in monkeys and humans, are associated with disrupted cortical large-scale correlations in both space and time (Barttfeld et al., 2015; Hahn et al., 2021); third, it has been demonstrated that both stationary and dynamic FC, particularly within the DMN, is typically reduced during anesthesia (Boveroux et al., 2010; Golkowski et al., 2019; Palanca et al., 2015); and fourth, we provide evidence suggesting that decreased large-scale BOLD coactivations across the DMN might be a signature of consciousness itself (i.e., presence or absence of behavioral responsiveness), showing that the behavior across DMN regions during anesthetized states compared to wakefulness suggests a more 'binary' nature, i.e., awake states are different from states with anesthesia, however there is this difference is not present between anesthesia-induced states (sevoflurane 3vol% vs. sevoflurane 2vol%).

However, there are some points which need to be considered; first, the global synchronization index (FF), is not sensitive to anticorrelations, which prevents us to reflect anticorrelated infra-slow BOLD

activity during the wakefulness states; second, our analyses are focused on FF distributions across a specific time-window (~25 TRs) based on Hahn and colleagues' results showing that this span of time provides sufficient sampling across time to give a robust separation of consciousness states (Hahn et al., 2021), however further studies are needed to overcome the limitation of distribution-based markers (Hahn et al., 2021); and fourth, it is worth mentioning that in contrast to previously proposed by Hahn and colleagues (Hahn et al., 2021), in our study the whole-brain synchronicity changes was not able to differentiate anesthesia-induced unconsciousness states from wakefulness. Thus, our results do not support the idea that brain-wide synchronization in fMRI data could reflect physiological signals dependent on level of consciousness/responsiveness as suggested by Scholvinck and colleagues (Scholvinck et al., 2010). The possibility that this difference originating from brain-wide synchronizations could be related to head movement artifacts cannot be excluded, especially considering that although both preprocessing pipelines are highly comparable, we have carefully performed an extensive movement artefact correction (see Methods: preprocessing fMRI data), including steps omitted by Hahn and colleagues, such as slice oriented motion correction (SLOMOCO). Furthermore, we have implemented a different 'whole-brain' parcellation, focusing on 5-mm sphere-ROIs time courses, and not on complete delineated anatomical ROIs as Hahn and colleagues to avoid introducing partial volume confound effects between areas.

4.2.2. VTA- and a-cBF-DMN functional connectivity is reduced during anesthesia-induced unconsciousness: summary results from first project

Using two independent fMRI data sets of healthy controls during wakefulness and anesthesia-induced unconsciousness with sevoflurane and propofol, respectively, we found that anesthetized states are characterized by a reduced VTA and a-cBF iFC. This reduction has been demonstrated independently of anesthetic agent, i.e., sevoflurane or propofol, anesthetic concentration, i.e., sevoflurane 3vol% or 2vol%, and anesthesia contrast, i.e., wakefulness pre- or post-anesthesia. Crucially, this reduction occurred mostly in areas associated with the DMN. Particularly for VTA, this reduction regionally overlaps posterior and anterior hubs of the DMN, while for the a-cBF, the reduction targets mainly the anterior DMN (**Fig. 20 & 21**). (*See detailed discussion above*)

4.2.3. Reduction of transient large-scale BOLD synchronizations across the DMN is mediated by reduced VTA-DMN but not by reduced a-cBF-DMN functional connectivity during anesthesia-induced unconsciousness

The goal of this study was to find the link between the reduction of BOLD fluctuations in large-synchrony across DMN regions and the reduction of functional connectivity between both VTA and a-cBF, respectively, to DMN during anesthesia induced unconsciousness. Our results demonstrate that the effect of sevoflurane 3vol% on transient large-scale synchronizations across the DMN was mediated by the change in correlated activity between VTA, but not a-cBF, and this network upon wakefulness post-intervention (**Fig. 23 A2**). Our study suggests that, possibly, coherent VTA-DMN activity is crucial for reestablishing structured synchronization pattern in the DMN. This interpretation is based on the following: first, recent studies have identified subcortical areas functionally and anatomically connected to the DMN, including VTA (Aguilar & McNally, 2022; Alves et al., 2019; Harrison et al., 2022; Li et al., 2021); second, recent evidence showing that cortical areas, including areas in the DMN, could be modulated by VTA during anesthesia- and disorder-induced unconsciousness, specifically it was demonstrated that functional connectivity of infra-slow activity between VTA and DMN is reduced in patients with disorders of consciousness, and increased with the administration of methylphenidate, a dopamine and norepinephrine reuptake inhibitor (Spindler et al., 2021); and third, several studies have demonstrated that stimulation of the VTA, e.g., electrical (Solt et al., 2014), optogenetic (Taylor et al., 2016), or chemo genetic (Oishi et al., 2017) induces wake-like behavior in rodents.

4.2.4. Limitations

As for the first project, is important to acknowledge that our BOLD fMRI datasets are derived from 3-Tesla fMRI scanner, which on the one side enables brain-wide analysis of brain activity, and on the other side, it is clearly limited in both its spatial and temporal resolution, particularly in the brainstem. Furthermore, we lack specificity in terms of nature of the signal, i.e., cholinergic for a-cBF or dopaminergic for VTA analyses (*See detailed discussion in first project*). Regarding our experimental and analytic approach, i.e., FF calculation and distribution analyses, it is important to mention that the FF is a measure of variability of neuronal spike trains commonly used in electrophysiological experiments, which when implemented using the BOLD signal it carries several limitations. First, the fMRI BOLD signal, a readout of infra-slow fluctuations of blood oxygenation in vessels in the brain,

only provides an indirect measure of neuronal activity based on a complex interaction between neurons, vascular cells and neuroglia called the neurovascular coupling, therefore our results of 'synchronicity' should be carefully interpreted. Second, to calculate the FF, we have reduced our continuous BOLD signal into countable single events by applying a trespassing threshold, evidently loosing information along the way; a systematic analysis using different thresholds is necessary. Third, the dependence of the FF on the intensity rate of events is still unclear, for example it has been observed in electrophysiological experiments that changes of intensity of spiking rates are equivalent to changing the length of the observation window with fixed intensity (Rajdl et al., 2020), it is unclear how this translates to BOLD event readouts and its relationship with wakefulness or states of unconsciousness. Fourth, regarding the mediation analysis, contrary to the FF outcome, i.e., scale parameters derived from FF fitted distribution, our VTA-DMN FC measure is based on averaged outcomes across the whole scanning time, which restricts our interpretation of conditional factors of anesthesia-induced unconsciousness. Fifth, future experiments with those anesthetics and consciousness-altered conditions are necessary to evaluate.

4.2.5. Conclusion

Results demonstrate reductions of transient BOLD large-scale synchronization across the DMN might be a signature of anesthesia-induced unconsciousness, which specifically upon wakefulness post-intervention with sevoflurane were mediated by the change of FC between the VTA and this network.

4.3. Subcortical activity in period prior burst-onset during sevoflurane-induced burst suppression state

Using simultaneous EEG-fMRI recordings from healthy participants during BS state induced with sevoflurane anesthesia we have shown that the period before the start of a burst is characterized by increased dynamic functional connectivity between cortical and subcortical areas, especially the brainstem and thalamus, which participation might be related to the length of the bursting event. Our results for the thalamus were supported by GLM analyses and regional-specific event-related responses. This finding supports the idea that subcortical regions might be causal in the generation of individual bursts in sevoflurane anesthesia BS.

4.3.1. Period prior burst-onset is associated to increased subcortical-cortical dynamic functional connectivity

Our time-resolved averaged dynamic correlation analysis using all bursts showed a significant increased connectivity between Cortex_BG and ARAS ROIs starting already at ~18 seconds, reaching the highest point at ~6 seconds and dropping ~2 seconds before the burst-onset (**Fig. 25 D**). Interestingly, our analyses dependent on burst-length, i.e., including only 'short' bursts, i.e., defined as bursts no longer than 10 TRs (~20 s), or 'long' bursts, i.e., defined as bursts longer than 20 TRs (~40 s) showed that the participation of the thalamus before the burst-onset might depend on the burst-length. This was evidenced by the increased connectivity of thalamic and cortical -including basal ganglia- ROIs before the burst-onset specially in the 'long' bursts (**Fig. 26 E2)**. These results demonstrate that, first, connectivity between cortical and subcortical areas, including ARAS and thalamic regions increased before the burst-onset; second, grouping bursts by length improved unraveling connectivity patterns, especially depicting participation of thalamo-cortical activity before a 'long' bursting event started and almost disappearing with shorter bursts.

Contrary to the view about BS being characterized by an isolated cortex (Steriade et al., 1994), this finding supports the idea that coherent cortico-subcortical activity is present before a single burst, hence, possibly, reflecting causation of bursts during BS induced with sevoflurane. This interpretation is based on previous literature: regarding the thalamus: first, sensory input triggers cortical EEG bursting activity during BS state (Kroeger & Amzica, 2007), which are morphologically analogous, e.g., in power, frequency, and duration, to the spontaneously-emergent bursts (Hudetz & Imas, 2007); second, in vitro electrophysiologic studies in auditory thalamocortical slices demonstrated that isoflurane in moderate concentration depresses polysynaptic bursts, i.e., those emerging from cortico-cortical connections, more than those monosynaptically driven, i.e., those emerging from thalamo-cortical afferents (Voss et al., 2019); and third, a recent study using high-speed calcium-imaging showed that unilateral thalamic inactivation caused a shift in the spatial distribution of cortical onset sites away from the inactivated hemisphere (Ming et al., 2020).

However, we cannot completely exclude the possibility that bursting activity during sevoflurane-induced BS could originate in the cortex as well, mainly because of two reasons: first, it might be that the analyzed bursts were all induced by external stimuli, especially from auditory nature, i.e., MRI sound during BS EEG-fMRI data recordings, and second, the 'short' bursts cortico-cortical connectivity pattern presents a strong trend of decreased connectivity at ~14 seconds before the burst-onset,

which could reflect the loss of global coherence due to specific reverberant activity in few areas. Nevertheless, our results are consistent with an EEG study in pediatric patients with severe epileptic and non-epileptic encephalopathies with BS pattern, where it was demonstrated that bursting periods were characterized by a significant cortico-subcortical directed coherence, while suppression periods, presented a non-directed cortico-cortical coherence (Japaridze et al., 2015). This suggests that probably there is a common mechanistic explanation for bursting global events independent of their origin, i.e., pathology-related BS patterns or pharmacologically-induced ones. Application of our research method to further characterize bursts of different origin could be helpful.

Regarding the role of Cortex_BG-ARAS interaction in the generation of single bursts, our results are consistent with animal experiments, which have shown that direct stimulation in the midbrain reticular formation during isoflurane-BS state produced single bursts (Orth et al., 2006), plus it has been proposed that extra-thalamic pathways, especially those originated in the midbrain, could play a role in the facilitation of spontaneous bursts and of those produced by directly of the brainstem nuclei (Golanov & Reis, 1995; Hudetz & Imas, 2007). Interestingly, a decreased connectivity between ARAS ROIs was evidenced in both 'short' as well as the 'long' bursts. We interpret this finding as indirect evidence indicating regional differentiation and consequently loss of coherence associated with, possibly, midbrain burst-generating activity.

4.3.2. Period prior to burst-onset is associated to increased subcortical BOLD activations: GLM analyses

The aim of this project was to investigate regional-specific BOLD activations during a period of ~18 seconds before the burst-onset during sevoflurane-induced BS. First, evaluating BOLD activity during the bursting events (i.e., periods of EEG high voltage activity), we could replicate previous findings from (Golkowski et al., 2019) about the positive coupling of EEG and BOLD signal across cortical areas, mainly temporal, frontal, and parietal regions, as well as subcortical areas, specifically basal ganglia, but not thalamus (after correcting for multiple comparison) (**Fig. 27 A & Tab. 12 *Original***). In our model, we included the global signal as a covariate of no interest, thus voxel-wise, the extend of our significant activations was reduced in comparison with the original paper. This indicates that although it has been demonstrated that anesthesia, i.e., subclinical as well as clinical concentration of sevoflurane, directly affects metabolic and cerebrovascular physiology, e.g., regional cerebral blood flow (rCBF), cerebral blood volume (rCBV) and cerebral metabolic rate of oxygen (rCMRO2) (Kaisti et al., 2003; Kaisti et al., 2002; Kolbitsch et al., 2001; Kolbitsch et al., 2000; Lorenz et al., 2001; Schlunzen

et al., 2004), neurovascular coupling seems to be preserved even in extreme brain state conditions such as BS. This has been observed in rats under BS conditions, where EEG and BOLD cortical signals where temporally and spatially highly correlated (Liu et al., 2011); in monkeys (Zhang et al., 2019) and in humans (Golkowski et al., 2019).

Next, evaluating the period prior burst-onset, our results showed that the BOLD activations in the cortex and basal ganglia followed a progressively increasing pattern of activations starting at ~18 seconds before the burst-onset, reaching its highest peak at for most of these ROIs, at timepoint 'zero' or burst-onset (**Fig. 27 B1**), suggesting that the GLM modelling of these regions' BOLD response fits better at the burst-onset time and confirmed by plotting the mean BOLD event-response of voxels within the cortex (**Fig. 29 A**). Interestingly, we found that thalamus regions did not follow the activation pattern as for the cortical and basal ganglia areas, but some nuclei depicted a sudden increase of activation at ~8 seconds (in medial thalamus) and at ~4 seconds (in posterior thalamus) prior burst-onset (**Fig. 28 B1-B2**). Critically, sudden thalamic BOLD activations were confirmed while studying specific bursts grouped by length. For instance, 'long' bursts, i.e., bursts with a minimal length of 20 TRs, showed increased activations in both the medial and the posterior thalamic nuclei, however in different timepoints as when including all bursts, at ~4 seconds (in medial thalamus) and at ~14 seconds (in posterior thalamus) (**Fig. 28 B2**). For the 'short' bursts, i.e., bursts with a maximal length of 10 TRs, medial thalamus' activations showed less pronounced peaks, e.g., at ~12 or ~4 seconds before the burst-onset; in posterior thalamus there is a more pronounced, but still not comparable to the 'long' bursts' one, at ~4 seconds prior to burst-onset (**Fig. 28 B1**).

BOLD activations before a global-bursting event are consistent with a previous study applying this same approach of artificially modifying the event-onset, where it was found that thalamic regional BOLD activity preceded generalized spike wave discharges by 6 seconds (Moeller et al., 2008). This might indicate a common underlying mechanisms of bursting global events, for example Liou and colleagues (Liou et al., 2019) observed that in a rodent epileptic model during BS induced by anesthesia, the thalamus triggered interictal bursts, plus inactivation of the ventroposterolateral thalamic nuclei reduced the rate of seizures (Liou et al., 2019). However, further research including bursting global events from different origins, for instance pharmacologically-induced with different anesthetics, and diseased-induced like in coma, encephalopathies, or epilepsy, are needed.

Our findings about increased pre-burst thalamic BOLD activations particularly for 'long' bursts were confirmed by the extraction of the mean event-related response, i.e., PSTH, of thalamic voxels and

the mean burst-modeled-BOLD for the burst event, where we found that particularly for medial thalamus there was a qualitatively accurate fit between time courses in comparison with posterior or anterior thalamic nuclei (**Fig. 29 B-D**). This is consistent with canonical electrophysiological experiments during BS in cats, where it was demonstrated that, during silent periods in cortical cells, i.e., suppression periods corroborated with electrocorticography (ECoG), there was a persistent electrical activity in ~30-40% of recorded thalamic neurons, located in ventral and centromedial thalamic areas (Steriade et al., 1994). Ii is important to mention that during timepoint 'zero' or burst-onset, the t-values for single voxels in the thalamus are high enough to reach significance, which means we cannot exclude the possibility that the thalamus does not show coherent BOLD fluctuations with the cortex hence with the EEG BS pattern as shown in previous studies (Liu et al., 2011).

Regarding further regional-specific BOLD activations with distinction of burst-length, e.g., cortical, and basal ganglia's activation pattern suggest a more homogenous behavior (**Fig. 28 A1-A2**), following the expected pattern as for the analysis including all events. Results for ARAS regions were inconclusive, although we see sudden increase in activations prior burst-onset, for example in the VTA at around ~6-4 seconds in all events as well as in the 'long' ones, the statistical values do not support any interpretation (**Fig. 27 C1-C2 & D1-D2**). For the rest of the ARAS nuclei, there is no specific pattern, which might indicate different BOLD dynamics which is not captured by the canonical HRF. Taking these results together with our dynamic functional connectivity ones, we suggest that subcortical activity, especially thalamic one, might be causal in the generation of single 'long' bursts during BS with sevoflurane. Our results do not suggest cortical activity as possible generator of a single burst during BS.

4.3.3. Limitations

As in our previous projects, there are several limitations: first, our BOLD fMRI datasets are derived from 3-Tesla fMRI scanner, which on the one side enables brain-wide analysis of brain activity, and on the other side, is clearly limited in its spatial resolution, particularly in the brainstem and deep structures as the thalamus. However, regarding the temporal resolution, it is recognized that BS has a slower timescale than neural activity associated with less-deep anesthetized states (i.e., 0.5 to 2Hz delta oscillations) (Ching et al., 2012), which is suitable for canonical BOLD responses. Second, regarding the methods used for these analyses, it is important to mention that our connectivity analyses were derived from parcel-averaged dynamic correlations, which disregards regional specificity, plus, the PJK approach is a novel method which needs further research to validate our present results. Third, as mentioned in the discussion, regarding our GLM analyses and region-specific

event-related responses, it is important to highlight that we found BOLD signal changes prior burst-onset longer than by 4 seconds, which is the canonical delay that has been described to elicit a BOLD response after a stimuli in an experiment (Glover, 1999). Specific BOLD-response modelling for a burst event is necessary to confirm these results. And fourth, our interpretations about causation should be taken carefully, effective connectivity analyses might solve this problem of directed connectivity.

4.3.4. Conclusion

Our findings demonstrate that just before the bursting global event, there is a significant increase in connectivity towards the cortex of subcortical areas, including thalamus and ARAS nuclei, but not to cortico-cortical connectivity. Thalamus-related results are supported by GLM and event-related response time courses.

4. Conclusion

In our first project, focusing on states of deep anesthesia, i.e., anesthesia-induced unconsciousness with sevoflurane 3vol% and 2vol%, or with propofol, we investigated the effect of these anesthetics on the intrinsic functional connectivity of both the VTA and a-cBF and its association with the effect of anesthesia on the so-called DMN, respectively. Here we demonstrated that independently of anesthetic, anesthetic concentration or anesthesia contrast, i.e., wakefulness pre- or post- anesthesia, anesthesia-induced unconsciousness is associated with both a reduced VTA and a a-cBF intrinsic functional connectivity, crucially, in areas included in the DMN. We further demonstrated that anesthesia-induced unconsciousness is associated with a reduced within-DMN functional connectivity and that these reductions were mediated by the connectivity reduction between VTA and DMN, independently of anesthetic agent, anesthetic concentration, or anesthesia contrast. We did not find a mediation effect of within-DMN connectivity reduction via a-cBF-DMN; however, we demonstrated that these were significantly correlated, especially for sevoflurane-induced anesthesia. These findings support the idea that the direct modulation of cortical dynamics represented by the reduction of the within-DMN during anesthetized states, are intrinsically related to lower-order anesthetic actions, i.e., direct effect on subcortical neuromodulatory systems associated with arousal processes represented by reduced VTA iFC and a-cBF iFC, respectively.

In our second project, also focusing on states of deep anesthesia, we investigated the effect of anesthesia on the transient large-scale BOLD synchronizations across DMN regions and its association with the reductions of VTA-DMN and a-cBF-DMN connectivity, respectively. We found first that there is a reduction of large-scale BOLD coactivations across DMN in anesthesia induced-states compared to wakefulness with sevoflurane and propofol, respectively, and second, that the reduction with sevoflurane was mediated by VTA-DMN connectivity reductions, specifically upon wakefulness post-anesthesia. We did not find a mediation via a-cBF-DMN connectivity. These results corroborate that anesthesia-induced unconsciousness is associated with a disruption of the within-organization of cortical dynamics, represented by the effect observed across the DMN, and additionally, our findings suggest that the recovery of the within-DMN organization might be influenced by the recovery of a coherent DMN and midbrain arousal system interaction. This supports the argument suggested by (Mashour, 2014): cortical anesthesia-induced changes might reflect a direct modulation from lower-order anesthetic actions.

Taken together, the findings from the first two projects provide evidence that *(i)* neuromodulatory brainstem connectivity to the cortex, particularly to the DMN is reduced during distinct states of anesthesia depth, and that *(ii)* this reduction is associated with the within-DMN connectivity changes signatures found during anesthesia-induced unconsciousness.

Finally, in our third project focusing on extreme brain states, i.e., burst suppression induced with sevoflurane, we studied cortico-cortical and cortico-subcortical connectivity patterns and the regional-specific BOLD activations in the period prior to burst-onset. Here we found a significant increased cortico-subcortical connectivity just before the start of a bursting global event, including ARAS and thalamic nuclei, but not a cortico-cortical one. Interestingly, thalamic participation was dependent on the length of the burst. This provides indirect evidence suggesting that subcortical activity, specially from the medial thalamus, could participate in the generation of single global bursting events during sevoflurane-induced burst suppression. Thalamic results were supported by regional BOLD activations before the burst-onset.

Overall, these results support the suggested 'bottom-up' model of anesthesia-induced unconsciousness about neuromodulatory brainstem systems' influence on the cortex, nevertheless due to important limitations of our methods, i.e., BOLD FC (correlation approach), potential influences from the cortex on the brainstem cannot be fully excluded, animal experiments are necessary.

6. Acknowledgments

I would like to thank the Anesthesiology department in Klinikum rechts der Isar, the participants and the colleagues involved in the design of experiment and recollection of data from the Sevoflurane and Propofol experiments, which I have used for my research project. Also, to the Neuroradiology department and my colleagues at the Neuro-Kopf-Zentrum where I conducted my projects and performed the analyses. Finally, I would like to thank my colleagues Rachel Nuttall for her help with the data preprocessing, Marlene Tahedl for her contribution on the cholinergic basal forebrain analyses and Fabian Hirsch for developing the partial jackknife correlation approach and for granting its application on the burst suppression data.

7. References

Aguilar, D. D., & McNally, J. M. (2022). Subcortical control of the default mode network: Role of the basal forebrain and implications for neuropsychiatric disorders. *Brain Res Bull*, *185*, 129-139. https://doi.org/10.1016/j.brainresbull.2022.05.005

Akrawi, W. P., Drummond, J. C., Kalkman, C. J., & Patel, P. M. (1996). A comparison of the electrophysiologic characteristics of EEG burst-suppression as produced by isoflurane, thiopental, etomidate, and propofol. *J Neurosurg Anesthesiol*, *8*(1), 40-46. https://doi.org/10.1097/00008506-199601000-00010

Alkire, M. T., Asher, C. D., Franciscus, A. M., & Hahn, E. L. (2009). Thalamic microinfusion of antibody to a voltage-gated potassium channel restores consciousness during anesthesia. *Anesthesiology*, *110*(4), 766-773. https://doi.org/10.1097/aln.0b013e31819c461c

Alkire, M. T., Haier, R. J., & Fallon, J. H. (2000). Toward a unified theory of narcosis: brain imaging evidence for a thalamocortical switch as the neurophysiologic basis of anesthetic-induced unconsciousness. *Conscious Cogn*, *9*(3), 370-386. https://doi.org/10.1006/ccog.1999.0423

Alkire, M. T., Hudetz, A. G., & Tononi, G. (2008). Consciousness and anesthesia. *Science*, *322*(5903), 876-880. https://doi.org/10.1126/science.1149213

Alkire, M. T., McReynolds, J. R., Hahn, E. L., & Trivedi, A. N. (2007). Thalamic microinjection of nicotine reverses sevoflurane-induced loss of righting reflex in the rat. *Anesthesiology*, *107*(2), 264-272. https://doi.org/10.1097/01.anes.0000270741.33766.24

Alkire, M. T., Pomfrett, C. J., Haier, R. J., Gianzero, M. V., Chan, C. M., Jacobsen, B. P., & Fallon, J. H. (1999). Functional brain imaging during anesthesia in humans: effects of halothane on global and regional cerebral glucose metabolism. *Anesthesiology*, *90*(3), 701-709. https://doi.org/10.1097/00000542-199903000-00011

Alves, P. N., Foulon, C., Karolis, V., Bzdok, D., Margulies, D. S., Volle, E., & Thiebaut de Schotten, M. (2019). An improved neuroanatomical model of the default-mode network reconciles previous neuroimaging and neuropathological findings. *Commun Biol*, *2*, 370. https://doi.org/10.1038/s42003-019-0611-3

Angel, A. (1991). The G. L. Brown lecture. Adventures in anaesthesia. *Exp Physiol*, *76*(1), 1-38. https://doi.org/10.1113/expphysiol.1991.sp003471

Arendt, T., Bigl, V., Tennstedt, A., & Arendt, A. (1985). Neuronal loss in different parts of the nucleus basalis is related to neuritic plaque formation in cortical target areas in Alzheimer's disease. *Neuroscience*, *14*(1), 1-14. https://doi.org/10.1016/0306-4522(85)90160-5

Aru, J., Suzuki, M., Rutiku, R., Larkum, M. E., & Bachmann, T. (2019). Coupling the State and Contents of Consciousness. *Front Syst Neurosci*, *13*, 43. https://doi.org/10.3389/fnsys.2019.00043

Ashburner, J. (2007). A fast diffeomorphic image registration algorithm. *Neuroimage*, *38*(1), 95-113. https://doi.org/10.1016/j.neuroimage.2007.07.007

Bar, K. J., de la Cruz, F., Schumann, A., Koehler, S., Sauer, H., Critchley, H., & Wagner, G. (2016). Functional connectivity and network analysis of midbrain and brainstem nuclei. *Neuroimage*, *134*, 53-63. https://doi.org/10.1016/j.neuroimage.2016.03.071

Barttfeld, P., Uhrig, L., Sitt, J. D., Sigman, M., Jarraya, B., & Dehaene, S. (2015). Signature of consciousness in the dynamics of resting-state brain activity. *Proc Natl Acad Sci U S A*, *112*(3), 887-892. https://doi.org/10.1073/pnas.1418031112

Bassett, D. S., & Sporns, O. (2017). Network neuroscience. *Nat Neurosci*, *20*(3), 353-364. https://doi.org/10.1038/nn.4502

Bastos, A. M., Donoghue, J. A., Brincat, S. L., Mahnke, M., Yanar, J., Correa, J., Waite, A. S., Lundqvist, M., Roy, J., Brown, E. N., & Miller, E. K. (2021). Neural effects of propofol-induced unconsciousness and its reversal using thalamic stimulation. *Elife*, *10*. https://doi.org/10.7554/eLife.60824

Beall, E. B., & Lowe, M. J. (2014). SimPACE: generating simulated motion corrupted BOLD data with synthetic-navigated acquisition for the development and evaluation of SLOMOCO: a new, highly effective slicewise motion correction. *Neuroimage*, *101*, 21-34. https://doi.org/10.1016/j.neuroimage.2014.06.038

Benarroch, E. E. (2010). Acetylcholine in the cerebral cortex: effects and clinical implications. *Neurology*, *75*(7), 659-665. https://doi.org/10.1212/WNL.0b013e3181ee267e

Biswal, B., Yetkin, F. Z., Haughton, V. M., & Hyde, J. S. (1995). Functional connectivity in the motor cortex of resting human brain using echo-planar MRI. *Magn Reson Med*, *34*(4), 537-541. https://doi.org/10.1002/mrm.1910340409

Biswal, B. B., Mennes, M., Zuo, X. N., Gohel, S., Kelly, C., Smith, S. M., Beckmann, C. F., Adelstein, J. S., Buckner, R. L., Colcombe, S., Dogonowski, A. M., Ernst, M., Fair, D., Hampson, M., Hoptman, M. J., Hyde, J. S., Kiviniemi, V. J., Kotter, R., Li, S. J., . . . Milham, M. P. (2010). Toward discovery science of human brain function. *Proc Natl Acad Sci U S A*, *107*(10), 4734-4739. https://doi.org/10.1073/pnas.0911855107

Bjorklund, A., & Dunnett, S. B. (2007). Dopamine neuron systems in the brain: an update. *Trends Neurosci*, *30*(5), 194-202. https://doi.org/10.1016/j.tins.2007.03.006

Bloem, B., Schoppink, L., Rotaru, D. C., Faiz, A., Hendriks, P., Mansvelder, H. D., van de Berg, W. D., & Wouterlood, F. G. (2014). Topographic mapping between basal forebrain cholinergic neurons and the medial prefrontal cortex in mice. *J Neurosci*, *34*(49), 16234-16246. https://doi.org/10.1523/JNEUROSCI.3011-14.2014

Bloom, F. E., & Iversen, L. L. (1971). Localizing 3H-GABA in nerve terminals of rat cerebral cortex by electron microscopic autoradiography. *Nature*, *229*(5287), 628-630. https://doi.org/10.1038/229628a0

Boly, M., Seth, A. K., Wilke, M., Ingmundson, P., Baars, B., Laureys, S., Edelman, D. B., & Tsuchiya, N. (2013). Consciousness in humans and non-human animals: recent advances and future directions. *Front Psychol*, *4*, 625. https://doi.org/10.3389/fpsyg.2013.00625

Boly, M., Tshibanda, L., Vanhaudenhuyse, A., Noirhomme, Q., Schnakers, C., Ledoux, D., Boveroux, P., Garweg, C., Lambermont, B., Phillips, C., Luxen, A., Moonen, G., Bassetti, C., Maquet, P., & Laureys, S. (2009). Functional connectivity in the default network during resting state is preserved in a vegetative but not in a brain dead patient. *Hum Brain Mapp*, *30*(8), 2393-2400. https://doi.org/10.1002/hbm.20672

Bonhomme, V., Staquet, C., Montupil, J., Defresne, A., Kirsch, M., Martial, C., Vanhaudenhuyse, A., Chatelle, C., Larroque, S. K., Raimondo, F., Demertzi, A., Bodart, O., Laureys, S., & Gosseries, O. (2019). General Anesthesia: A Probe to Explore Consciousness. *Front Syst Neurosci*, *13*, 36. https://doi.org/10.3389/fnsys.2019.00036

Boveroux, P., Vanhaudenhuyse, A., Bruno, M. A., Noirhomme, Q., Lauwick, S., Luxen, A., Degueldre, C., Plenevaux, A., Schnakers, C., Phillips, C., Brichant, J. F., Bonhomme, V., Maquet, P., Greicius, M. D., Laureys, S., & Boly, M. (2010). Breakdown of within- and between-network resting state functional magnetic resonance imaging connectivity during propofol-induced loss of consciousness. *Anesthesiology*, *113*(5), 1038-1053. https://doi.org/10.1097/ALN.0b013e3181f697f5

Boynton, G. M., Engel, S. A., Glover, G. H., & Heeger, D. J. (1996). Linear systems analysis of functional magnetic resonance imaging in human V1. *J Neurosci*, *16*(13), 4207-4221. https://www.ncbi.nlm.nih.gov/pubmed/8753882

Bremer, F. (1935). *Cerveau "isolé" et physiologie du sommeil*. Masson. https://books.google.de/books?id=j3H9swEACAAJ

Bressler, S. L., & Menon, V. (2010). Large-scale brain networks in cognition: emerging methods and principles. *Trends Cogn Sci*, *14*(6), 277-290. https://doi.org/10.1016/j.tics.2010.04.004

Brown, E. N., Lydic, R., & Schiff, N. D. (2010). General anesthesia, sleep, and coma. *N Engl J Med*, *363*(27), 2638-2650. https://doi.org/10.1056/NEJMra0808281

Brown, E. N., Pavone, K. J., & Naranjo, M. (2018). Multimodal General Anesthesia: Theory and Practice. *Anesth Analg*, *127*(5), 1246-1258. https://doi.org/10.1213/ANE.0000000000003668

Brown, E. N., Purdon, P. L., & Van Dort, C. J. (2011). General anesthesia and altered states of arousal: a systems neuroscience analysis. *Annu Rev Neurosci*, *34*, 601-628. https://doi.org/10.1146/annurev-neuro-060909-153200

Bruinsma, T. J., Sarma, V. V., Oh, Y., Jang, D. P., Chang, S. Y., Worrell, G. A., Lowe, V. J., Jo, H. J., & Min, H. K. (2018). The Relationship Between Dopamine Neurotransmitter Dynamics and the Blood-Oxygen-Level-Dependent (BOLD) Signal: A Review of Pharmacological Functional Magnetic Resonance Imaging. *Front Neurosci*, *12*, 238. https://doi.org/10.3389/fnins.2018.00238

Buckner, R. L., Andrews-Hanna, J. R., & Schacter, D. L. (2008). The brain's default network: anatomy, function, and relevance to disease. *Ann N Y Acad Sci*, *1124*, 1-38. https://doi.org/10.1196/annals.1440.011

Buxton, R. B. (2013). The physics of functional magnetic resonance imaging (fMRI). *Rep Prog Phys*, *76*(9), 096601. https://doi.org/10.1088/0034-4885/76/9/096601

Buzsaki, G., Bickford, R. G., Ponomareff, G., Thal, L. J., Mandel, R., & Gage, F. H. (1988). Nucleus basalis and thalamic control of neocortical activity in the freely moving rat. *J Neurosci*, *8*(11), 4007-4026. https://www.ncbi.nlm.nih.gov/pubmed/3183710

Byun, J. I., Cha, K. S., Kim, M., Lee, W. J., Lee, H. S., Sunwoo, J. S., Shin, J. W., Kim, T. J., Jun, J. S., Kim, H. J., Shin, W. C., Schenck, C. H., Lee, S. K., & Jung, K. Y. (2022). Association of Nucleus Basalis of Meynert Functional Connectivity and Cognition in Idiopathic Rapid-Eye-Movement Sleep Behavior Disorder. *J Clin Neurol*, *18*(5), 562-570. https://doi.org/10.3988/jcn.2022.18.5.562

Campagna, J. A., Miller, K. W., & Forman, S. A. (2003). Mechanisms of actions of inhaled anesthetics. *N Engl J Med*, *348*(21), 2110-2124. https://doi.org/10.1056/NEJMra021261

Castaigne, P., Lhermitte, F., Buge, A., Escourolle, R., Hauw, J. J., & Lyon-Caen, O. (1981). Paramedian thalamic and midbrain infarct: clinical and neuropathological study. *Ann Neurol*, *10*(2), 127-148. https://doi.org/10.1002/ana.410100204

Cauda, F., Micon, B. M., Sacco, K., Duca, S., D'Agata, F., Geminiani, G., & Canavero, S. (2009). Disrupted intrinsic functional connectivity in the vegetative state. *J Neurol Neurosurg Psychiatry*, *80*(4), 429-431. https://doi.org/10.1136/jnnp.2007.142349

Cavanna, F., Vilas, M. G., Palmucci, M., & Tagliazucchi, E. (2018). Dynamic functional connectivity and brain metastability during altered states of consciousness. *Neuroimage*, *180*(Pt B), 383-395. https://doi.org/10.1016/j.neuroimage.2017.09.065

Chao-Gan, Y., & Yu-Feng, Z. (2010). DPARSF: A MATLAB Toolbox for "Pipeline" Data Analysis of Resting-State fMRI. *Front Syst Neurosci*, *4*, 13. https://doi.org/10.3389/fnsys.2010.00013

Chemali, J. J., Van Dort, C. J., Brown, E. N., & Solt, K. (2012). Active emergence from propofol general anesthesia is induced by methylphenidate. *Anesthesiology*, *116*(5), 998-1005. https://doi.org/10.1097/ALN.0b013e3182518bfc

Ching, S., Purdon, P. L., Vijayan, S., Kopell, N. J., & Brown, E. N. (2012). A neurophysiological-metabolic model for burst suppression. *Proc Natl Acad Sci U S A*, *109*(8), 3095-3100. https://doi.org/10.1073/pnas.1121461109

Cloostermans, M. C., van Meulen, F. B., Eertman, C. J., Hom, H. W., & van Putten, M. J. (2012). Continuous electroencephalography monitoring for early prediction of neurological outcome in postanoxic patients after cardiac arrest: a prospective cohort study. *Crit Care Med*, *40*(10), 2867-2875. https://doi.org/10.1097/CCM.0b013e31825b94f0

Cole, D. M., Oei, N. Y., Soeter, R. P., Both, S., van Gerven, J. M., Rombouts, S. A., & Beckmann, C. F. (2013). Dopamine-dependent architecture of cortico-subcortical network connectivity. *Cereb Cortex*, *23*(7), 1509-1516. https://doi.org/10.1093/cercor/bhs136

Dahlstroem, A., & Fuxe, K. (1964). Evidence for the Existence of Monoamine-Containing Neurons in the Central Nervous System. I. Demonstration of Monoamines in the Cell Bodies of Brain Stem Neurons. *Acta Physiol Scand Suppl*, SUPPL 232:231-255. https://www.ncbi.nlm.nih.gov/pubmed/14229500

De Rubeis, D. A., & Young, G. B. (2001). Continuous EEG monitoring in a patient with massive carbamazepine overdose. *J Clin Neurophysiol*, *18*(2), 166-168. https://doi.org/10.1097/00004691-200103000-00008

Dean, J. G., Fields, C. W., Brito, M. A., Silverstein, B. H., Rybicki-Kler, C., Fryzel, A. M., Groenhout, T., Liu, T., Mashour, G. A., & Pal, D. (2022). Inactivation of Prefrontal Cortex Attenuates Behavioral Arousal Induced by Stimulation of Basal Forebrain During Sevoflurane Anesthesia. *Anesth Analg*, *134*(6), 1140-1152. https://doi.org/10.1213/ANE.0000000000006011

DeFelipe, J., & Farinas, I. (1992). The pyramidal neuron of the cerebral cortex: morphological and chemical characteristics of the synaptic inputs. *Prog Neurobiol*, *39*(6), 563-607. https://doi.org/10.1016/0301-0082(92)90015-7

Dehaene, S., & Changeux, J. P. (2011). Experimental and theoretical approaches to conscious processing. *Neuron*, *70*(2), 200-227. https://doi.org/10.1016/j.neuron.2011.03.018

Demertzi, A., Tagliazucchi, E., Dehaene, S., Deco, G., Barttfeld, P., Raimondo, F., Martial, C., Fernandez-Espejo, D., Rohaut, B., Voss, H. U., Schiff, N. D., Owen, A. M., Laureys, S., Naccache, L., & Sitt, J. D. (2019). Human consciousness is supported by dynamic complex patterns of brain signal coordination. *Sci Adv*, *5*(2), eaat7603. https://doi.org/10.1126/sciadv.aat7603

Denoyer, M., Sallanon, M., Buda, C., Kitahama, K., & Jouvet, M. (1991). Neurotoxic lesion of the mesencephalic reticular formation and/or the posterior hypothalamus does not alter waking in the cat. *Brain Res*, *539*(2), 287-303. https://doi.org/10.1016/0006-8993(91)91633-c

Detari, L., & Vanderwolf, C. H. (1987). Activity of identified cortically projecting and other basal forebrain neurones during large slow waves and cortical activation in anaesthetized rats. *Brain Res*, *437*(1), 1-8. https://doi.org/10.1016/0006-8993(87)91521-6

Detsch, O., Kochs, E., Siemers, M., Bromm, B., & Vahle-Hinz, C. (2002). Increased responsiveness of cortical neurons in contrast to thalamic neurons during isoflurane-induced EEG bursts in rats. *Neurosci Lett*, *317*(1), 9-12. https://doi.org/10.1016/s0304-3940(01)02419-3

Dosenbach, N. U., Nardos, B., Cohen, A. L., Fair, D. A., Power, J. D., Church, J. A., Nelson, S. M., Wig, G. S., Vogel, A. C., Lessov-Schlaggar, C. N., Barnes, K. A., Dubis, J. W., Feczko, E., Coalson, R. S., Pruett, J. R., Jr., Barch, D. M., Petersen, S. E., & Schlaggar, B. L. (2010). Prediction of individual brain maturity using fMRI. *Science*, *329*(5997), 1358-1361. https://doi.org/10.1126/science.1194144

Drew, P. J., Mateo, C., Turner, K. L., Yu, X., & Kleinfeld, D. (2020). Ultra-slow Oscillations in fMRI and Resting-State Connectivity: Neuronal and Vascular Contributions and Technical Confounds. *Neuron*, *107*(5), 782-804. https://doi.org/10.1016/j.neuron.2020.07.020

Du, C., Volkow, N. D., Koretsky, A. P., & Pan, Y. (2014). Low-frequency calcium oscillations accompany deoxyhemoglobin oscillations in rat somatosensory cortex. *Proc Natl Acad Sci U S A*, *111*(43), E4677-4686. https://doi.org/10.1073/pnas.1410800111

Eden, U. T., & Kramer, M. A. (2010). Drawing inferences from Fano factor calculations. *J Neurosci Methods*, *190*(1), 149-152. https://doi.org/10.1016/j.jneumeth.2010.04.012

Edlow, B. L. (2021). Dopaminergic modulation of human consciousness via default mode network connectivity. *Proc Natl Acad Sci U S A*, *118*(31). https://doi.org/10.1073/pnas.2111268118

Edlow, B. L., Haynes, R. L., Takahashi, E., Klein, J. P., Cummings, P., Benner, T., Greer, D. M., Greenberg, S. M., Wu, O., Kinney, H. C., & Folkerth, R. D. (2013). Disconnection of the ascending arousal system in traumatic coma. *J Neuropathol Exp Neurol*, *72*(6), 505-523. https://doi.org/10.1097/NEN.0b013e3182945bf6

Edlow, B. L., Takahashi, E., Wu, O., Benner, T., Dai, G., Bu, L., Grant, P. E., Greer, D. M., Greenberg, S. M., Kinney, H. C., & Folkerth, R. D. (2012). Neuroanatomic connectivity of the human ascending arousal system critical to consciousness and its disorders. *J Neuropathol Exp Neurol*, *71*(6), 531-546. https://doi.org/10.1097/NEN.0b013e3182588293

Eger, E. I., 2nd, Saidman, L. J., & Brandstater, B. (1965). Minimum alveolar anesthetic concentration: a standard of anesthetic potency. *Anesthesiology*, *26*(6), 756-763. https://doi.org/10.1097/00000542-196511000-00010

el-Maghrabi, E. A., & Eckenhoff, R. G. (1993). Inhibition of dopamine transport in rat brain synaptosomes by volatile anesthetics. *Anesthesiology*, *78*(4), 750-756. https://doi.org/10.1097/00000542-199304000-00019

Fallon, J. H., & Moore, R. Y. (1978). Catecholamine innervation of the basal forebrain. IV. Topography of the dopamine projection to the basal forebrain and neostriatum. *J Comp Neurol*, *180*(3), 545-580. https://doi.org/10.1002/cne.901800310

Fan, B., Pang, L., Li, S., Zhou, X., Lv, Z., Chen, Z., & Zheng, J. (2022). Correlation Between the Functional Connectivity of Basal Forebrain Subregions and Vigilance Dysfunction in Temporal Lobe Epilepsy With and Without Focal to Bilateral Tonic-Clonic Seizure. *Front Psychiatry*, *13*, 888150. https://doi.org/10.3389/fpsyt.2022.888150

Fariello, R. G., Chun, R. W., Doro, J. M., Buncic, J. R., & Prichard, J. S. (1977). EEG recognition of Aicardi's syndrome. *Arch Neurol*, *34*(9), 563-566. https://doi.org/10.1001/archneur.1977.00500210065012

Feldman, J. L., Mitchell, G. S., & Nattie, E. E. (2003). Breathing: rhythmicity, plasticity, chemosensitivity. *Annu Rev Neurosci*, *26*, 239-266. https://doi.org/10.1146/annurev.neuro.26.041002.131103

Ferron, J. F., Kroeger, D., Chever, O., & Amzica, F. (2009). Cortical inhibition during burst suppression induced with isoflurane anesthesia. *J Neurosci*, *29*(31), 9850-9860. https://doi.org/10.1523/JNEUROSCI.5176-08.2009

Fiset, P., Paus, T., Daloze, T., Plourde, G., Meuret, P., Bonhomme, V., Hajj-Ali, N., Backman, S. B., & Evans, A. C. (1999). Brain mechanisms of propofol-induced loss of consciousness in humans: a positron emission tomographic study. *J Neurosci*, *19*(13), 5506-5513. https://www.ncbi.nlm.nih.gov/pubmed/10377359

Fleischmann, A., Pilge, S., Kiel, T., Kratzer, S., Schneider, G., & Kreuzer, M. (2018). Substance-Specific Differences in Human Electroencephalographic Burst Suppression Patterns. *Front Hum Neurosci*, *12*, 368. https://doi.org/10.3389/fnhum.2018.00368

Fox, M. D., & Raichle, M. E. (2007). Spontaneous fluctuations in brain activity observed with functional magnetic resonance imaging. *Nat Rev Neurosci*, *8*(9), 700-711. https://doi.org/10.1038/nrn2201

Fox, M. D., Snyder, A. Z., Vincent, J. L., Corbetta, M., Van Essen, D. C., & Raichle, M. E. (2005). The human brain is intrinsically organized into dynamic, anticorrelated functional networks. *Proc Natl Acad Sci U S A*, *102*(27), 9673-9678. https://doi.org/10.1073/pnas.0504136102

Franks, N. P. (2008). General anaesthesia: from molecular targets to neuronal pathways of sleep and arousal. *Nat Rev Neurosci*, *9*(5), 370-386. https://doi.org/10.1038/nrn2372

Fritz, H. J., Ray, N., Dyrba, M., Sorg, C., Teipel, S., & Grothe, M. J. (2019). The corticotopic organization of the human basal forebrain as revealed by regionally selective functional connectivity profiles. *Hum Brain Mapp*, *40*(3), 868-878. https://doi.org/10.1002/hbm.24417

Fukunaga, M., Horovitz, S. G., van Gelderen, P., de Zwart, J. A., Jansma, J. M., Ikonomidou, V. N., Chu, R., Deckers, R. H., Leopold, D. A., & Duyn, J. H. (2006). Large-amplitude, spatially correlated fluctuations in BOLD fMRI signals during extended rest and early sleep stages. *Magn Reson Imaging*, *24*(8), 979-992. https://doi.org/10.1016/j.mri.2006.04.018

Gamou, S., Fukuda, S., Ogura, M., Sakamoto, H., & Morita, S. (2010). Microinjection of propofol into the perifornical area induces sedation with decreasing cortical acetylcholine release in rats. *Anesth Analg*, *111*(2), 395-402. https://doi.org/10.1213/ANE.0b013e3181e24776

Garcia-Cabezas, M. A., Martinez-Sanchez, P., Sanchez-Gonzalez, M. A., Garzon, M., & Cavada, C. (2009). Dopamine innervation in the thalamus: monkey versus rat. *Cereb Cortex*, *19*(2), 424-434. https://doi.org/10.1093/cercor/bhn093

Garcia-Cabezas, M. A., Rico, B., Sanchez-Gonzalez, M. A., & Cavada, C. (2007). Distribution of the dopamine innervation in the macaque and human thalamus. *Neuroimage*, *34*(3), 965-984. https://doi.org/10.1016/j.neuroimage.2006.07.032

Gargouri, F., Gallea, C., Mongin, M., Pyatigorskaya, N., Valabregue, R., Ewenczyk, C., Sarazin, M., Yahia-Cherif, L., Vidailhet, M., & Lehericy, S. (2019). Multimodal magnetic resonance imaging investigation of basal forebrain damage and cognitive deficits in Parkinson's disease. *Mov Disord*, *34*(4), 516-525. https://doi.org/10.1002/mds.27561

Ghashghaei, H. T., & Barbas, H. (2001). Neural interaction between the basal forebrain and functionally distinct prefrontal cortices in the rhesus monkey. *Neuroscience*, *103*(3), 593-614. https://doi.org/10.1016/s0306-4522(00)00585-6

Gili, T., Saxena, N., Diukova, A., Murphy, K., Hall, J. E., & Wise, R. G. (2013). The thalamus and brainstem act as key hubs in alterations of human brain network connectivity induced by mild propofol sedation. *J Neurosci*, *33*(9), 4024-4031. https://doi.org/10.1523/JNEUROSCI.3480-12.2013

Giordano, G. M., Stanziano, M., Papa, M., Mucci, A., Prinster, A., Soricelli, A., & Galderisi, S. (2018). Functional connectivity of the ventral tegmental area and avolition in subjects with schizophrenia: a resting state functional MRI study. *Eur Neuropsychopharmacol*, *28*(5), 589-602. https://doi.org/10.1016/j.euroneuro.2018.03.013

Glover, G. H. (1999). Deconvolution of impulse response in event-related BOLD fMRI. *Neuroimage*, *9*(4), 416-429. https://doi.org/10.1006/nimg.1998.0419

Glover, G. H., Li, T. Q., & Ress, D. (2000). Image-based method for retrospective correction of physiological motion effects in fMRI: RETROICOR. *Magn Reson Med*, *44*(1), 162-167. https://doi.org/10.1002/1522-2594(200007)44:1<162::aid-mrm23>3.0.co;2-e

Goense, J., Merkle, H., & Logothetis, N. K. (2012). High-resolution fMRI reveals laminar differences in neurovascular coupling between positive and negative BOLD responses. *Neuron*, *76*(3), 629-639. https://doi.org/10.1016/j.neuron.2012.09.019

Goense, J. B., & Logothetis, N. K. (2008). Neurophysiology of the BOLD fMRI signal in awake monkeys. *Curr Biol*, *18*(9), 631-640. https://doi.org/10.1016/j.cub.2008.03.054

Golanov, E. V., & Reis, D. J. (1995). Vasodilation evoked from medulla and cerebellum is coupled to bursts of cortical EEG activity in rats. *Am J Physiol*, *268*(2 Pt 2), R454-467. https://doi.org/10.1152/ajpregu.1995.268.2.R454

Golkowski, D., Larroque, S. K., Vanhaudenhuyse, A., Plenevaux, A., Boly, M., Di Perri, C., Ranft, A., Schneider, G., Laureys, S., Jordan, D., Bonhomme, V., & Ilg, R. (2019). Changes in Whole Brain Dynamics and Connectivity Patterns during Sevoflurane- and Propofol-induced Unconsciousness Identified by Functional Magnetic Resonance Imaging. *Anesthesiology*, *130*(6), 898-911. https://doi.org/10.1097/ALN.0000000000002704

Golkowski, D., Ranft, A., Kiel, T., Riedl, V., Kohl, P., Rohrer, G., Pientka, J., Berger, S., Preibisch, C., Zimmer, C., Mashour, G. A., Schneider, G., Kochs, E. F., Ilg, R., & Jordan, D. (2017). Coherence of BOLD signal and electrical activity in the human brain during deep sevoflurane anesthesia. *Brain Behav*, *7*(7), e00679. https://doi.org/10.1002/brb3.679

Gradin, V. B., Waiter, G., O'Connor, A., Romaniuk, L., Stickle, C., Matthews, K., Hall, J., & Douglas Steele, J. (2013). Salience network-midbrain dysconnectivity and blunted reward signals in schizophrenia. *Psychiatry Res*, *211*(2), 104-111. https://doi.org/10.1016/j.pscychresns.2012.06.003

Greicius, M. D., Kiviniemi, V., Tervonen, O., Vainionpaa, V., Alahuhta, S., Reiss, A. L., & Menon, V. (2008). Persistent default-mode network connectivity during light sedation. *Hum Brain Mapp*, *29*(7), 839-847. https://doi.org/10.1002/hbm.20537

Greicius, M. D., Krasnow, B., Reiss, A. L., & Menon, V. (2003). Functional connectivity in the resting brain: a network analysis of the default mode hypothesis. *Proc Natl Acad Sci U S A*, *100*(1), 253-258. https://doi.org/10.1073/pnas.0135058100

Gui, H., Liu, C., He, H., Zhang, J., Chen, H., & Zhang, Y. (2021). Dopaminergic Projections From the Ventral Tegmental Area to the Nucleus Accumbens Modulate Sevoflurane Anesthesia in Mice. *Front Cell Neurosci*, *15*, 671473. https://doi.org/10.3389/fncel.2021.671473

Guldenmund, P., Demertzi, A., Boveroux, P., Boly, M., Vanhaudenhuyse, A., Bruno, M. A., Gosseries, O., Noirhomme, Q., Brichant, J. F., Bonhomme, V., Laureys, S., & Soddu, A. (2013). Thalamus, brainstem and salience network connectivity changes during propofol-induced sedation and unconsciousness. *Brain Connect*, *3*(3), 273-285. https://doi.org/10.1089/brain.2012.0117

Haber, S. N., & Fudge, J. L. (1997). The primate substantia nigra and VTA: integrative circuitry and function. *Crit Rev Neurobiol*, *11*(4), 323-342. https://doi.org/10.1615/critrevneurobiol.v11.i4.40

Hadley, J. A., Nenert, R., Kraguljac, N. V., Bolding, M. S., White, D. M., Skidmore, F. M., Visscher, K. M., & Lahti, A. C. (2014). Ventral tegmental area/midbrain functional connectivity and response to antipsychotic medication in schizophrenia. *Neuropsychopharmacology*, *39*(4), 1020-1030. https://doi.org/10.1038/npp.2013.305

Hahn, G., Zamora-Lopez, G., Uhrig, L., Tagliazucchi, E., Laufs, H., Mantini, D., Kringelbach, M. L., Jarraya, B., & Deco, G. (2021). Signature of consciousness in brain-wide synchronization patterns of monkey and human fMRI signals. *Neuroimage*, *226*, 117470. https://doi.org/10.1016/j.neuroimage.2020.117470

Hao, X., Ou, M., Zhang, D., Zhao, W., Yang, Y., Liu, J., Yang, H., Zhu, T., Li, Y., & Zhou, C. (2020). The Effects of General Anesthetics on Synaptic Transmission. *Curr Neuropharmacol*, *18*(10), 936-965. https://doi.org/10.2174/1570159X18666200227125854

Harrison, B. J., Davey, C. G., Savage, H. S., Jamieson, A. J., Leonards, C. A., Moffat, B. A., Glarin, R. K., & Steward, T. (2022). Dynamic subcortical modulators of human default mode network function. *Cereb Cortex*, *32*(19), 4345-4355. https://doi.org/10.1093/cercor/bhab487

Hartikainen, K. M., Rorarius, M., Perakyla, J. J., Laippala, P. J., & Jantti, V. (1995). Cortical reactivity during isoflurane burst-suppression anesthesia. *Anesth Analg*, *81*(6), 1223-1228. https://doi.org/10.1097/00000539-199512000-00018

Hayes, A. F., & Rockwood, N. J. (2017). Regression-based statistical mediation and moderation analysis in clinical research: Observations, recommendations, and implementation. *Behav Res Ther*, *98*, 39-57. https://doi.org/10.1016/j.brat.2016.11.001

Heckers, S., Geula, C., & Mesulam, M. M. (1992). Cholinergic innervation of the human thalamus: dual origin and differential nuclear distribution. *J Comp Neurol*, *325*(1), 68-82. https://doi.org/10.1002/cne.903250107

Heeger, D. J., & Ress, D. (2002). What does fMRI tell us about neuronal activity? *Nat Rev Neurosci*, *3*(2), 142-151. https://doi.org/10.1038/nrn730

Hemmings, H. C., Jr. (2009). Sodium channels and the synaptic mechanisms of inhaled anaesthetics. *Br J Anaesth*, *103*(1), 61-69. https://doi.org/10.1093/bja/aep144

Hemmings, H. C., Jr., Akabas, M. H., Goldstein, P. A., Trudell, J. R., Orser, B. A., & Harrison, N. L. (2005). Emerging molecular mechanisms of general anesthetic action. *Trends Pharmacol Sci*, *26*(10), 503-510. https://doi.org/10.1016/j.tips.2005.08.006

Hendrickx, J. F. A., & De Wolf, A. M. (2022). End-tidal Anesthetic Concentration: Monitoring, Interpretation, and Clinical Application. *Anesthesiology*, *136*(6), 985-996. https://doi.org/10.1097/ALN.0000000000004218

Hirose, M., Haginoya, K., Yokoyama, H., Tanaka, S., Uematsu, M., Kaneta, T., Takayanagi, M., Kon, K., Yoshihara, Y., Iinuma, K., & Tsuchiya, S. (2010). Functional cortical deafferentation from the subcortical structures in a patient with early myoclonic encephalopathy: a functional neuroimaging study. *Epilepsia*, *51*(4), 699-702. https://doi.org/10.1111/j.1528-1167.2009.02399.x

Horovitz, S. G., Braun, A. R., Carr, W. S., Picchioni, D., Balkin, T. J., Fukunaga, M., & Duyn, J. H. (2009). Decoupling of the brain's default mode network during deep sleep. *Proc Natl Acad Sci U S A*, *106*(27), 11376-11381. https://doi.org/10.1073/pnas.0901435106

Horovitz, S. G., Fukunaga, M., de Zwart, J. A., van Gelderen, P., Fulton, S. C., Balkin, T. J., & Duyn, J. H. (2008). Low frequency BOLD fluctuations during resting wakefulness and light sleep: a simultaneous EEG-fMRI study. *Hum Brain Mapp*, *29*(6), 671-682. https://doi.org/10.1002/hbm.20428

Huang, Z., Wang, Z., Zhang, J., Dai, R., Wu, J., Li, Y., Liang, W., Mao, Y., Yang, Z., Holland, G., Zhang, J., & Northoff, G. (2014). Altered temporal variance and neural synchronization of spontaneous brain activity in anesthesia. *Hum Brain Mapp*, *35*(11), 5368-5378. https://doi.org/10.1002/hbm.22556

Hudetz, A. G., & Imas, O. A. (2007). Burst activation of the cerebral cortex by flash stimuli during isoflurane anesthesia in rats. *Anesthesiology*, *107*(6), 983-991. https://doi.org/10.1097/01.anes.0000291471.80659.55

Hudetz, A. G., Liu, X., & Pillay, S. (2015). Dynamic repertoire of intrinsic brain states is reduced in propofol-induced unconsciousness. *Brain Connect*, *5*(1), 10-22. https://doi.org/10.1089/brain.2014.0230

Huels, E. R., Groenhout, T., Fields, C. W., Liu, T., Mashour, G. A., & Pal, D. (2021). Inactivation of Prefrontal Cortex Delays Emergence From Sevoflurane Anesthesia. *Front Syst Neurosci*, *15*, 690717. https://doi.org/10.3389/fnsys.2021.690717

Imas, O. A., Ropella, K. M., Ward, B. D., Wood, J. D., & Hudetz, A. G. (2005). Volatile anesthetics disrupt frontal-posterior recurrent information transfer at gamma frequencies in rat. *Neurosci Lett*, *387*(3), 145-150. https://doi.org/10.1016/j.neulet.2005.06.018

Japaridze, N., Muthuraman, M., Reinicke, C., Moeller, F., Anwar, A. R., Mideksa, K. G., Pressler, R., Deuschl, G., Stephani, U., & Siniatchkin, M. (2015). Neuronal Networks during Burst Suppression as Revealed by Source Analysis. *PLoS One*, *10*(4), e0123807. https://doi.org/10.1371/journal.pone.0123807

Jones, B. E. (2004). Activity, modulation and role of basal forebrain cholinergic neurons innervating the cerebral cortex. *Prog Brain Res*, *145*, 157-169. https://doi.org/10.1016/S0079-6123(03)45011-5

Jones, B. E., & Beaudet, A. (1987). Distribution of acetylcholine and catecholamine neurons in the cat brainstem: a choline acetyltransferase and tyrosine hydroxylase immunohistochemical study. *J Comp Neurol*, *261*(1), 15-32. https://doi.org/10.1002/cne.902610103

Jones, B. E., & Yang, T. Z. (1985). The efferent projections from the reticular formation and the locus coeruleus studied by anterograde and retrograde axonal transport in the rat. *J Comp Neurol*, *242*(1), 56-92. https://doi.org/10.1002/cne.902420105

Jones, M. V., & Harrison, N. L. (1993). Effects of volatile anesthetics on the kinetics of inhibitory postsynaptic currents in cultured rat hippocampal neurons. *J Neurophysiol*, *70*(4), 1339-1349. https://doi.org/10.1152/jn.1993.70.4.1339

Jordan, D., Ilg, R., Riedl, V., Schorer, A., Grimberg, S., Neufang, S., Omerovic, A., Berger, S., Untergehrer, G., Preibisch, C., Schulz, E., Schuster, T., Schroter, M., Spoormaker, V., Zimmer, C., Hemmer, B., Wohlschlager, A., Kochs, E. F., & Schneider, G. (2013). Simultaneous electroencephalographic and functional magnetic resonance imaging indicate impaired cortical top-down processing in association with anesthetic-induced unconsciousness. *Anesthesiology*, *119*(5), 1031-1042. https://doi.org/10.1097/ALN.0b013e3182a7ca92

Kafashan, M., Ching, S., & Palanca, B. J. (2016). Sevoflurane Alters Spatiotemporal Functional Connectivity Motifs That Link Resting-State Networks during Wakefulness. *Front Neural Circuits*, *10*, 107. https://doi.org/10.3389/fncir.2016.00107

Kaisti, K. K., Langsjo, J. W., Aalto, S., Oikonen, V., Sipila, H., Teras, M., Hinkka, S., Metsahonkala, L., & Scheinin, H. (2003). Effects of sevoflurane, propofol, and adjunct nitrous oxide on regional cerebral blood flow, oxygen consumption, and blood volume in humans. *Anesthesiology*, *99*(3), 603-613. https://doi.org/10.1097/00000542-200309000-00015

Kaisti, K. K., Metsahonkala, L., Teras, M., Oikonen, V., Aalto, S., Jaaskelainen, S., Hinkka, S., & Scheinin, H. (2002). Effects of surgical levels of propofol and sevoflurane anesthesia on cerebral blood flow in healthy subjects studied with positron emission tomography. *Anesthesiology*, *96*(6), 1358-1370. https://doi.org/10.1097/00000542-200206000-00015

Kebabian, J. W., Beaulieu, M., & Itoh, Y. (1984). Pharmacological and biochemical evidence for the existence of two categories of dopamine receptor. *Can J Neurol Sci*, *11*(1 Suppl), 114-117. https://doi.org/10.1017/s0317167100046254

Kebabian, J. W., & Calne, D. B. (1979). Multiple receptors for dopamine. *Nature*, *277*(5692), 93-96. https://doi.org/10.1038/277093a0

Keita, H., Henzel-Rouelle, D., Dupont, H., Desmonts, J. M., & Mantz, J. (1999). Halothane and isoflurane increase spontaneous but reduce the N-methyl-D-aspartate-evoked dopamine release in rat striatal slices: evidence for direct presynaptic effects. *Anesthesiology*, *91*(6), 1788-1797. https://doi.org/10.1097/00000542-199912000-00033

Kelly, C., de Zubicaray, G., Di Martino, A., Copland, D. A., Reiss, P. T., Klein, D. F., Castellanos, F. X., Milham, M. P., & McMahon, K. (2009). L-dopa modulates functional connectivity in striatal cognitive and motor networks: a double-blind placebo-controlled study. *J Neurosci*, *29*(22), 7364-7378. https://doi.org/10.1523/JNEUROSCI.0810-09.2009

Kenny, J. D., Taylor, N. E., Brown, E. N., & Solt, K. (2015). Dextroamphetamine (but Not Atomoxetine) Induces Reanimation from General Anesthesia: Implications for the Roles of Dopamine and Norepinephrine in Active Emergence. *PLoS One*, *10*(7), e0131914. https://doi.org/10.1371/journal.pone.0131914

Kenny, J. D., Westover, M. B., Ching, S., Brown, E. N., & Solt, K. (2014). Propofol and sevoflurane induce distinct burst suppression patterns in rats. *Front Syst Neurosci*, *8*, 237. https://doi.org/10.3389/fnsys.2014.00237

Kikuchi, T., Wang, Y., Sato, K., & Okumura, F. (1998). In vivo effects of propofol on acetylcholine release from the frontal cortex, hippocampus and striatum studied by intracerebral microdialysis in freely moving rats. *Br J Anaesth*, *80*(5), 644-648. https://doi.org/10.1093/bja/80.5.644

Koch, C., Massimini, M., Boly, M., & Tononi, G. (2016). Neural correlates of consciousness: progress and problems. *Nat Rev Neurosci*, *17*(5), 307-321. https://doi.org/10.1038/nrn.2016.22

Kohno, M., Okita, K., Morales, A. M., Robertson, C. L., Dean, A. C., Ghahremani, D. G., Sabb, F. W., Rawson, R. A., Mandelkern, M. A., Bilder, R. M., & London, E. D. (2016). Midbrain functional connectivity and ventral striatal dopamine D2-type receptors: link to impulsivity in methamphetamine users. *Mol Psychiatry*, *21*(11), 1554-1560. https://doi.org/10.1038/mp.2015.223

Kolbitsch, C., Lorenz, I. H., Hormann, C., Kremser, C., Schocke, M., Felber, S., Moser, P. L., Hinteregger, M., Pfeiffer, K. P., & Benzer, A. (2001). Sevoflurane and nitrous oxide increase regional cerebral blood flow (rCBF) and regional cerebral blood volume (rCBV) in a drug-specific manner in human volunteers. *Magn Reson Imaging*, *19*(10), 1253-1260. https://doi.org/10.1016/s0730-725x(01)00465-9

Kolbitsch, C., Lorenz, I. H., Hormann, C., Schocke, M., Kremser, C., Zschiegner, F., Lockinger, A., Pfeiffer, K. P., Felber, S., & Benzer, A. (2000). A subanesthetic concentration of sevoflurane increases regional cerebral blood flow and regional cerebral blood volume and decreases regional mean transit time and regional cerebrovascular resistance in volunteers. *Anesth Analg*, *91*(1), 156-162. https://doi.org/10.1097/00000539-200007000-00029

Kolmac, C., & Mitrofanis, J. (1999). Organization of the basal forebrain projection to the thalamus in rats. *Neurosci Lett*, *272*(3), 151-154. https://doi.org/10.1016/s0304-3940(99)00614-x

Krimmel, S. R., White, M. G., Panicker, M. H., Barrett, F. S., Mathur, B. N., & Seminowicz, D. A. (2019). Resting state functional connectivity and cognitive task-related activation of the human claustrum. *Neuroimage*, *196*, 59-67. https://doi.org/10.1016/j.neuroimage.2019.03.075

Kroeger, D., & Amzica, F. (2007). Hypersensitivity of the anesthesia-induced comatose brain. *J Neurosci*, *27*(39), 10597-10607. https://doi.org/10.1523/JNEUROSCI.3440-07.2007

Lakens, D. (2013). Calculating and reporting effect sizes to facilitate cumulative science: a practical primer for t-tests and ANOVAs. *Front Psychol*, *4*, 863. https://doi.org/10.3389/fpsyg.2013.00863

Lambrakis, C. C., Lancman, M. E., & Romano, C. (1999). Asynchronous and asymmetric burst-suppression in a patient with a corpus callosum lesion. *Clin Neurophysiol*, *110*(1), 103-105. https://doi.org/10.1016/s0013-4694(98)00102-3

Lancaster, J. L., Woldorff, M. G., Parsons, L. M., Liotti, M., Freitas, C. S., Rainey, L., Kochunov, P. V., Nickerson, D., Mikiten, S. A., & Fox, P. T. (2000). Automated Talairach atlas labels for functional brain mapping. *Hum Brain Mapp*, *10*(3), 120-131. https://doi.org/10.1002/1097-0193(200007)10:3<120::aid-hbm30>3.0.co;2-8

Laureys, S. (2005). The neural correlate of (un)awareness: lessons from the vegetative state. *Trends Cogn Sci*, *9*(12), 556-559. https://doi.org/10.1016/j.tics.2005.10.010

Lee, M., Sanz, L. R. D., Barra, A., Wolff, A., Nieminen, J. O., Boly, M., Rosanova, M., Casarotto, S., Bodart, O., Annen, J., Thibaut, A., Panda, R., Bonhomme, V., Massimini, M., Tononi, G., Laureys, S., Gosseries, O., & Lee, S. W. (2022). Quantifying arousal and awareness in altered states of consciousness using interpretable deep learning. *Nat Commun*, *13*(1), 1064. https://doi.org/10.1038/s41467-022-28451-0

Lee, R. S., Steffensen, S. C., & Henriksen, S. J. (2001). Discharge profiles of ventral tegmental area GABA neurons during movement, anesthesia, and the sleep-wake cycle. *J Neurosci*, *21*(5), 1757-1766. https://www.ncbi.nlm.nih.gov/pubmed/11222665

Leung, L. S., & Luo, T. (2021). Cholinergic Modulation of General Anesthesia. *Curr Neuropharmacol*, *19*(11), 1925-1936. https://doi.org/10.2174/1570159X19666210421095504

Lewis, L. D., Ching, S., Weiner, V. S., Peterfreund, R. A., Eskandar, E. N., Cash, S. S., Brown, E. N., & Purdon, P. L. (2013). Local cortical dynamics of burst suppression in the anaesthetized brain. *Brain*, *136*(Pt 9), 2727-2737. https://doi.org/10.1093/brain/awt174

Lewis, L. D., Voigts, J., Flores, F. J., Schmitt, L. I., Wilson, M. A., Halassa, M. M., & Brown, E. N. (2015). Thalamic reticular nucleus induces fast and local modulation of arousal state. *Elife*, *4*, e08760. https://doi.org/10.7554/eLife.08760

Li, J., Curley, W. H., Guerin, B., Dougherty, D. D., Dalca, A. V., Fischl, B., Horn, A., & Edlow, B. L. (2021). Mapping the subcortical connectivity of the human default mode network. *Neuroimage*, *245*, 118758. https://doi.org/10.1016/j.neuroimage.2021.118758

Liou, J. Y., Baird-Daniel, E., Zhao, M., Daniel, A., Schevon, C. A., Ma, H., & Schwartz, T. H. (2019). Burst suppression uncovers rapid widespread alterations in network excitability caused by an acute seizure focus. *Brain*, *142*(10), 3045-3058. https://doi.org/10.1093/brain/awz246

Lioudyno, M. I., Birch, A. M., Tanaka, B. S., Sokolov, Y., Goldin, A. L., Chandy, K. G., Hall, J. E., & Alkire, M. T. (2013). Shaker-related potassium channels in the central medial nucleus of the thalamus are important molecular targets for arousal suppression by volatile general anesthetics. *J Neurosci*, *33*(41), 16310-16322. https://doi.org/10.1523/JNEUROSCI.0344-13.2013

Liu, X., Zhu, X. H., Zhang, Y., & Chen, W. (2011). Neural origin of spontaneous hemodynamic fluctuations in rats under burst-suppression anesthesia condition. *Cereb Cortex*, *21*(2), 374-384. https://doi.org/10.1093/cercor/bhq105

Logothetis, N. K., Pauls, J., Augath, M., Trinath, T., & Oeltermann, A. (2001). Neurophysiological investigation of the basis of the fMRI signal. *Nature*, *412*(6843), 150-157. https://doi.org/10.1038/35084005

Logothetis, N. K., & Wandell, B. A. (2004). Interpreting the BOLD signal. *Annu Rev Physiol*, *66*, 735-769. https://doi.org/10.1146/annurev.physiol.66.082602.092845

Lorenz, I. H., Kolbitsch, C., Hormann, C., Schocke, M., Felber, S., Zschiegner, F., Hinteregger, M., Kremser, C., Pfeiffer, K. P., & Benzer, A. (2001). Subanesthetic concentration of sevoflurane increases regional cerebral blood flow more, but regional cerebral blood volume less, than subanesthetic concentration of isoflurane in human volunteers. *J Neurosurg Anesthesiol*, *13*(4), 288-295. https://doi.org/10.1097/00008506-200110000-00002

Luiten, P. G., Gaykema, R. P., Traber, J., & Spencer, D. G., Jr. (1987). Cortical projection patterns of magnocellular basal nucleus subdivisions as revealed by anterogradely transported Phaseolus vulgaris leucoagglutinin. *Brain Res*, *413*(2), 229-250. https://doi.org/10.1016/0006-8993(87)91014-6

Lukatch, H. S., Kiddoo, C. E., & Maciver, M. B. (2005). Anesthetic-induced burst suppression EEG activity requires glutamate-mediated excitatory synaptic transmission. *Cereb Cortex*, *15*(9), 1322-1331. https://doi.org/10.1093/cercor/bhi015

Lukatch, H. S., & MacIver, M. B. (1996). Synaptic mechanisms of thiopental-induced alterations in synchronized cortical activity. *Anesthesiology*, *84*(6), 1425-1434. https://doi.org/10.1097/00000542-199606000-00019

Luo, T. Y., Cai, S., Qin, Z. X., Yang, S. C., Shu, Y., Liu, C. X., Zhang, Y., Zhang, L., Zhou, L., Yu, T., & Yu, S. Y. (2020). Basal Forebrain Cholinergic Activity Modulates Isoflurane and Propofol Anesthesia. *Front Neurosci*, *14*, 559077. https://doi.org/10.3389/fnins.2020.559077

Lydic, R., & Baghdoyan, H. A. (2005). Sleep, anesthesiology, and the neurobiology of arousal state control. *Anesthesiology*, *103*(6), 1268-1295. https://doi.org/10.1097/00000542-200512000-00024

Ma, X., Fu, S., Yin, Y., Wu, Y., Wang, T., Xu, G., Liu, M., Xu, Y., Tian, J., & Jiang, G. (2021). Aberrant Functional Connectivity of Basal Forebrain Subregions with Cholinergic System in Short-term and Chronic Insomnia Disorder. *J Affect Disord*, *278*, 481-487. https://doi.org/10.1016/j.jad.2020.09.103

Mackinnon, D. P., Lockwood, C. M., & Williams, J. (2004). Confidence Limits for the Indirect Effect: Distribution of the Product and Resampling Methods. *Multivariate Behav Res*, *39*(1), 99. https://doi.org/10.1207/s15327906mbr3901_4

Markello, R. D., Spreng, R. N., Luh, W. M., Anderson, A. K., & De Rosa, E. (2018). Segregation of the human basal forebrain using resting state functional MRI. *Neuroimage*, *173*, 287-297. https://doi.org/10.1016/j.neuroimage.2018.02.042

Markram, H., Toledo-Rodriguez, M., Wang, Y., Gupta, A., Silberberg, G., & Wu, C. (2004). Interneurons of the neocortical inhibitory system. *Nat Rev Neurosci*, *5*(10), 793-807. https://doi.org/10.1038/nrn1519

Martuzzi, R., Ramani, R., Qiu, M., Rajeevan, N., & Constable, R. T. (2010). Functional connectivity and alterations in baseline brain state in humans. *Neuroimage*, *49*(1), 823-834. https://doi.org/10.1016/j.neuroimage.2009.07.028

Mashour, G. A. (2014). Top-down mechanisms of anesthetic-induced unconsciousness. *Front Syst Neurosci*, *8*, 115. https://doi.org/10.3389/fnsys.2014.00115

Mashour, G. A., & Hudetz, A. G. (2018). Neural Correlates of Unconsciousness in Large-Scale Brain Networks. *Trends Neurosci*, *41*(3), 150-160. https://doi.org/10.1016/j.tins.2018.01.003

Mashour, G. A., Pal, D., & Brown, E. N. (2022). Prefrontal cortex as a key node in arousal circuitry. *Trends Neurosci*, *45*(10), 722-732. https://doi.org/10.1016/j.tins.2022.07.002

Mazziotta, J., Toga, A., Evans, A., Fox, P., Lancaster, J., Zilles, K., Woods, R., Paus, T., Simpson, G., Pike, B., Holmes, C., Collins, L., Thompson, P., MacDonald, D., Iacoboni, M., Schormann, T., Amunts, K., Palomero-Gallagher, N., Geyer, S., . . . Mazoyer, B. (2001). A probabilistic atlas and reference system for the human brain: International Consortium for Brain Mapping (ICBM). *Philos Trans R Soc Lond B Biol Sci*, *356*(1412), 1293-1322. https://doi.org/10.1098/rstb.2001.0915

McCormick, D. A. (1992). Neurotransmitter actions in the thalamus and cerebral cortex and their role in neuromodulation of thalamocortical activity. *Prog Neurobiol*, *39*(4), 337-388. https://doi.org/10.1016/0301-0082(92)90012-4

Meng, D., Li, X., Bauer, M., Taylor, J. P., Auer, D. P., & Alzheimer's Disease Neuroimaging, I. (2018). Altered Nucleus Basalis Connectivity Predicts Treatment Response in Mild Cognitive Impairment. *Radiology*, *289*(3), 775-785. https://doi.org/10.1148/radiol.2018180092

Mesulam, M. M., Mufson, E. J., Levey, A. I., & Wainer, B. H. (1983). Cholinergic innervation of cortex by the basal forebrain: cytochemistry and cortical connections of the septal area, diagonal band nuclei, nucleus basalis (substantia innominata), and hypothalamus in the rhesus monkey. *J Comp Neurol*, *214*(2), 170-197. https://doi.org/10.1002/cne.902140206

Metherate, R., Cox, C. L., & Ashe, J. H. (1992). Cellular bases of neocortical activation: modulation of neural oscillations by the nucleus basalis and endogenous acetylcholine. *J Neurosci*, *12*(12), 4701-4711. https://www.ncbi.nlm.nih.gov/pubmed/1361197

Meuret, P., Backman, S. B., Bonhomme, V., Plourde, G., & Fiset, P. (2000). Physostigmine reverses propofol-induced unconsciousness and attenuation of the auditory steady state response and bispectral index in human volunteers. *Anesthesiology*, *93*(3), 708-717. https://doi.org/10.1097/00000542-200009000-00020

Miller, J. W., & Ferrendelli, J. A. (1990). The central medial nucleus: thalamic site of seizure regulation. *Brain Res*, *508*(2), 297-300. https://doi.org/10.1016/0006-8993(90)90411-4

Miller, J. W., Hall, C. M., Holland, K. D., & Ferrendelli, J. A. (1989). Identification of a median thalamic system regulating seizures and arousal. *Epilepsia*, *30*(4), 493-500. https://doi.org/10.1111/j.1528-1157.1989.tb05331.x

Ming, Q., Liou, J. Y., Yang, F., Li, J., Chu, C., Zhou, Q., Wu, D., Xu, S., Luo, P., Liang, J., Li, D., Pryor, K. O., Lin, W., Schwartz, T. H., & Ma, H. (2020). Isoflurane-Induced Burst Suppression Is a Thalamus-Modulated, Focal-Onset Rhythm With Persistent Local Asynchrony and Variable Propagation Patterns in Rats. *Front Syst Neurosci*, *14*, 599781. https://doi.org/10.3389/fnsys.2020.599781

Missale, C., Nash, S. R., Robinson, S. W., Jaber, M., & Caron, M. G. (1998). Dopamine receptors: from structure to function. *Physiol Rev*, *78*(1), 189-225. https://doi.org/10.1152/physrev.1998.78.1.189

Mitra, A., Kraft, A., Wright, P., Acland, B., Snyder, A. Z., Rosenthal, Z., Czerniewski, L., Bauer, A., Snyder, L., Culver, J., Lee, J. M., & Raichle, M. E. (2018). Spontaneous Infra-slow Brain Activity Has Unique Spatiotemporal Dynamics and Laminar Structure. *Neuron*, *98*(2), 297-305 e296. https://doi.org/10.1016/j.neuron.2018.03.015

Moeller, F., Siebner, H. R., Wolff, S., Muhle, H., Boor, R., Granert, O., Jansen, O., Stephani, U., & Siniatchkin, M. (2008). Changes in activity of striato-thalamo-cortical network precede generalized spike wave discharges. *Neuroimage*, *39*(4), 1839-1849. https://doi.org/10.1016/j.neuroimage.2007.10.058

Monti, J. M., & Monti, D. (2007). The involvement of dopamine in the modulation of sleep and waking. *Sleep Med Rev*, *11*(2), 113-133. https://doi.org/10.1016/j.smrv.2006.08.003

Monti, M. M., Lutkenhoff, E. S., Rubinov, M., Boveroux, P., Vanhaudenhuyse, A., Gosseries, O., Bruno, M. A., Noirhomme, Q., Boly, M., & Laureys, S. (2013). Dynamic change of global and local information processing in propofol-induced loss and recovery of consciousness. *PLoS Comput Biol*, *9*(10), e1003271. https://doi.org/10.1371/journal.pcbi.1003271

Morales, M., & Margolis, E. B. (2017). Ventral tegmental area: cellular heterogeneity, connectivity and behaviour. *Nat Rev Neurosci*, *18*(2), 73-85. https://doi.org/10.1038/nrn.2016.165

Moruzzi, G., & Magoun, H. W. (1949). Brain stem reticular formation and activation of the EEG. *Electroencephalogr Clin Neurophysiol*, *1*(4), 455-473. https://www.ncbi.nlm.nih.gov/pubmed/18421835

Mueller, F., Musso, F., London, M., de Boer, P., Zacharias, N., & Winterer, G. (2018). Pharmacological fMRI: Effects of subanesthetic ketamine on resting-state functional connectivity in the default mode network, salience network, dorsal attention network and executive control network. *Neuroimage Clin*, *19*, 745-757. https://doi.org/10.1016/j.nicl.2018.05.037

Murty, V. P., Shermohammed, M., Smith, D. V., Carter, R. M., Huettel, S. A., & Adcock, R. A. (2014). Resting state networks distinguish human ventral tegmental area from substantia nigra. *Neuroimage*, *100*, 580-589. https://doi.org/10.1016/j.neuroimage.2014.06.047

Nakajima, M., & Halassa, M. M. (2017). Thalamic control of functional cortical connectivity. *Curr Opin Neurobiol*, *44*, 127-131. https://doi.org/10.1016/j.conb.2017.04.001

Nakamura, Y., Okada, N., Koshiyama, D., Kamiya, K., Abe, O., Kunimatsu, A., Okanoya, K., Kasai, K., & Koike, S. (2020). Differences in Functional Connectivity Networks Related to the Midbrain Dopaminergic

System-Related Area in Various Psychiatric Disorders. *Schizophr Bull*. https://doi.org/10.1093/schbul/sbz121

Nakamura, Y., Okada, N., Kunimatsu, A., Kasai, K., & Koike, S. (2018). Anatomical Templates of the Midbrain Ventral Tegmental Area and Substantia Nigra for Asian Populations. *Front Psychiatry*, *9*, 383. https://doi.org/10.3389/fpsyt.2018.00383

Nemoto, C., Murakawa, M., Hakozaki, T., Imaizumi, T., Isosu, T., & Obara, S. (2013). Effects of dexmedetomidine, midazolam, and propofol on acetylcholine release in the rat cerebral cortex in vivo. *J Anesth*, *27*(5), 771-774. https://doi.org/10.1007/s00540-013-1589-5

Nir, T., Or-Borichev, A., Izraitel, E., Hendler, T., Lerner, Y., & Matot, I. (2019). Transient subcortical functional connectivity upon emergence from propofol sedation in human male volunteers: evidence for active emergence. *Br J Anaesth*, *123*(3), 298-308. https://doi.org/10.1016/j.bja.2019.05.038

Nir, T., Raizman, R., Meningher, I., Jacob, Y., Huang, K. H., Schwartz, A. E., Brallier, J. W., Ahn, H., Kundu, P., Tang, C. Y., Delman, B. N., McCormick, P. J., Scarpa, J., Sano, M., Deiner, S. G., Livny, A., Baxter, M. G., & Mincer, J. S. (2022). Lateralisation of subcortical functional connectivity during and after general anaesthesia. *Br J Anaesth*, *128*(1), 65-76. https://doi.org/10.1016/j.bja.2021.08.033

Niu, B., Fang, Y., Miao, J. M., Yu, Y., Cao, F., Chen, H. X., Zhang, Z. G., Mei, W., & Tian, Y. K. (2014). Minimal alveolar concentration of sevoflurane for induction of isoelectric electroencephalogram in middle-aged adults. *Br J Anaesth*, *112*(1), 72-78. https://doi.org/10.1093/bja/aet280

Norton, L., Hutchison, R. M., Young, G. B., Lee, D. H., Sharpe, M. D., & Mirsattari, S. M. (2012). Disruptions of functional connectivity in the default mode network of comatose patients. *Neurology*, *78*(3), 175-181. https://doi.org/10.1212/WNL.0b013e31823fcd61

O'Connor, D. H., Fukui, M. M., Pinsk, M. A., & Kastner, S. (2002). Attention modulates responses in the human lateral geniculate nucleus. *Nat Neurosci*, *5*(11), 1203-1209. https://doi.org/10.1038/nn957

Ogawa, S., Lee, T. M., Kay, A. R., & Tank, D. W. (1990). Brain magnetic resonance imaging with contrast dependent on blood oxygenation. *Proc Natl Acad Sci U S A*, *87*(24), 9868-9872. https://doi.org/10.1073/pnas.87.24.9868

Ohtahara, S., Ohtsuka, Y., Yamatogi, Y., & Oka, E. (1987). The early-infantile epileptic encephalopathy with suppression-burst: developmental aspects. *Brain Dev*, *9*(4), 371-376. https://doi.org/10.1016/s0387-7604(87)80110-9

Oishi, Y., Suzuki, Y., Takahashi, K., Yonezawa, T., Kanda, T., Takata, Y., Cherasse, Y., & Lazarus, M. (2017). Activation of ventral tegmental area dopamine neurons produces wakefulness through dopamine D2-like receptors in mice. *Brain Struct Funct*, *222*(6), 2907-2915. https://doi.org/10.1007/s00429-017-1365-7

Orth, M., Bravo, E., Barter, L., Carstens, E., & Antognini, J. F. (2006). The differential effects of halothane and isoflurane on electroencephalographic responses to electrical microstimulation of the reticular formation. *Anesth Analg*, *102*(6), 1709-1714. https://doi.org/10.1213/01.ane.0000205752.00303.94

Ostermann, M. E., Young, B., Sibbald, W. J., & Nicolle, M. W. (2000). Coma mimicking brain death following baclofen overdose. *Intensive Care Med*, *26*(8), 1144-1146. https://doi.org/10.1007/s001340051330

Pal, D., Dean, J. G., Liu, T., Li, D., Watson, C. J., Hudetz, A. G., & Mashour, G. A. (2018). Differential Role of Prefrontal and Parietal Cortices in Controlling Level of Consciousness. *Curr Biol*, *28*(13), 2145-2152 e2145. https://doi.org/10.1016/j.cub.2018.05.025

Palanca, B. J., Mitra, A., Larson-Prior, L., Snyder, A. Z., Avidan, M. S., & Raichle, M. E. (2015). Resting-state Functional Magnetic Resonance Imaging Correlates of Sevoflurane-induced Unconsciousness. *Anesthesiology*, *123*(2), 346-356. https://doi.org/10.1097/ALN.0000000000000731

Palomero-Gallagher, N., Mohlberg, H., Zilles, K., & Vogt, B. (2008). Cytology and receptor architecture of human anterior cingulate cortex. *J Comp Neurol*, *508*(6), 906-926. https://doi.org/10.1002/cne.21684

Pan, H., Liu, S., Miao, D., & Yuan, Y. (2018). Sample size determination for mediation analysis of longitudinal data. *BMC Med Res Methodol*, *18*(1), 32. https://doi.org/10.1186/s12874-018-0473-2

Paraskeva, A., Papilas, K., Fassoulaki, A., Melemeni, A., & Papadopoulos, G. (2002). Physostigmine does not antagonize sevoflurane anesthesia assessed by bispectral index or enhances recovery. *Anesth Analg*, *94*(3), 569-572; table of contents. https://doi.org/10.1097/00000539-200203000-00017

Parent, A., Pare, D., Smith, Y., & Steriade, M. (1988). Basal forebrain cholinergic and noncholinergic projections to the thalamus and brainstem in cats and monkeys. *J Comp Neurol*, *277*(2), 281-301. https://doi.org/10.1002/cne.902770209

Parvizi, J., & Damasio, A. (2001). Consciousness and the brainstem. *Cognition*, *79*(1-2), 135-160. https://doi.org/10.1016/s0010-0277(00)00127-x

Parvizi, J., & Damasio, A. R. (2003). Neuroanatomical correlates of brainstem coma. *Brain*, *126*(Pt 7), 1524-1536. https://doi.org/10.1093/brain/awg166

Patel, A. X., Kundu, P., Rubinov, M., Jones, P. S., Vertes, P. E., Ersche, K. D., Suckling, J., & Bullmore, E. T. (2014). A wavelet method for modeling and despiking motion artifacts from resting-state fMRI time series. *Neuroimage*, *95*, 287-304. https://doi.org/10.1016/j.neuroimage.2014.03.012

Peduto, V. A., Concas, A., Santoro, G., Biggio, G., & Gessa, G. L. (1991). Biochemical and electrophysiologic evidence that propofol enhances GABAergic transmission in the rat brain. *Anesthesiology*, *75*(6), 1000-1009. https://doi.org/10.1097/00000542-199112000-00012

Peltier, S. J., Kerssens, C., Hamann, S. B., Sebel, P. S., Byas-Smith, M., & Hu, X. (2005). Functional connectivity changes with concentration of sevoflurane anesthesia. *Neuroreport*, *16*(3), 285-288. https://doi.org/10.1097/00001756-200502280-00017

Peng, J., Wang, P., Zhou, N., & Zhu, J. (2009). Partial Correlation Estimation by Joint Sparse Regression Models. *J Am Stat Assoc*, *104*(486), 735-746. https://doi.org/10.1198/jasa.2009.0126

Pergola, G., Danet, L., Pitel, A. L., Carlesimo, G. A., Segobin, S., Pariente, J., Suchan, B., Mitchell, A. S., & Barbeau, E. J. (2018). The Regulatory Role of the Human Mediodorsal Thalamus. *Trends Cogn Sci*, *22*(11), 1011-1025. https://doi.org/10.1016/j.tics.2018.08.006

Peterson, A. C., Zhang, S., Hu, S., Chao, H. H., & Li, C. R. (2017). The Effects of Age, from Young to Middle Adulthood, and Gender on Resting State Functional Connectivity of the Dopaminergic Midbrain. *Front Hum Neurosci*, *11*, 52. https://doi.org/10.3389/fnhum.2017.00052

Phillis, J. W., & York, D. H. (1968). Pharmacological studies on a cholinergic inhibition in the cerebral cortex. *Brain Res*, *10*(3), 297-306. https://doi.org/10.1016/0006-8993(68)90201-1

Plourde, G., Chartrand, D., Fiset, P., Font, S., & Backman, S. B. (2003). Antagonism of sevoflurane anaesthesia by physostigmine: effects on the auditory steady-state response and bispectral index. *Br J Anaesth*, *91*(4), 583-586. https://doi.org/10.1093/bja/aeg209

Posner, J. B. (1978). Coma and other states of consciousness: the differential diagnosis of brain death. *Ann N Y Acad Sci*, *315*, 215-227. https://doi.org/10.1111/j.1749-6632.1978.tb50340.x

Poulet, J. F., Fernandez, L. M., Crochet, S., & Petersen, C. C. (2012). Thalamic control of cortical states. *Nat Neurosci*, *15*(3), 370-372. https://doi.org/10.1038/nn.3035

Poulet, J. F. A., & Crochet, S. (2018). The Cortical States of Wakefulness. *Front Syst Neurosci*, *12*, 64. https://doi.org/10.3389/fnsys.2018.00064

Purdon, P. L., Sampson, A., Pavone, K. J., & Brown, E. N. (2015). Clinical Electroencephalography for Anesthesiologists: Part I: Background and Basic Signatures. *Anesthesiology*, *123*(4), 937-960. https://doi.org/10.1097/ALN.0000000000000841

Raichle, M. E. (2015). The brain's default mode network. *Annu Rev Neurosci*, *38*, 433-447. https://doi.org/10.1146/annurev-neuro-071013-014030

Raichle, M. E., MacLeod, A. M., Snyder, A. Z., Powers, W. J., Gusnard, D. A., & Shulman, G. L. (2001). A default mode of brain function. *Proc Natl Acad Sci U S A*, *98*(2), 676-682. https://doi.org/10.1073/pnas.98.2.676

Rajdl, K., Lansky, P., & Kostal, L. (2020). Fano Factor: A Potentially Useful Information. *Front Comput Neurosci*, *14*, 569049. https://doi.org/10.3389/fncom.2020.569049

Ranft, A., Golkowski, D., Kiel, T., Riedl, V., Kohl, P., Rohrer, G., Pientka, J., Berger, S., Thul, A., Maurer, M., Preibisch, C., Zimmer, C., Mashour, G. A., Kochs, E. F., Jordan, D., & Ilg, R. (2016). Neural Correlates of Sevoflurane-induced Unconsciousness Identified by Simultaneous Functional Magnetic Resonance Imaging and Electroencephalography. *Anesthesiology*, *125*(5), 861-872. https://doi.org/10.1097/ALN.0000000000001322

Redinbaugh, M. J., Phillips, J. M., Kambi, N. A., Mohanta, S., Andryk, S., Dooley, G. L., Afrasiabi, M., Raz, A., & Saalmann, Y. B. (2020). Thalamus Modulates Consciousness via Layer-Specific Control of Cortex. *Neuron*, *106*(1), 66-75 e12. https://doi.org/10.1016/j.neuron.2020.01.005

Ries, C. R., & Puil, E. (1999). Mechanism of anesthesia revealed by shunting actions of isoflurane on thalamocortical neurons. *J Neurophysiol*, *81*(4), 1795-1801. https://doi.org/10.1152/jn.1999.81.4.1795

Rosenblum, W. I. (2015). Immediate, irreversible, posttraumatic coma: a review indicating that bilateral brainstem injury rather than widespread hemispheric damage is essential for its production. *J Neuropathol Exp Neurol*, *74*(3), 198-202. https://doi.org/10.1097/NEN.0000000000000170

Rossetti, A. O., Carrera, E., & Oddo, M. (2012). Early EEG correlates of neuronal injury after brain anoxia. *Neurology*, *78*(11), 796-802. https://doi.org/10.1212/WNL.0b013e318249f6bb

Saalmann, Y. B., & Kastner, S. (2015). The cognitive thalamus. *Front Syst Neurosci*, *9*, 39. https://doi.org/10.3389/fnsys.2015.00039

Saalmann, Y. B., Pinsk, M. A., Wang, L., Li, X., & Kastner, S. (2012). The pulvinar regulates information transmission between cortical areas based on attention demands. *Science*, *337*(6095), 753-756. https://doi.org/10.1126/science.1223082

Sabaroedin, K., Razi, A., Chopra, S., Tran, N., Pozaruk, A., Chen, Z., Finlay, A., Nelson, B., Allott, K., Alvarez-Jimenez, M., Graham, J., Yuen, H. P., Harrigan, S., Cropley, V., Sharma, S., Saluja, B., Williams, R., Pantelis, C., Wood, S. J., . . . Fornito, A. (2022). Frontostriatothalamic effective connectivity and dopaminergic function in the psychosis continuum. *Brain*. https://doi.org/10.1093/brain/awac018

Samann, P. G., Wehrle, R., Hoehn, D., Spoormaker, V. I., Peters, H., Tully, C., Holsboer, F., & Czisch, M. (2011). Development of the brain's default mode network from wakefulness to slow wave sleep. *Cereb Cortex*, *21*(9), 2082-2093. https://doi.org/10.1093/cercor/bhq295

Sanchez-Gonzalez, M. A., Garcia-Cabezas, M. A., Rico, B., & Cavada, C. (2005). The primate thalamus is a key target for brain dopamine. *J Neurosci*, *25*(26), 6076-6083. https://doi.org/10.1523/JNEUROSCI.0968-05.2005

Sanders, R. D., Tononi, G., Laureys, S., & Sleigh, J. W. (2012). Unresponsiveness not equal unconsciousness. *Anesthesiology*, *116*(4), 946-959. https://doi.org/10.1097/ALN.0b013e318249d0a7

Saneto, R. P., & Sotero de Menezes, M. (2007). Persistence of suppression-bursts in a patient with Ohtahara syndrome. *J Child Neurol*, *22*(5), 631-634. https://doi.org/10.1177/0883073807303220

Sarter, M., & Bruno, J. P. (2000). Cortical cholinergic inputs mediating arousal, attentional processing and dreaming: differential afferent regulation of the basal forebrain by telencephalic and brainstem afferents. *Neuroscience*, *95*(4), 933-952. https://doi.org/10.1016/s0306-4522(99)00487-x

Schiff, N. D. (2008). Central thalamic contributions to arousal regulation and neurological disorders of consciousness. *Ann N Y Acad Sci*, *1129*, 105-118. https://doi.org/10.1196/annals.1417.029

Schiff, N. D., & Plum, F. (2000). The role of arousal and "gating" systems in the neurology of impaired consciousness. *J Clin Neurophysiol*, *17*(5), 438-452. https://doi.org/10.1097/00004691-200009000-00002

Schlunzen, L., Vafaee, M. S., Cold, G. E., Rasmussen, M., Nielsen, J. F., & Gjedde, A. (2004). Effects of subanaesthetic and anaesthetic doses of sevoflurane on regional cerebral blood flow in healthy volunteers. A positron emission tomographic study. *Acta Anaesthesiol Scand*, *48*(10), 1268-1276. https://doi.org/10.1111/j.1399-6576.2004.00505.x

Scholvinck, M. L., Maier, A., Ye, F. Q., Duyn, J. H., & Leopold, D. A. (2010). Neural basis of global resting-state fMRI activity. *Proc Natl Acad Sci U S A*, *107*(22), 10238-10243. https://doi.org/10.1073/pnas.0913110107

Schroter, M. S., Spoormaker, V. I., Schorer, A., Wohlschlager, A., Czisch, M., Kochs, E. F., Zimmer, C., Hemmer, B., Schneider, G., Jordan, D., & Ilg, R. (2012). Spatiotemporal reconfiguration of large-scale brain functional networks during propofol-induced loss of consciousness. *J Neurosci*, *32*(37), 12832-12840. https://doi.org/10.1523/JNEUROSCI.6046-11.2012

Schrouff, J., Perlbarg, V., Boly, M., Marrelec, G., Boveroux, P., Vanhaudenhuyse, A., Bruno, M. A., Laureys, S., Phillips, C., Pelegrini-Issac, M., Maquet, P., & Benali, H. (2011). Brain functional integration decreases during propofol-induced loss of consciousness. *Neuroimage*, *57*(1), 198-205. https://doi.org/10.1016/j.neuroimage.2011.04.020

Schulte, D., Callado, L. F., Davidson, C., Phillips, P. E., Roewer, N., Schulte am Esch, J., & Stamford, J. A. (2000). Propofol decreases stimulated dopamine release in the rat nucleus accumbens by a mechanism independent of dopamine D2, GABAA and NMDA receptors. *Br J Anaesth*, *84*(2), 250-253. https://doi.org/10.1093/oxfordjournals.bja.a013413

Schulz, J., Zimmermann, J., Sorg, C., Menegaux, A., & Brandl, F. (2022). Magnetic resonance imaging of the dopamine system in schizophrenia - A scoping review. *Front Psychiatry*, *13*, 925476. https://doi.org/10.3389/fpsyt.2022.925476

Schwalm, M., Schmid, F., Wachsmuth, L., Backhaus, H., Kronfeld, A., Aedo Jury, F., Prouvot, P. H., Fois, C., Albers, F., van Alst, T., Faber, C., & Stroh, A. (2017). Cortex-wide BOLD fMRI activity reflects locally-recorded slow oscillation-associated calcium waves. *Elife*, *6*. https://doi.org/10.7554/eLife.27602

Sessler, C. N., Grap, M. J., & Ramsay, M. A. (2008). Evaluating and monitoring analgesia and sedation in the intensive care unit. *Crit Care*, *12 Suppl 3*, S2. https://doi.org/10.1186/cc6148

Settell, M. L., Testini, P., Cho, S., Lee, J. H., Blaha, C. D., Jo, H. J., Lee, K. H., & Min, H. K. (2017). Functional Circuitry Effect of Ventral Tegmental Area Deep Brain Stimulation: Imaging and Neurochemical Evidence of Mesocortical and Mesolimbic Pathway Modulation. *Front Neurosci*, *11*, 104. https://doi.org/10.3389/fnins.2017.00104

Shafiei, G., Zeighami, Y., Clark, C. A., Coull, J. T., Nagano-Saito, A., Leyton, M., Dagher, A., & Misic, B. (2019). Dopamine Signaling Modulates the Stability and Integration of Intrinsic Brain Networks. *Cereb Cortex*, *29*(1), 397-409. https://doi.org/10.1093/cercor/bhy264

Shanker, A., Abel, J. H., Schamberg, G., & Brown, E. N. (2021). Etiology of Burst Suppression EEG Patterns. *Front Psychol*, *12*, 673529. https://doi.org/10.3389/fpsyg.2021.673529

Shichino, T., Murakawa, M., Adachi, T., Arai, T., Miyazaki, Y., & Mori, K. (1998). Effects of inhalation anaesthetics on the release of acetylcholine in the rat cerebral cortex in vivo. *Br J Anaesth*, *80*(3), 365-370. https://doi.org/10.1093/bja/80.3.365

Shichino, T., Murakawa, M., Adachi, T., Nakao, S., Shinomura, T., Kurata, J., & Mori, K. (1997). Effects of isoflurane on in vivo release of acetylcholine in the rat cerebral cortex and striatum. *Acta Anaesthesiol Scand*, *41*(10), 1335-1340. https://doi.org/10.1111/j.1399-6576.1997.tb04654.x

Shmuel, A., & Leopold, D. A. (2008). Neuronal correlates of spontaneous fluctuations in fMRI signals in monkey visual cortex: Implications for functional connectivity at rest. *Hum Brain Mapp*, *29*(7), 751-761. https://doi.org/10.1002/hbm.20580

Shrout, P. E., & Bolger, N. (2002). Mediation in experimental and nonexperimental studies: new procedures and recommendations. *Psychol Methods*, *7*(4), 422-445. https://www.ncbi.nlm.nih.gov/pubmed/12530702

Shyr, M. H., Tsai, T. H., Yang, C. H., Chen, H. M., Ng, H. F., & Tan, P. P. (1997). Propofol anesthesia increases dopamine and serotonin activities at the somatosensory cortex in rats: a microdialysis study. *Anesth Analg*, *84*(6), 1344-1348. https://doi.org/10.1097/00000539-199706000-00031

Silva, J. H., Gomez, R. S., Diniz, P. H., Gomez, M. V., & Guatimosim, C. (2007). The effect of sevoflurane on the release of [3H]dopamine from rat brain cortical slices. *Brain Res Bull*, *72*(4-6), 309-314. https://doi.org/10.1016/j.brainresbull.2007.01.011

Sleigh, J., Warnaby, C., & Tracey, I. (2018). General anaesthesia as fragmentation of selfhood: insights from electroencephalography and neuroimaging. *Br J Anaesth*, *121*(1), 233-240. https://doi.org/10.1016/j.bja.2017.12.038

Smith, G., D'Cruz, J. R., Rondeau, B., & Goldman, J. (2022). General Anesthesia for Surgeons. In *StatPearls*. https://www.ncbi.nlm.nih.gov/pubmed/29630251

Snider, S. B., Bodien, Y. G., Bianciardi, M., Brown, E. N., Wu, O., & Edlow, B. L. (2019). Disruption of the ascending arousal network in acute traumatic disorders of consciousness. *Neurology*, *93*(13), e1281-e1287. https://doi.org/10.1212/WNL.0000000000008163

Solt, K., Cotten, J. F., Cimenser, A., Wong, K. F., Chemali, J. J., & Brown, E. N. (2011). Methylphenidate actively induces emergence from general anesthesia. *Anesthesiology*, *115*(4), 791-803. https://doi.org/10.1097/ALN.0b013e31822e92e5

Solt, K., Van Dort, C. J., Chemali, J. J., Taylor, N. E., Kenny, J. D., & Brown, E. N. (2014). Electrical stimulation of the ventral tegmental area induces reanimation from general anesthesia. *Anesthesiology*, *121*(2), 311-319. https://doi.org/10.1097/ALN.0000000000000117

Spindler, L. R. B., Luppi, A. I., Adapa, R. M., Craig, M. M., Coppola, P., Peattie, A. R. D., Manktelow, A. E., Finoia, P., Sahakian, B. J., Williams, G. B., Allanson, J., Pickard, J. D., Menon, D. K., & Stamatakis, E. A. (2021). Dopaminergic brainstem disconnection is common to pharmacological and pathological consciousness perturbation. *Proc Natl Acad Sci U S A*, *118*(30). https://doi.org/10.1073/pnas.2026289118

Stamatakis, E. A., Adapa, R. M., Absalom, A. R., & Menon, D. K. (2010). Changes in resting neural connectivity during propofol sedation. *PLoS One*, *5*(12), e14224. https://doi.org/10.1371/journal.pone.0014224

Starzl, T. E., Taylor, C. W., & Magoun, H. W. (1951). Ascending conduction in reticular activating system, with special reference to the diencephalon. *J Neurophysiol*, *14*(6), 461-477. https://doi.org/10.1152/jn.1951.14.6.461

Stecker, M. M., Cheung, A. T., Pochettino, A., Kent, G. P., Patterson, T., Weiss, S. J., & Bavaria, J. E. (2001). Deep hypothermic circulatory arrest: II. Changes in electroencephalogram and evoked potentials during rewarming. *Ann Thorac Surg*, *71*(1), 22-28. https://doi.org/10.1016/s0003-4975(00)02021-x

Steriade, M. (2001). Impact of network activities on neuronal properties in corticothalamic systems. *J Neurophysiol*, *86*(1), 1-39. https://doi.org/10.1152/jn.2001.86.1.1

Steriade, M., Amzica, F., & Contreras, D. (1994). Cortical and thalamic cellular correlates of electroencephalographic burst-suppression. *Electroencephalogr Clin Neurophysiol*, *90*(1), 1-16. https://doi.org/10.1016/0013-4694(94)90108-2

Steriade, M., & Glenn, L. L. (1982). Neocortical and caudate projections of intralaminar thalamic neurons and their synaptic excitation from midbrain reticular core. *J Neurophysiol*, *48*(2), 352-371. https://doi.org/10.1152/jn.1982.48.2.352

Steriade, M., Pare, D., Parent, A., & Smith, Y. (1988). Projections of cholinergic and non-cholinergic neurons of the brainstem core to relay and associational thalamic nuclei in the cat and macaque monkey. *Neuroscience*, *25*(1), 47-67. https://doi.org/10.1016/0306-4522(88)90006-1

Swank, R. L., & Watson, C. W. (1949). Effects of barbiturates and ether on spontaneous electrical activity of dog brain. *J Neurophysiol*, *12*(2), 137-160. https://doi.org/10.1152/jn.1949.12.2.137

Tagliazucchi, E., Balenzuela, P., Fraiman, D., & Chialvo, D. R. (2012). Criticality in large-scale brain FMRI dynamics unveiled by a novel point process analysis. *Front Physiol*, *3*, 15. https://doi.org/10.3389/fphys.2012.00015

Tagliazucchi, E., von Wegner, F., Morzelewski, A., Brodbeck, V., Jahnke, K., & Laufs, H. (2013). Breakdown of long-range temporal dependence in default mode and attention networks during deep sleep. *Proc Natl Acad Sci U S A*, *110*(38), 15419-15424. https://doi.org/10.1073/pnas.1312848110

Tasserie, J., Uhrig, L., Sitt, J. D., Manasova, D., Dupont, M., Dehaene, S., & Jarraya, B. (2022). Deep brain stimulation of the thalamus restores signatures of consciousness in a nonhuman primate model. *Sci Adv*, *8*(11), eabl5547. https://doi.org/10.1126/sciadv.abl5547

Taylor, A. J., Kim, J. H., & Ress, D. (2022). Temporal stability of the hemodynamic response function across the majority of human cerebral cortex. *Hum Brain Mapp*, *43*(16), 4924-4942. https://doi.org/10.1002/hbm.26047

Taylor, N. E., Van Dort, C. J., Kenny, J. D., Pei, J., Guidera, J. A., Vlasov, K. Y., Lee, J. T., Boyden, E. S., Brown, E. N., & Solt, K. (2016). Optogenetic activation of dopamine neurons in the ventral tegmental area induces reanimation from general anesthesia. *Proc Natl Acad Sci U S A*, *113*(45), 12826-12831. https://doi.org/10.1073/pnas.1614340113

Thompson, W. H., Richter, C. G., Plaven-Sigray, P., & Fransson, P. (2018). Simulations to benchmark time-varying connectivity methods for fMRI. *PLoS Comput Biol*, *14*(5), e1006196. https://doi.org/10.1371/journal.pcbi.1006196

Threlkeld, Z. D., Bodien, Y. G., Rosenthal, E. S., Giacino, J. T., Nieto-Castanon, A., Wu, O., Whitfield-Gabrieli, S., & Edlow, B. L. (2018). Functional networks reemerge during recovery of consciousness after acute severe traumatic brain injury. *Cortex*, *106*, 299-308. https://doi.org/10.1016/j.cortex.2018.05.004

Toner, C. C., Connelly, K., Whelpton, R., Bains, S., Michael-Titus, A. T., McLaughlin, D. P., & Stamford, J. A. (2001). Effects of sevoflurane on dopamine, glutamate and aspartate release in an in vitro model of cerebral ischaemia. *Br J Anaesth*, *86*(4), 550-554. https://doi.org/10.1093/bja/86.4.550

Tononi, G. (2012). Integrated information theory of consciousness: an updated account. *Arch Ital Biol*, *150*(2-3), 56-90. https://doi.org/10.4449/aib.v149i5.1388

Tononi, G., & Edelman, G. M. (1998). Consciousness and complexity. *Science*, *282*(5395), 1846-1851. https://doi.org/10.1126/science.282.5395.1846

Tononi, G., & Koch, C. (2008). The neural correlates of consciousness: an update. *Ann N Y Acad Sci*, *1124*, 239-261. https://doi.org/10.1196/annals.1440.004

Tononi, G., & Koch, C. (2015). Consciousness: here, there and everywhere? *Philos Trans R Soc Lond B Biol Sci*, *370*(1668). https://doi.org/10.1098/rstb.2014.0167

Tucker, M. R., Hann, J. R., & Phillips, C. L. (1984). Subanesthetic doses of ketamine, diazepam, and nitrous oxide for adult outpatient sedation. *J Oral Maxillofac Surg*, *42*(10), 668-672. https://doi.org/10.1016/0278-2391(84)90210-6

Turchi, J., Chang, C., Ye, F. Q., Russ, B. E., Yu, D. K., Cortes, C. R., Monosov, I. E., Duyn, J. H., & Leopold, D. A. (2018). The Basal Forebrain Regulates Global Resting-State fMRI Fluctuations. *Neuron*, *97*(4), 940-952 e944. https://doi.org/10.1016/j.neuron.2018.01.032

Uhrig, L., Dehaene, S., & Jarraya, B. (2014). Cerebral mechanisms of general anesthesia. *Ann Fr Anesth Reanim*, *33*(2), 72-82. https://doi.org/10.1016/j.annfar.2013.11.005

Van der Werf, Y. D., Witter, M. P., & Groenewegen, H. J. (2002). The intralaminar and midline nuclei of the thalamus. Anatomical and functional evidence for participation in processes of arousal and awareness. *Brain Res Brain Res Rev*, *39*(2-3), 107-140. https://doi.org/10.1016/s0165-0173(02)00181-9

Van Dijk, K. R., Hedden, T., Venkataraman, A., Evans, K. C., Lazar, S. W., & Buckner, R. L. (2010). Intrinsic functional connectivity as a tool for human connectomics: theory, properties, and optimization. *J Neurophysiol*, *103*(1), 297-321. https://doi.org/10.1152/jn.00783.2009

Van Horn, S. C., & Sherman, S. M. (2004). Differences in projection patterns between large and small corticothalamic terminals. *J Comp Neurol*, *475*(3), 406-415. https://doi.org/10.1002/cne.20187

Vanhaudenhuyse, A., Noirhomme, Q., Tshibanda, L. J., Bruno, M. A., Boveroux, P., Schnakers, C., Soddu, A., Perlbarg, V., Ledoux, D., Brichant, J. F., Moonen, G., Maquet, P., Greicius, M. D., Laureys, S., & Boly, M. (2010). Default network connectivity reflects the level of consciousness in non-communicative brain-damaged patients. *Brain*, *133*(Pt 1), 161-171. https://doi.org/10.1093/brain/awp313

Vincent, J. L., Patel, G. H., Fox, M. D., Snyder, A. Z., Baker, J. T., Van Essen, D. C., Zempel, J. M., Snyder, L. H., Corbetta, M., & Raichle, M. E. (2007). Intrinsic functional architecture in the anaesthetized monkey brain. *Nature*, *447*(7140), 83-86. https://doi.org/10.1038/nature05758

Vincent, K. F., Zhang, E. R., Kato, R., Cho, A., Moody, O. A., & Solt, K. (2021). Return of the Righting Reflex Does Not Portend Recovery of Cognitive Function in Anesthetized Rats. *Front Syst Neurosci*, *15*, 762096. https://doi.org/10.3389/fnsys.2021.762096

Voss, L. J., Garcia, P. S., Hentschke, H., & Banks, M. I. (2019). Understanding the Effects of General Anesthetics on Cortical Network Activity Using Ex Vivo Preparations. *Anesthesiology*, *130*(6), 1049-1063. https://doi.org/10.1097/ALN.0000000000002554

Wagner, G., de la Cruz, F., Kohler, S., & Bar, K. J. (2017). Treatment Associated Changes of Functional Connectivity of Midbrain/Brainstem Nuclei in Major Depressive Disorder. *Sci Rep*, *7*(1), 8675. https://doi.org/10.1038/s41598-017-09077-5

Wang, J., Xu, Y., Deshpande, G., Li, K., Sun, P., & Liang, P. (2021). The Effect of Light Sedation with Midazolam on Functional Connectivity of the Dorsal Attention Network. *Brain Sci*, *11*(8). https://doi.org/10.3390/brainsci11081107

Wang, Y., Yu, T., Yuan, C., Yuan, J., Luo, Z., Pan, Y., Zhang, Y., Zhang, Y., & Yu, B. (2016). Effects of propofol on the dopamine, metabolites and GABAA receptors in media prefrontal cortex in freely moving rats. *Am J Transl Res*, *8*(5), 2301-2308. https://www.ncbi.nlm.nih.gov/pubmed/27347337

Westover, M. B., Ching, S., Kumaraswamy, V. M., Akeju, S. O., Pierce, E., Cash, S. S., Kilbride, R., Brown, E. N., & Purdon, P. L. (2015). The human burst suppression electroencephalogram of deep hypothermia. *Clin Neurophysiol*, *126*(10), 1901-1914. https://doi.org/10.1016/j.clinph.2014.12.022

Whishaw, I. Q. (1976). The effects of alcohol and atropine on EEG and behavior in the rabbit. *Psychopharmacology (Berl)*, *48*(1), 83-90. https://doi.org/10.1007/BF00423311

White, N. S., & Alkire, M. T. (2003). Impaired thalamocortical connectivity in humans during general-anesthetic-induced unconsciousness. *Neuroimage*, *19*(2 Pt 1), 402-411. https://doi.org/10.1016/s1053-8119(03)00103-4

Xie, G., Deschamps, A., Backman, S. B., Fiset, P., Chartrand, D., Dagher, A., & Plourde, G. (2011). Critical involvement of the thalamus and precuneus during restoration of consciousness with

physostigmine in humans during propofol anaesthesia: a positron emission tomography study. *Br J Anaesth*, *106*(4), 548-557. https://doi.org/10.1093/bja/aeq415

Xu, P., Klaasen, N. G., Opmeer, E. M., Pijnenborg, G. H. M., van Tol, M. J., Liemburg, E. J., & Aleman, A. (2019). Intrinsic mesocorticolimbic connectivity is negatively associated with social amotivation in people with schizophrenia. *Schizophr Res*, *208*, 353-359. https://doi.org/10.1016/j.schres.2019.01.023

Yan, C. G., Wang, X. D., Zuo, X. N., & Zang, Y. F. (2016). DPABI: Data Processing & Analysis for (Resting-State) Brain Imaging. *Neuroinformatics*, *14*(3), 339-351. https://doi.org/10.1007/s12021-016-9299-4

Yeo, B. T., Krienen, F. M., Sepulcre, J., Sabuncu, M. R., Lashkari, D., Hollinshead, M., Roffman, J. L., Smoller, J. W., Zollei, L., Polimeni, J. R., Fischl, B., Liu, H., & Buckner, R. L. (2011). The organization of the human cerebral cortex estimated by intrinsic functional connectivity. *J Neurophysiol*, *106*(3), 1125-1165. https://doi.org/10.1152/jn.00338.2011

Yetnikoff, L., Lavezzi, H. N., Reichard, R. A., & Zahm, D. S. (2014). An update on the connections of the ventral mesencephalic dopaminergic complex. *Neuroscience*, *282*, 23-48. https://doi.org/10.1016/j.neuroscience.2014.04.010

Yli-Hankala, A., Jantti, V., Pyykko, I., & Lindgren, L. (1993). Vibration stimulus induced EEG bursts in isoflurane anaesthesia. *Electroencephalogr Clin Neurophysiol*, *87*(4), 215-220. https://doi.org/10.1016/0013-4694(93)90021-m

Zaborszky, L., Csordas, A., Mosca, K., Kim, J., Gielow, M. R., Vadasz, C., & Nadasdy, Z. (2015). Neurons in the basal forebrain project to the cortex in a complex topographic organization that reflects corticocortical connectivity patterns: an experimental study based on retrograde tracing and 3D reconstruction. *Cereb Cortex*, *25*(1), 118-137. https://doi.org/10.1093/cercor/bht210

Zhang, S., Hu, S., Chao, H. H., & Li, C. S. (2016). Resting-State Functional Connectivity of the Locus Coeruleus in Humans: In Comparison with the Ventral Tegmental Area/Substantia Nigra Pars Compacta and the Effects of Age. *Cereb Cortex*, *26*(8), 3413-3427. https://doi.org/10.1093/cercor/bhv172

Zhang, X., Pan, W. J., & Keilholz, S. D. (2020). The relationship between BOLD and neural activity arises from temporally sparse events. *Neuroimage*, *207*, 116390. https://doi.org/10.1016/j.neuroimage.2019.116390

Zhang, Z., Cai, D. C., Wang, Z., Zeljic, K., Wang, Z., & Wang, Y. (2019). Isoflurane-Induced Burst Suppression Increases Intrinsic Functional Connectivity of the Monkey Brain. *Front Neurosci*, *13*, 296. https://doi.org/10.3389/fnins.2019.00296

Zhou, X., Wang, Y., Zhang, C., Wang, M., Zhang, M., Yu, L., & Yan, M. (2015). The Role of Dopaminergic VTA Neurons in General Anesthesia. *PLoS One*, *10*(9), e0138187. https://doi.org/10.1371/journal.pone.0138187

List of publications

Zimmermann J., Nuttall R., Golkowski, D., Schneider G., Ranft A., Rüdiger Ilg., Wollschläger A., Sorg C., The impact of sevoflurane on functional connectivity in forebrain intrinsic networks is mediated by midbrain ventral tegmental area [*in process of resubmission*].

Schulz, J., Zimmermann, J., Sorg, C., Menegaux, A., & Brandl, F. (2022). Magnetic resonance imaging of the dopamine system in schizophrenia - A scoping review. *Frontiers in psychiatry*, *13*, 925476. https://doi.org/10.3389/fpsyt.2022.925476

Nuttall, R., Jäger, C., Zimmermann, J., Archila-Melendez, M. E., Preibisch, C., Taylor, P., Sauseng, P., Wohlschläger, A., Sorg, C., & Dowsett, J. (2022). Evoked responses to rhythmic visual stimulation vary across sources of intrinsic alpha activity in humans. *Scientific reports*, *12*(1), 5986. https://doi.org/10.1038/s41598-022-09922-2

Schmitz-Koep, B., Zimmermann, J., Menegaux, A., Nuttall, R., Bäuml, J. G., Schneider, S. C., Daamen, M., Boecker, H., Zimmer, C., Wolke, D., Bartmann, P., Hedderich, D. M., & Sorg, C. (2021). Within amygdala: Basolateral parts are selectively impaired in premature-born adults. *NeuroImage. Clinical*, *31*, 102780. https://doi.org/10.1016/j.nicl.2021.102780

Hedderich, D. M., Menegaux, A., Schmitz-Koep, B., Nuttall, R., Zimmermann, J., Schneider, S. C., Bäuml, J. G., Daamen, M., Boecker, H., Wilke, M., Zimmer, C., Wolke, D., Bartmann, P., Sorg, C., & Gaser, C. (2021). Increased Brain Age Gap Estimate (BrainAGE) in Young Adults After Premature Birth. *Frontiers in aging neuroscience*, *13*, 653365. https://doi.org/10.3389/fnagi.2021.653365

Schmitz-Koep, B., Zimmermann, J., Menegaux, A., Nuttall, R., Bäuml, J. G., Schneider, S. C., Daamen, M., Boecker, H., Zimmer, C., Wolke, D., Bartmann, P., Hedderich, D. M., & Sorg, C. (2021). Decreased amygdala volume in adults after premature birth. *Scientific reports*, *11*(1), 5403. https://doi.org/10.1038/s41598-021-84906-2

International Conferences

Society for Neuroscience (SfN) International Virtual Conference Neuroscience 2021 (Chicago-USA) (November 8-11)

Poster Presentation: P637.04. *Analysis of the disruption of DMN synchronicity under effects of Sevoflurane and contributions of VTA-DMN FC to the emergence from general anaesthesia.*

FENS Forum 2022 (Paris-France) (July 9-13)

Poster Presentation: #6902. *Increasing cortico-subcortical connectivity predicts a bursting event during sevoflurane-induced burst suppression state in humans*